THE GEOLOGY, GEOCHEMISTRY AND MOLYBDENITE MINERALISATION OF THE KIGOM COMPLEX

BY

JOSEPH ITAH OMADA

IN FULFILLMENT OF THE REQUIREMENTS OF THE POSTGRADUATE SCHOOL, AHMADU BELLO UNIVERSITY, ZARIA, FOR THE AWARD OF A Ph.D GEOLOGY (MINERAL EXPLORATION) IN THE DEPARTMENT OF GEOLOGY, AHMADU BELLO UNIVERSITY,ZARIA

DEPARTMENT OF GEOLOGY
FACULTY OF SCIENCE
AHMADU BELLO UNIVERSITY, ZARIA

SEPTEMBER, 1992

DECLARATION

I declare that the information contained in this thesis is my work and that it has not been presented in any form for any award elsewhere. Information obtained from other literary publications have been dully acknowledged.



J.I. Omada

20/1/93

Date

CERTIFICATION

This project thesis entitled "The Geology, Geochemistry and Molybdenite mineralisation of the Kigom complex" by J.I. Omada meets the regulations governing the award of the degree of a Ph.D Geology in the Department of Geology, Ahmadu Bello University, Zaria and is approved for its contribution to knowledge and literary presentation.

Dr. S.K Abaa — 30/03/93

Chairman, supervisory committee — Date

Dr. C.D. OKUJENI — 30/03/93

Member, supervisory committee — Date

Dr. S.K Abaa — 30/03/93

Head of Department — Date

— 8/2/94

Dean, Postgraduate School — Date

ACKNOWLEDGEMENT

May I express my gratitude to Canadian International Development Agency who provided the funds for the analyses and for my stay in Canada; the authorities of the Ahmadu Bello University, Zaria, through the Head of Geology, A.B.U., who nominated me to serve on the C.I.D.A. sponsored project; McGill University, Canada, for giving me admission to the University for the purpose of completing the thesis.

I am greatly indebted to Dr. S.I. Abaa, Prof. R. F. Martin and Dr. C. D. Okujeni who supervised this project and critically reviewed the manuscript. Their suggestions and encouragement greatly improved the thesis. The financial support of Prof. R.F. Martin in the probe work also is gratefully acknowledged.

I am grateful to my wife, Margaret, and children; Enebojojo and Enyojo, and for bearing and praying with me during the difficult times and my sister Hannah who had to make a lot of sacrifices during this period. The encouragement of E.A. Bala and the other staff members of the Department of Geology, A.B.U., Zaria, is acknowledged.

Above all, I am grateful to God who gave me sufficient grace and strength to reach this stage of the work.

ABSTRACT

Field, geological and geochemical studies of the Kigom complex and the associated molybdenite mineralisation have been undertaken.

The Kigom complex, one of the late Jurassic intracratonic granitic intrusions into the Nigerian-Niger basement, consists of four categories of granite with gradational contacts between them: the fayalite-bearing aegirine microgranite (oldest), the arfvedsonite granite, the riebeckite granite and the riebeckite-aegirine-biotite granite (youngest). The granites are hypersolvus containing microperthites with modified exsolution textures of the coexisting feldspars. Close to the amphiboles, the perthites are enriched in K-feldspar. This modification may reflect the local removal of Na consumed in the late growth of sodic amphiboles suggesting that the K^+ for Na^+ ion exchange was most active in the rocks as late magmatic minerals were being deposited. The amphiboles, optically both arfvedsonite and riebeckite, but compositionally riebeckitic arfvedsonites, are oikocrystic containing inclusions of perthite and quartz. Late hydrothermal alterations along cleavages and at margins of the amphibloles produced aegirine, magnetite, and biotite as the K-rich fluid had long reaction time with the subsolidus minerals; a process that becomes prevalent in-the-latter granites. Astrophyl1ite, flourite, thorite, and zircon are common accessory minerals in the rocks.

The Kigom granites typically display enrichment patterns characteristic of peralkaline anorogenic A-type granites: high $Si0_2$, Na_20, K_20, Fe_20_3 (total Fe), Zr, Rb, Nb, F, and Y, and low Sr and Ba. Differentiation indices clearly show that the perthites differentiated early in the crystallisation history and that the degree of peralkalinity increases from the older to the younger facies following the trend of final consolidation of the magma responsible for the Kigom complex. This is related to the later alkali metasomatism by an alkali-rich fluid into the system such that the more altered rocks are the most enriched in trace elements. The trace element ratios are those characteristic of late-granites, while their high values are indicative of shallow-level subvolcanic intrusions. The granites of the Kigom complex have very low Mg/Mg+Fe ratio indicating a crustal source.

Molybdenite mineralisation is of low-grade and occurs disseminated in riebeckite granite at the contact between it and the arfvedsonite granite, and the basement migmatite. The molybdenite generally has inclusions of perthite with which it, in places, has blunt contacts. Pyrite, which essentially constitutes the outer zone of the mineralisation, as well as chalcopyrite, galena, helvite, and sphalerite are also common in the ore zone. Whole-rock and trace element studies of the ore zone indicate that the Mo mineralisation, like most of the trace elements, represent rest concentrations of elements which were initially present in the magma but incompatible with the silicates and were therefore deposited at relatively lower Eh/pH conditions at which stage the

vapour phase was supersaturated in Mo. The Mo in the melt was introduced into it from the source. Molybdenite mineralisation elsewhere in the world also are typically known to be associated with calc-alkaline and peralkaline magma series at a contact with earlier granites and or the host rocks.

The Kigom has evolved as a peralkaline water-saturated and F- and volatile-rich shallow-level subvolcanic magma; a condition favourable for Mo enrichment.

Table of contents

Title page i

Declaration ii

Certification iii

Acknowledgement iv

Abstract v

Table of Contents viii

List of Tables xii

List of Figures xiv

List of Plates xvii

Abbreviations xix

CHAPTER ONE INTRODUCTION 1

1.1 Aims, Objectives and Scope of work

1.2 Location of Study Area

1.3 Climate and Vegetation

1.4 Relief and Drainage

1.5 Accessibility

CHAPTER TWO LITERATURE REVIEW 10

2.1 Introduction

2.2 Petrological associations

2.3 The geochemistry of Mo

2.4 The concentration of Mo in magmas

2.5 Types of molybdenite deposits

2.5.1 The porphyry or disseminated type

Examples of porphyry or disseminated Mo deposits

A-type granites

I-type granites

2.5.2 The vein-type molybdenite mineralisation

2.5.3 Other types of Mo mineralisation

CHAPTER THREE REGIONAL GEOLOGY 27

3.1 Introduction

3.2 Geological setting

3.3 Tectonic setting

3.4 Geological and geochemical characteristics

3.5 The basement of the Kigom complex

3.6 The Older Basalts

CHAPTER FOUR FIELD OCCURRENCE AND PETROGRAPHY 43

4.1 Introduction

4.2 Field occurrence

4.3 Petrography

4.3.1 The chilled margin

4.3.2 The aegirine microgranite

4.3.3 The arfvedsonite granite

4.3.4 The riebeckite granite

4.3.5 The riebeckite-aegirine-biotite granite

4.3.6 The pegmatites

4.3.7 The rhyolitic dykes

4.4 Mineral Paragenesis

CHAPTER FIVE MINERALISATION 69

5.1 Introduction

5.2 Mode of occurrence

5.3 Ore petrography

CHAPTER SIX GEOCHEMISTRY 83

6.1 Introduction

6.2 Analytical methods

6.3 Whole-rock geochemistry

6.3.1 The major oxides

6.3.2 The trace elements

6.4 Mineral chemistry

CHAPTER SEVEN DISCUSSION 134

7.1 Introduction

7.2 Petrogenesis

7.2.1 Textural and mineralogical evidence

7.2.2 Hydrothermal alterations

7.3.3 Geochemical evidence

7.3.4 Sequence of evolution

7.4 Genesis of molybdenite mineralisation

7.5 Mo deposit grade

CHAPTER EIGHT CONCLUSION 145

8.1 Conclusion

8.2 Recommendation

LIST OF REFERENCES 150

APPENDIX 172

List of Tables

Table 1 The possible uses of molybdenite in the alloy, steel, and chemical industries

Table 2 Classification and characteristics of molybdenum stockwork deposits

Table 3 Whole-rock geochemical analyses of some of the Nigerian Younger Granite complexes

Table 4 Average geochemical composition of the basement migmatite around the Kigom complex

Table 5 Geochemical analyses of pegmatite in the basement migmatite of the study area compared with pegmatite elsewhere in Nigeria

Table 6 Geochemical analyses of dolerite dykes in the basement migmatite and of the older basalt of the study area compared with compositions of an alkaline basalt

Table 7 Whole-rock major oxides geochemical analyses of the major rock units of the Kigom complex

Table 8 Whole-rock major oxide analyses of the riebeckite granite at the ore zone of the Kigom complex

Table 9 Whole-rock major oxide and normative compositions of the Dykes associated with the Kigom complex

Table 10 Whole-rock trace element composition of the granites of the Kigom complex and at the ore zone

Table 11 Whole-rock trace element analyses of the Dykes associated with the Kigom complex

Table 12 The composition of fayalite in the aegirine microgranite of the Kigom complex

Table 13 The composition of amphiboles from the Kigom complex

Table 14 The composition of biotite in the Kigom complex

Table 15 The composition of aegirine in the Kigom complex

Table 16 The composition of astrophyllite in the ore zone of riebeckite granite of the Kigom complex

List of Figures

Figure 1 The general geology and distribution of the Nigerian Younger Granite complexes

Figure 2 Aerial photo interpretation map of the Kigom complex and the surrounding areas

Figure 3 Schematic representation of the relationship between stockwork molybdenum deposits and arc magma chemistry in a convergent plate margin setting

Figure 4 The Colorado Mineral Belt

Figure 5 Section showing generalized geology and ore zones of Climax, Colorado

Figure 6 Map showing molybdenum deposits in relation to Tertiary stocks and gravity contours, Colorado

Figure 7 $Na_2O + K_2O$ versus SiO_2 plot for the dolerite dyke

Figure 8 Aerial photograph of the Kigom and the surrounding rocks

Figure 9 The geology of the Kigom complex

Figure 10 Rose diagram of the joints on the Kigom complex

Figure 11 Pattern of distribution of the sulphide mineralisation at the ore zone of the Kigom complex

Figure 12 Silica and Alumina Distribution plot for the Kigom granites

Figure 13 Na_2O and K_2O Distribution plot for the Kigom granites

Figure 14 CaO, MnO, and TiO_2 Distribution plot for the Kigom granites

Figure 15 Alkali/Silica plot for the Kigom granites

Figure 16 Alumina saturation and alkali saturation plot for the Kigom granites
Figure 17 Q-Ab-Or triangular plot for the Kigom granites
Figure 18 Or-Ab-An triangular plot for the Kigom granites
Figure 19 Alkali distribution plot for the ore zone
Figure 20 The distribution of Zr in the granites of the Kigom complex
Figure 21 Distribution plot for the trace elements Rb, Li, Zn, Nb, and Y in the granites of the Kigom complex
Figure 22 Distribution plot for Sr, Cr, Be, and Ba in the granites of the Kigom complex
Figure 23 Distribution plot for Mo, W, and Sn in the granites of the Kigom complex
Figure 24 Distribution plot for Cu, Pb, Zn, Th and U for the Kigom granites
Figure 25 Distribution plot for F in the granites of the Kigom complex
Figure 26 Ba-Rb-Sr triangular plot for the granites of the Kigom complex
Figure 27 Distribution plot for Pb in the ore zone of the riebeckite granite
Figure 28 Distribution plot for Mo and F for the ore zone of the riebeckite granite
Figure 29 Distribution plot for Cu, Zn, U and Th for the ore zone of the riebeckite granite

Figure 30 Distribution plot for Zr in the ore zone of the Kigom complex

Figure 31 The distribution of Nb, Y and Rb in the ore zone of the riebeckite granite

Figure 32 Distribution plot for W, Sn, Be, Ag, Ba and Sr for the ore zone of the riebeckite granite

Figure 33 Amphibole classification diagram

Figure 34 The Ca + Al^{IV} versus Si + Na + K plot for the amphiboles in the Kigom complex.

Figure 35 Plot of amphiboles from Giret et al. (1980), Borley (1963), and Strong and Taylor (1984)

Figure 36 The graphical representation of the evolution of rock types associated with the Nigerian ring complexes (After Jacobson et al. (1958) and Bowden and Kinnaird (1976)).

List of Plates

Plate 1 Typical outcrop pattern of the Younger granite complexes as exemplified by the Kigom complex

Plate 2 Photomicrograph of the basement migmatite in the study area

Plate 3 Photomicrograph of the dolerite dyke in the basement migmatite of the study area

Plate 4a Photograph of part of the weathered older basalt being escavated for alluvial tin

Plate 4b Photograph of Basalt crater and photomicrograph of the Newer Basalt in the study area

Plate 5 Photograph of the rhyolite dyke

Plate 6 Photomicrograph of the aegirine microgranite

Plate 7 Photograph and photomicrograph of the fayalite crystals in the aegirine microgranite

Plate 8 Photograph of the arfvedsonite granite

Plate 9 Photomicrograph of part of the arfvedsonite granite

Plate 10 Photomicrograph of part of the arfvedsonite granite

Plate 11 Photomicrograph of the riebeckite granite showing texturally altered perthite

Plate 12 Photomicrograph of parts of the riebeckite granite showing inclusions of perthite in late quartz

Plate 13 Photomicrograph of riebeckite crystals in riebeckite granite

Plate 14 Photomicrograph of riebeckite granite showing euhedral crystals of zircon and fluorite

Plate 15 Photomicrograph of the riebeckite-aegirine-biotite granite showing the altered riebeckite

Plate 16 Photomicrograph of the felsic dyke

Plate 17 Photomicrograph of rhyolite in the study area

Plate 18a Photograph of parts of the adit by the Fidelity mining syndicate

Plate 18b Photograph of the abondoned treatment site for the molybdenite mine

Plate 19 Photograph of the molybdenite zone showing the disseminated mineralisation

Plate 20 Photograph of the ore zone showing the forms of occurrence of molybdenite

Plate 21 Photomicrograph of the ore zone showing the alteration of perthite and amphibole to biotite

Plate 22 Photomicrograph of the ore zone showing the growth of astrophyllite along planes of perthite

Plate 23 Photomicrograph of parts of the ore zone showing the contact relationship between helvite and molybdenite

Plate 24 Photomicrograph of altered perthite in the molybdenite zone of the ore zone

Abbreviations, Definitions, Glossaries and Symbols

abs.	abstract
ann.	annual
bull.	bulletin
Can.	Canadian
Conf.	conference
Contr.	contribution
Econ.	economic
ed.	editor
eds.	editors
e.g.	for example
Equip.	equipment
Fig.	figure
Finl.	Finland
Geol.	Geology
Geophysc.	geophysical
Geosc.	geosciences
Journ.	Journal
Mag.	magazine
Met.	metallurgy
Min.	mining
Minr.	mineralogical
Pac.	pacific
Rev.	revision
Sci.	Science

Soc.	Society
Surv.	survey
v.	volume
Vs	versus

CHAPTER ONE

INTRODUCTION

1.1 AIMS, OBJECTIVES AND SCOPE OF WORK

The Jurassic Younger Granites of Nigeria are high level anorogenic granitic plutons intruded into the Precambrian - Lower Palaeozoic basement which consists of gneisses, migmatite and deformed granites. The intrusions occur mostly as ring complexes but also as cupolas. Over 40 individual Complexes ranging in size from 1,500 km^2 to less than 2 km^2 have been recognised in Nigeria (Fig. 1). In the case of many of the individual complexes [e.g., Tibchi: Ike (1979), Ririwai: Abaa (1978), Martin and Bowden (1981), Bowden (1982)], both peralkaline and peraluminuous granites constitute over 90% by volume of all rocks. Essentially peralkaline or peraluminous complexes are also common.

In terms of mineralisation, the Younger Granite Complexes represent distinctive granitic suites that are mineralised in tin and do in fact constitute the best example of a tin metallogenetic province. Apart from Sn mineralisation, substantial quantities of Zn, Cu, U, Nb, Th and REE also have been reported (Bowden and van Breeman, 1972; Kinnaird, 1979; Bowden, 1982; Abaa, 1985,1991; Imeokparia, 1985). The enrichment of some of the Complexes in Mo and W, so that whole-rock concentrations attain 45 and 60 ppm, respectively, also has been reported [e.g., the Jarawa Complex:

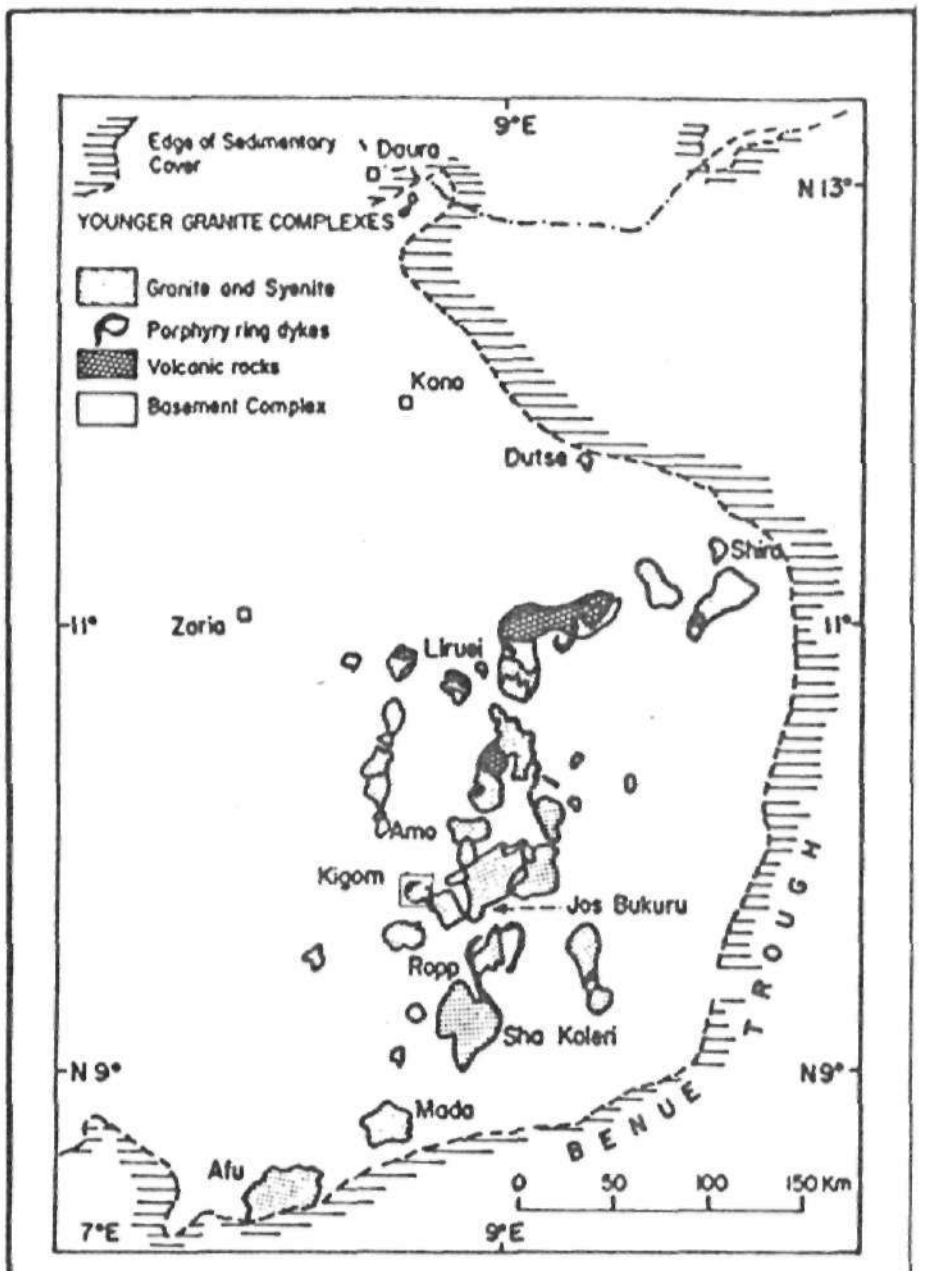


FIGURE 1. General geology and distribution of the Nigerian Younger granite complexes (after Jacobson *et al.*, 1958).

Imeokparia (1985)]. Of all the complexes, only the Kigom complex is richly mineralised in Mo. Yet, it is among the least studied. Apart from the report of Mo mineralisation in the Kigom complex by Jacobson et al. (1958) and, subsequently, a short account of a visit by Garner (1959) at the time that the Fidelity Mining Syndicate owned by one Mr. N. Yassin (licence No. ML 13655) was developing a mine, there has been no further study of the Kigom Complex and the associated Mo mineralisation.

A detailed study of the geology and the geochemistry of the Kigom complex and the associated mineralisation is, therefore, necessary to highlight the distinctiveness of the complex and its implications on the genesis of the Mo deposit. It should be interesting to know in which way the Kigom complex may differ from the other complexes of the province which generally are not Mo-mineralised. In addition, a study of the Mo deposit should be of great interest to the country since Mo is essential in the iron, steel and chemical industries (Table 1).

The objectives of the study include;

i) To review existing literature on the geological and tectonic setting, geochemistry, and mechanism of concentration of Mo in granites, and on some of the major deposits of molybdenite in the world

ii) To present results of geological mapping of the Kigom Complex and the surrounding areas on a scale of 1:50,000

iii) To investigate existing geological structures in the Kigom complex and their possible controls on mineralisation. This

Table 1. The possible use of molybdenum in the alloy, steel and chemical industries.

INDUSTRY	USES
Alloy (Iron and Steel)	hardening alloy (for strength and ductility)
Steel	manufacture of aircraft, automobiles, oil machinery, shafts, valves, pumps, gears, high speed tools, pins, bolts, guns, armour plates, dies, wire, etc
Iron	improves cast iron for industries, railroad and automobiles
Chemical	catalysts, dyes, lithographic inks and lubricants

involves air-photo interpretation and field mapping

iv) To document, through petrographic and mineralogical studies, the rock units of the Kigom complex

v) To determine the distribution of major and trace elements in representative samples of the major rock units with a view to determining their bulk chemical composition and enrichment pattern

vi) To determine the average concentration of molybdenite in the ore zone and to compare with ore grades mined elsewhere in the world and

vii) To deduce the likely conditions of Mo mineralisation, to relate this to the existing models for the concentration of Mo in granites and to discuss the evolution of the magma.

Age dating of rocks and REE data of the rocks of the study area will not be covered in this work.

1.2 LOCATION OF STUDY AREA

The study area is located 40 km southwest of Jos between Longitudes 9°40'N and 9°48'N and Latitudes 8°35'E and 8°39'E. It is part of Naraguta sheet 168 (1:100,000). It covers an area of 178.19 km^2 with the Kigom complex occupying 25 Km^2 of this area. The Kigom Complex is located in the central part of the belt of the Younger Granites and lies to the west-southwest of the Jos-Bukuru Complex (Fig. 1). Politically, the Kigom marks the boundary between Plateau and Kaduna States.

1.3 CLIMATE AND VEGETATION

The Jos Plateau area being part of sub-Saharan Africa, has two seasons. The wet season begins in April and ends in mid-October, whereas the dry season begins in mid-October and ends in March. Temperatures vary between 25° and 35°C during the wet season, and between 9° and 18°C during the dry season.

The Jos Plateau is sparsely vegetated. Wide river channels have thick alluvium and, therefore, not much vegetation. A typical example is the River Kaduna, which passes west and south of the study area. Shrubs and grasses wither very quickly during the dry season.

1.4 RELIEF AND DRAINAGE

The Jos Plateau area is geographically distinct from the surrounding areas. It is generally flat, with each of the Younger Granite Complexes constituting a topographic high. These complexes have sharp contacts and stand nearly vertically with respect to the surrounding rocks (Plate 1).

Drainage is of both trellis type and dendritic. However, there is a prominence of the trellis pattern over the dendritic, because of the very strong control of fractures on the drainage pattern. The aerial interpretation map of the study area (Fig. 2), shows that most of the fractures are continuous. The steams trend mainly N-S, NE-SW, and NW-SE. These correspond to the general regional structural patterns.

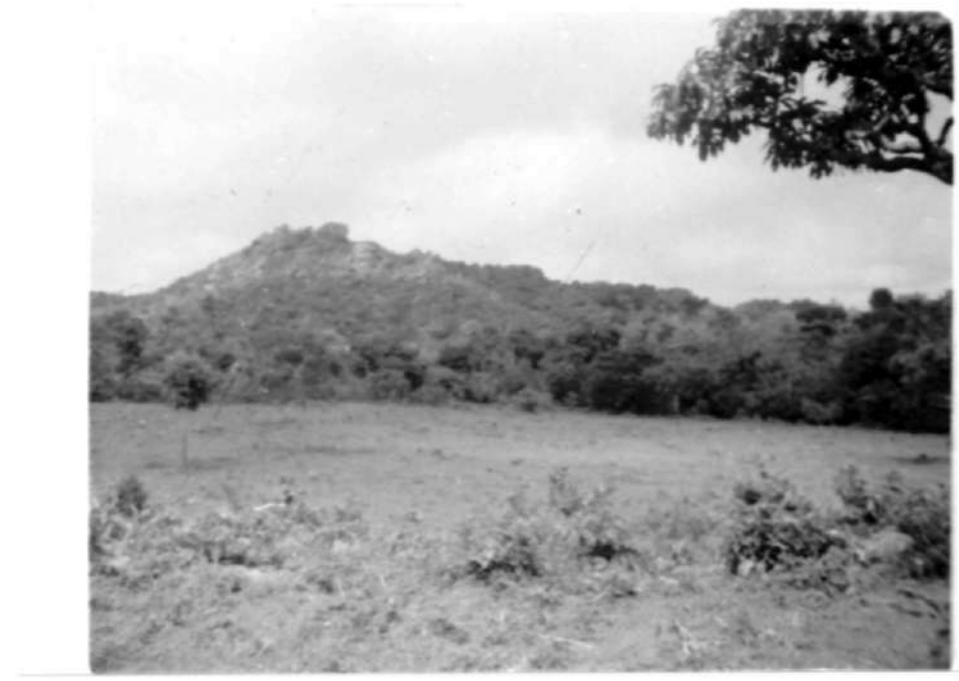


Plate 1. Typical outcrop pattern of the Younger granite complexes as exemplified by the Kigom complex.

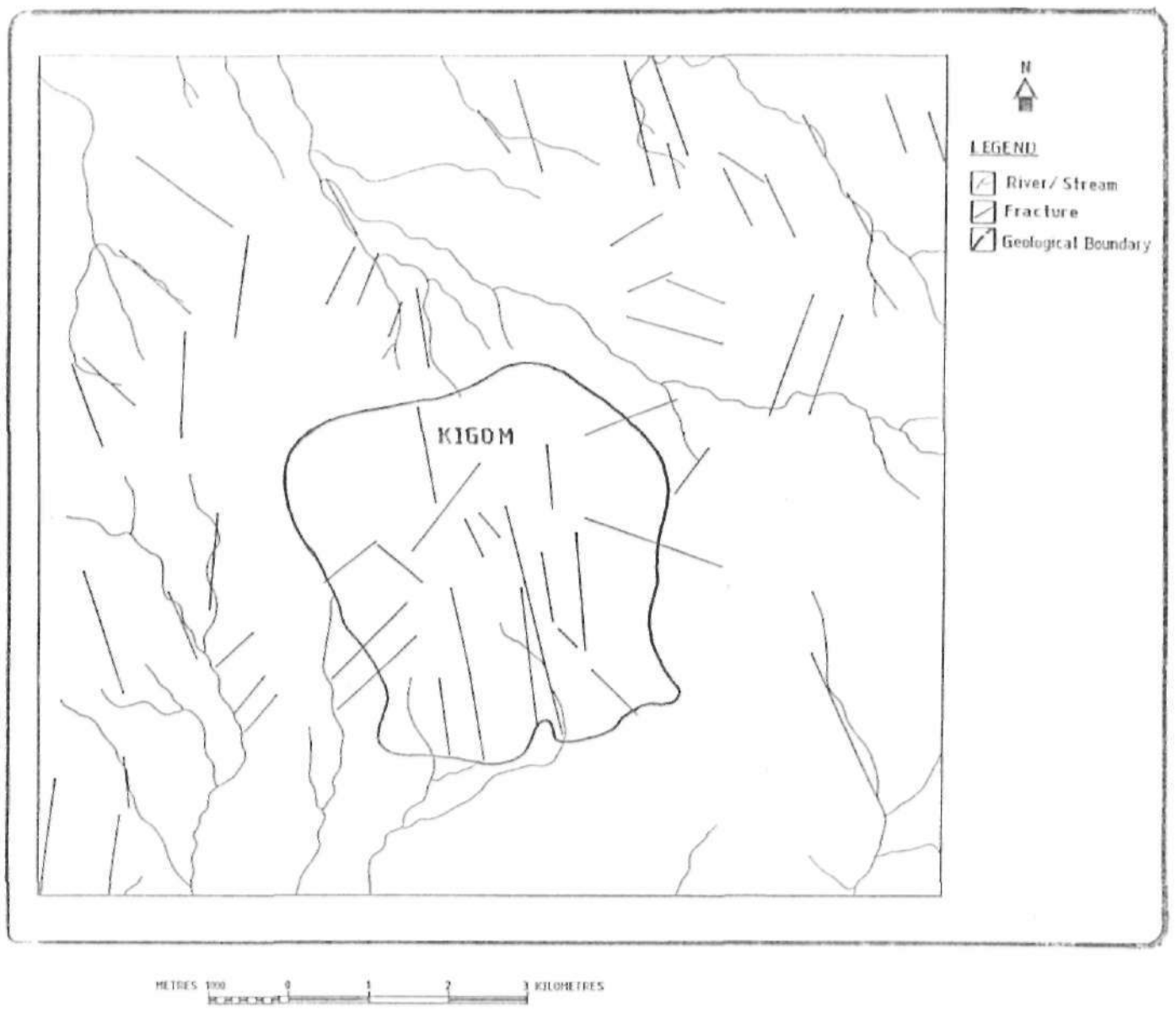


Fig. 2. Aerial photo interpretation of the Kigom Complex, part of sheet 168 Naraguta S.W.

1.5 ACCESSIBILITY

The study area is relatively accessible by means of the Jos-Bukuru-K.Vom road which is paved, and then secondary roads, namely the K.Vom-Ganawuri-Daw-Telema road or the K.Vom-MaiAngwa-Kishesho-Kigom road. These secondary roads are motorable in both the wet and dry seasons, but may require a four-wheel-drive vehicle in the wet season. Access to most parts of the Kigom Complex can only be made by foot because of the steep relief.

CHAPTER TWO

LITERATURE REVIEW

2.1 INTRODUCTION

This chapter reviews the literature on the geological and tectonic settings of molybdenite mineralisation, the mechanism of concentration of MoS_2 in granites, and the geochemistry of Mo. The geology and genesis of some of the major deposits also are reviewed.

2.2 PETROLOGICAL ASSOCIATIONS

Calc-alkaline, and alkaline magmatic series are associated with Mo deposits (Fig. 3). Deposits associated with calc-alkaline suites can be divided into the stockwork type and the disseminated type depending on the depth of formation, features of alteration and characteristics of exsolution of the magmatic fluids. The Mo deposits associated with alkali-calcic and alkaline suites occur mainly in the form of stockworks. Such deposits may be syenite- and monzonite-related or granite-related (Westra and Keith, 1981). Granitic systems that bear Mo develop in and adjacent to epizonal plutons (Mutschler et al., 1981).

Using chemical criteria, Chappell and White (1974), and Pitcher (1983) classified granites into the I-, S-, A-, and M-types. Each type is related to tectonic setting and source mineralogy, and can be assigned specific types of metal associations. In this classification, Mo is associated with both the I- and the A-type granites. These are, respectively, granites related to subduction and to within-plate magmatism.

A-type granites, to which category the Kigom complex belongs, are developed in a tensional environment like a back-arc basin, an area of bending in the subducting slab, or areas of mid-plate transtensional faulting. These tensions could be established soon after an orogenic event (Pitcher, 1983) and thus post-orogenic or as intracratonic rifting within a non-orogenic crust. The F-rich A-type granites, a post-orogenic granite, of the Colorado Mineral belt (Fig. 4), for example, are considered to have been derived by partial melting of the lower crust (Stein and Hannah, 1985) during incipient extension related to the development of the Rio Grande Rift after subduction-related magmatism of Laramide age had ceased (Stein, 1985, 1988; Geraghty et al., 1988; Bookstrom, 1981; Thompson and Burke, 1974; Keith, 1978). The anorogenic Younger Granite complexes of Nigeria, the Bordvika granites within the Oslo rift, Norway (Gyeti and Schonwandt, 1979) and the W-bearing Black Pearl albite stock, Arizona (Schmitz and Burt, 1990) represent granitic intrusions into a non-orogenic craton. The details of mineralisation characteristics of some of these Mo-bearing granites will be discussed later.

AHMADU BELLO UNIVERSITY
KASHIM IBRAHIM LIBRARY

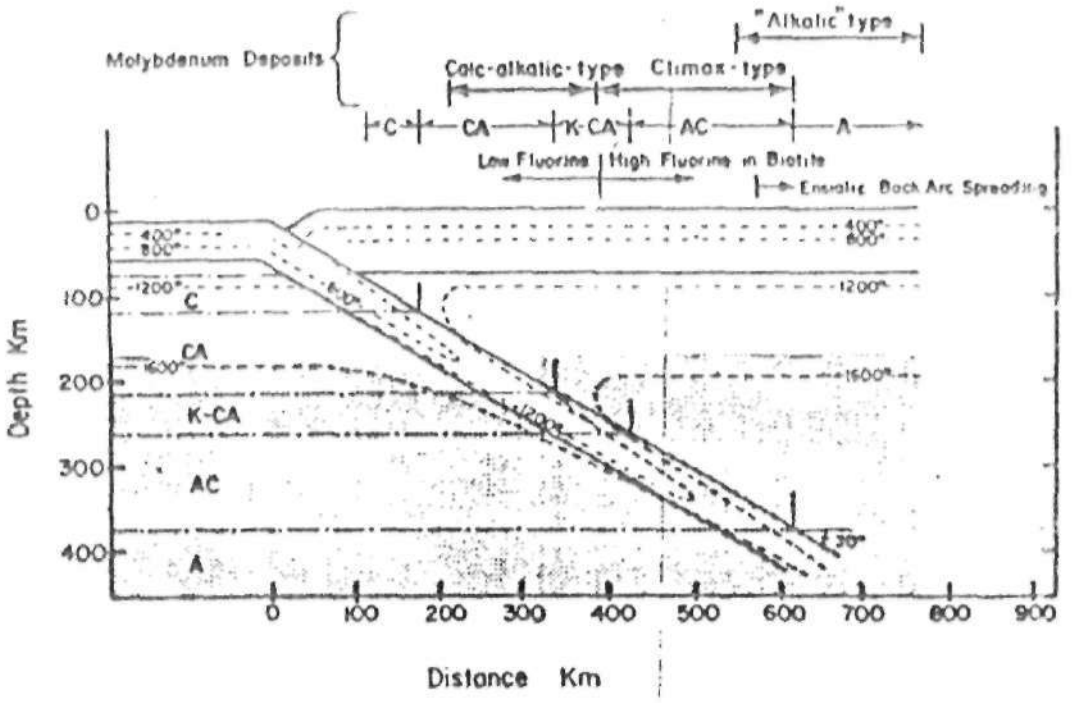


Figure 3. Schematic representation of the relationship between stockwork molybdenum deposits and arc magma chemistry in a convergent plate margin setting (after Westra and Keith (1981). Schematic geothermal configuration after Toksoz et al. (1971). Shaded area outlines zone in which phlogopite is no longer stable. Note that the stability limit of phlogopite in the mantle is strongly dependednt on the thermal configuration one adopts. The upper stability limit of phlogopite as shown is based on experimental data by Wendlandt and Eggler (1980) and a geotherm configuration (not shown) proposed by Anderson et al. (1978).

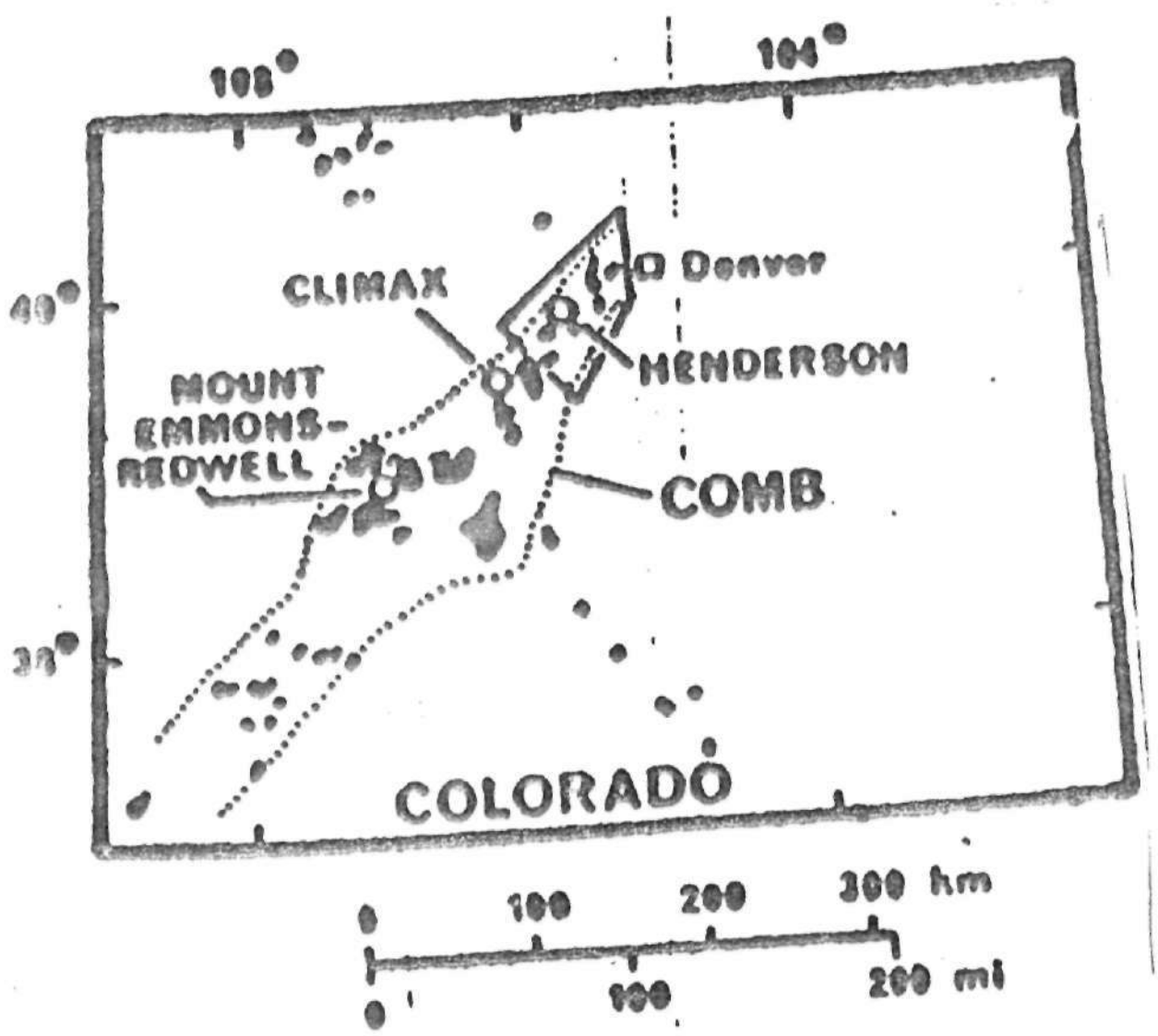


Figure 4. The Colorado Mineral Belt. (After Stein, 1985).

In relation to magma types, the calc-alkaline, the high-K calc-alkaline, and alkaline Mo-mineralised suites are related to a convergent plate margin setting, subduction, and intracratonic rifting, respectively. Each of these have distinctive trace-element associations.

The alphabet classification of granites is, however, considered to be unreliable with respect to metal associations (Hannah and Stein, 1990), as some rocks do show dual affinities. The Taylor Creek Rhyolite of the Black Range, New Mexico, for example, shows an affinity with I- type granites using $\delta^{18}O$ values (7‰) (Rye et al. 1990), and with A-type granites using mineralogical and chemical studies (Hannah and Stein, 1990). The Taylor Creek magma apparently had an origin in the lower crust but contains variable proportions of mantle components (Reece et al., 1990). Thus the rhyolite can only be loosely classified as A-type granites and hence the associated tin mineralisation is controlled by processes related to source mineralogy, order of crystallisation, and fluid exsolution rather than tectonic setting.

2.3 THE GEOCHEMISTRY OF Mo

Mo, a transition element, belongs to Group IVB of the periodic table. Its chemistry, like that of W, involves a wide range of oxidation states, from 2+ to 6+. Under reducing conditions and in acid media, Mo^{4+} is the most stable, and forms the sulphide molybdenite (MoS_2) (Manheim, 1974; Uzkut, 1974), the most important

of the Mo minerals economically. It has a hexagonal structure, in which layers are held by van der Waals bonds. Under oxidising conditions, Mo^{6+} is the most stable; Mo occurs in the form of complexes, for example, in minerals such as ferrimolybdite ($Fe_2^{+3}(Mo^{+6}O_4)_3.8H_2O$, orthorhombic), molybdeniferous scheelite (powellite) ($CaMoO_4$, tetragonal), and wulfenite ($PbMoO_4$). Other Mo-bearing minerals include chillagite [$Pb(Mo,W)O_4$, tetragonal], ilsemanite [$Mo_3O_8.nH_2O$, amorphous MoS_2], koechlinite [Bi_2MoO_6, orthorhombic], lindgrenite [$Cu_3^{+2}(MoO_4)_2(OH)_2$, monoclinic], eosite ($Ca(Mo,V)O_4$, tetragonal], molybdite [MoO_3, orthorhombic], molybdofornacite {$Pb_2Cu^{+2}[(As,P)O_4][(Mo^{+6},Cr^{+6})O_4(OH)$, monoclinic}, and jordisite (MoS_2, amorphous). The 2+ oxidation state is very unstable and thus unlikely to occur in nature.

Mo is incompatible with the major rock-forming minerals (Krauskopf, 1979), and thus it is present only at low levels of concentration in crustal rocks (1-2 ppm, on average). Tungsten-bearing minerals, such as scheelite and huebnerite, do carry Mo [800 and 900 ppm, respectively], and minerals containing Ti^{4+} and Fe^{3+}, for example, titanite, ilmenite, and titaniferous magnetite, do have preferential accumulation of Mo (Manheim and Landergren, 1978). The association of Mo with Ti^{4+} and Fe^{3+} is partly due to the similarity in their ionic radius: 0.68 Å, 0.67 Å, and 0.68 Å, respectively, for Mo^{4+}, Fe^{3+}, and Ti^{4+} (Manheim and Landergreen, 1978). Molybdenite can be co-precipitated with fine-grained sulphides such as pyrite, chalcopyrite, sphalerite, and galena, such that Mo deposits can be rich in Cu, Zn and Fe.

2.4 THE CONCENTRATION OF Mo IN MAGMAS

Crystallising magmas have low initial contents of Mo. In melts of granodioritic, granitic, and quartz monzonitic compositions, Mo is transported as the molybdate anion complex (Uzkut, 1974). As crystallisation proceeds and the residual melt becomes increasingly rich in fluids, the concentration of Mo and many other initially incompatible elements increases in the magma. Thus Mo concentration takes place at the top of magma chambers by a combination of processes of magmatic differentiation, for example, fractional crystallisation and thermogravitational diffusion as well as by volatile transfer (Westra and Keith, 1981).

Wyllie and Tuttle (1964), Wyllie (1979), and Glyuk and Trufanova (1977) have shown that high initial alkali contents and high concentrations of F drastically lower the solidus temperature of felsic melts and reduce melt viscosity. At low temperatures and with reduced viscosity following the crystallisation of most of the silicates, concentrations of initially incompatible elements such as Mo, W, Zr, Y and Sn are enhanced, especially in peralkaline melts.

The experimental data of Webster and Holloway (1990) on the partitioning of F and Cl between magmatic hydrothermal fluids and highly evolved granitic magmas show that the differing behaviour of Cl versus F in a silicate melt and associated aqueous fluid strongly influences metal distribution in the system. The effects of increased F contents are to decrease melt viscosity, increase

diffusion rates of cations and volatiles, decrease both liquidus and solidus temperatures, and increase thermal stability of hydrous phases. The effects of increased Cl, on the other hand, are to increase the solubility of alkalis with respect to Al in the fluid, increase the partitioning of Zn, Cu, Pb, W, Mn, REE, Li, Rb, Cs, Nb, Y, Sr, and Ba from the melt into the fluid, which occurs markedly in a F-free system. Whereas Mo deposits associated with calc-alkaline rocks are related to F-poor and Cl-rich magmas, Mo deposits associated with peralkaline rocks typically involve F-rich systems.

The role of host rocks in Mo-bearing granitic rocks has been a subject of discussion. Many investigators of the stockwork Mo deposits (e.g., Wallace et al., 1978; Kamilli, 1978; Ganster, 1976; Stein and Hannah 1985) believe that Mo in the hydrothermal system was derived entirely from the crystallising magma; in their opinion, the host rocks played little or no role in Mo concentration. For example, Hannah and Stein (1986) showed that, at Climax, the ore fluids and the metals and sulphur they carried were derived entirely within the igneous system.

As a result of its incompatibility with the major rock-forming minerals, Mo tends to be concentrated in the highly differentiated, near-eutectic or near minimum granitic residue (Westra and Keith, 1981) and in the vapour phase (Mutschler et al., 1981). In the hydrothermal environment, Mo could be enriched through a Mo-rich vapour phase associated with a late magmatic H_2O-saturated silicate melt (Isuk, 1976) or vapour transport of

oxymolybdate or halogen compounds (Arutyunyan, 1969; Shesherba, 1970; Glemser and Wendlandt, 1963) or molybdate, oxymolybdate, and molybdate complexes in hydrothermal fluids (Khitarov et al., 1967; Smith et al., 1980).

Using thermodynamic extrapolations, Smith et al. (1980) suggested that Mo concentration in the hydrothermal fluid coexisting with a felsic melt may reach several thousand parts per million (ppm) at 350°C, and that the solubility decreases drastically between 350 and 300°C.

2.5 TYPES OF MOLYBDENITE DEPOSIT

Characteristics of Mo deposits are summarized in Table 2. These will be reviewed in turn.

2.5.1 The Porphyry or the disseminated type

Of the known molybdenite deposits, those of the porphyry or the disseminated type are the most enriched and the most numerous. Generally, these are hosted in granitic rocks of calc-alkaline or alkaline character, and are associated with hydrothermal and metasomatic activity having some form of structural control. The deposit may be of stockwork type and show breccia pipes in which the sulphides are dispersed through relatively large volumes of altered and fractured rocks.

Table 2. Classification and characteristics of molybdenum stockwork Deposits

	Porphyry or disseminated		vein type	others
magma type	calc-alkaline	alkaline	usually associated with calc-alkaline granitic rocks and quartzo-feldsparthic veins	contact metasomatic zones and tactite bodies of silicfied limestone adjacentto intrusive granitic rocks. Also in black shales
Geotect. setting	compressive continental plate margin and subduction zones	intracratonic rift zones or back arcs		
Geologic setting	usually associated with later injections and or hydrothermal activities	usually associated with later injections and or hydrothermal activities		
Petrochemistry				
Rb ppm	100-350	>200	-	-
Sr ppm	100-800	<100		
Nb ppm	<10	15-140		
Examples	Climax Urad- Henderson Questa	Bordvika Mt Pleasant Kigom		

The calc-alkaline group includes the high K calc-alkaline of Westra and Keith (1981). Compiled from Westra and Keith (1981), Jensen and Bateman (1981), and Blossom (1989).

Examples of Porphyry or Disseminated Mo Deposits

a) A-type granites

The Climax deposit is an example of large-scale disseminated mineralisation, with an average grade of < 0.4% MoS_2 in several million tonnes of ore. The orebody lies in the Precambrian terrane of the Colorado mineral belt (Fig. 4) at an altitude of 3,390 m. The mineralisation is related to the hydrothermal activity associated with H_2O-saturated peralkaline magma that intruded Precambrian rocks in mid-Tertiary times and formed at least four composite stocks (Figs. 5 & 6). The ores are confined to the first three injections; a complex stockwork having circular plan. These igneous units have been metasomatically altered by the associated hydrothermal activity. There is a spatial and genetic relationship between the ore and the enclosing precambrian host-rocks (Jensen and Bateman, 1981). Mutschler et al. (1981) suggested that the source plutons for the Climax, Urad-Henderson (see below), and the Mount Emmons - Redwell basin, Colorado, are small epizonal plugs of granite porphyry.

The Urad-Henderson orebody, also located in the Colorado mineral belt, has a mineable grade of 0.49% MoS_2. It occurs in a fractured and hydrothermally altered granite in a portion of a composite granite porphyry stock. The granites are metaluminous in composition and were intruded at about the same time as in the case of Climax (Seedorff, 1985).

The Bordvika molybdenite deposit occurs within the Oslo rift, Norway. It is located in the central part of the Glitrevann Cauldron in a granitic stock surrounded by syenitic ring dykes with general inward dips (Schonwandt and Gyeti, 1977; Gyeti and Schonwandt, 1979; Oftedahl, 1953). The Glitrevann granitic stock consists of three units of peralkaline composition, namely, black quartz-feldspar porphyry, grey quartz-feldspar porphyry, and aplitic granite. Molybdenite mineralisation occurs in the central part of the stock, which has been hydrothermally altered into the potassic, sericitic, argillic and propylitic zones. Molybdenite occurs either in veins with quartz, feldspars and mica or as stockworks or breccia fillings (Gyeti and Schonwandt, 1979). The largest deposits, the Munka and the Bjorntjarn, are located in the contact zone between the youngest granites and gneissic supracrustal host-rocks. The granites associated with mineralisation form geographically well-defined cupolas on top of the underlying batholiths (Ohander, 1985; Ohander and Nisca, 1985), for example, in the Vidsel area (Isaksson, 1982). In the Vidsel area, major molybdenite enrichments are found in aplites associated with the roof zone of the pluton.

b) I-type granites

The Kemess Porphyry Cu-Mo deposit occurs in andesitic to basaltic flows and tuffs that can be correlated with the Savage Mountain Formation of the upper Triassic Tarela Group within the

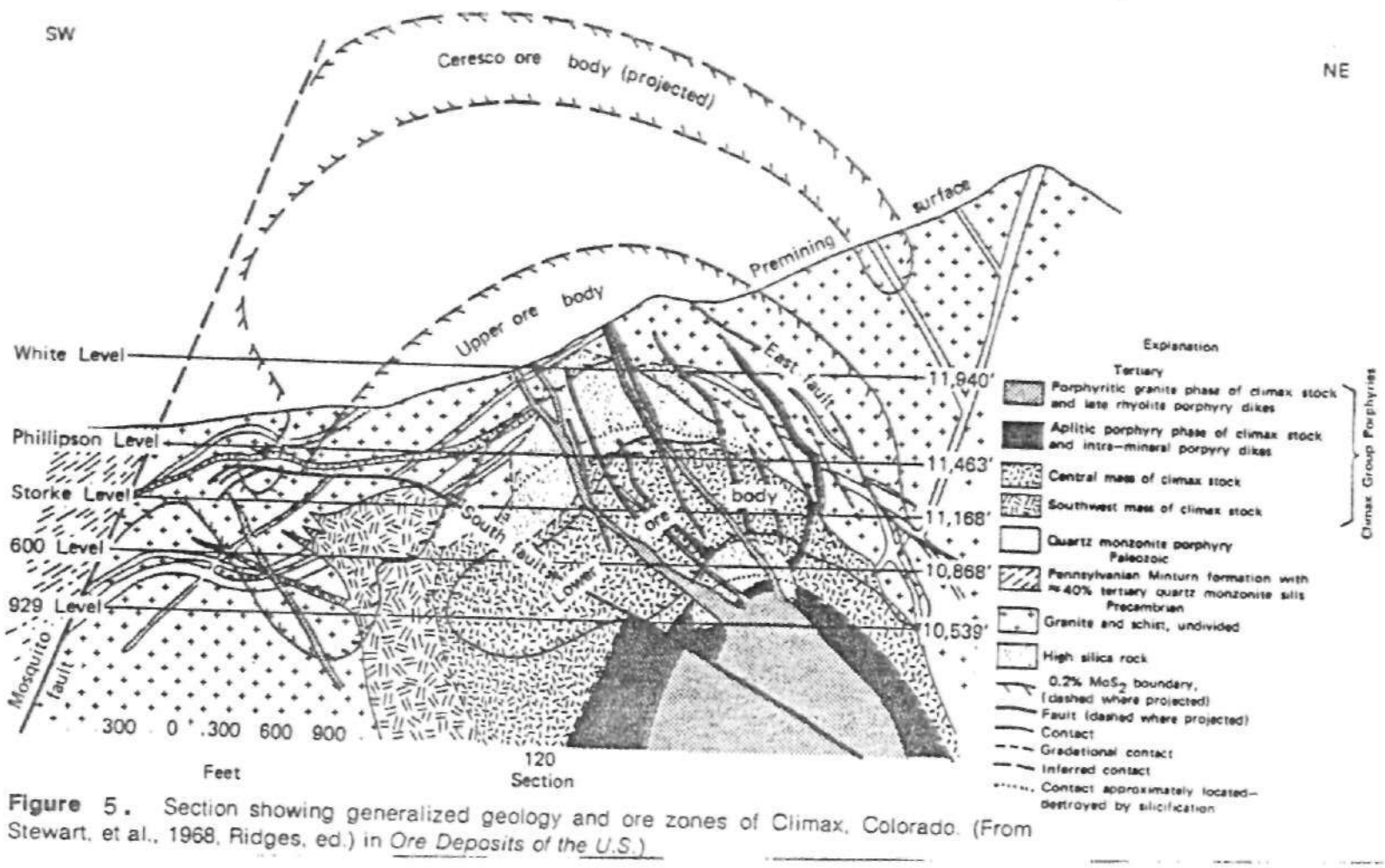


Figure 5. Section showing generalized geology and ore zones of Climax, Colorado. (From Stewart, et al., 1968, Ridges, ed.) in *Ore Deposits of the U.S.*)

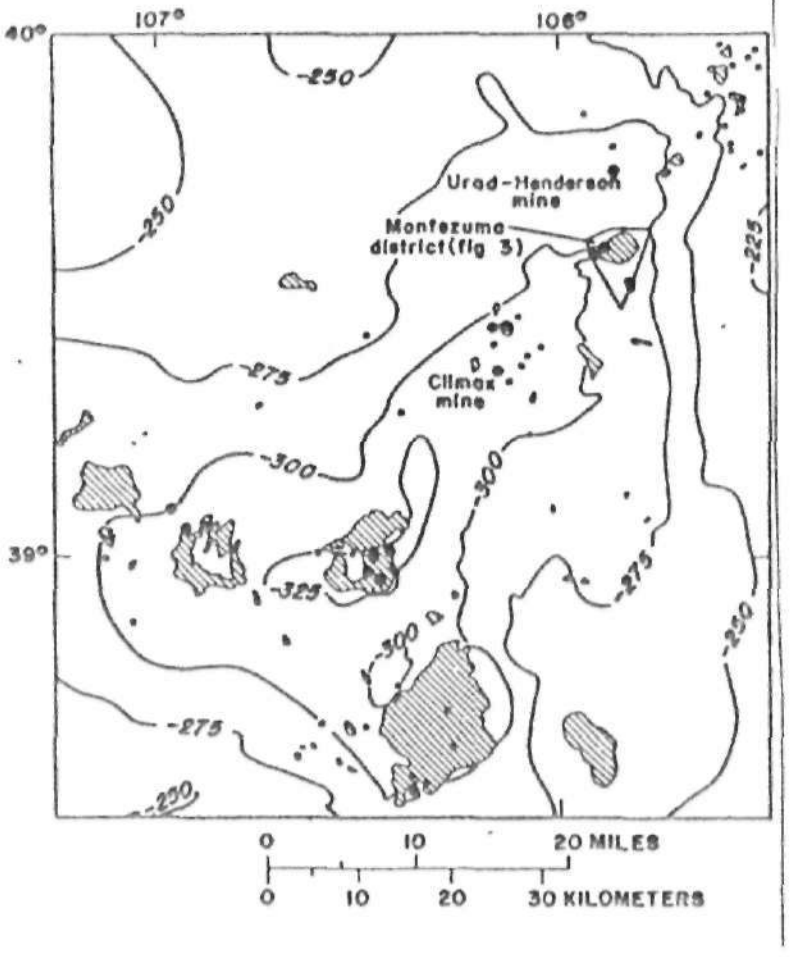


Figure 6. Map showing molybdenum deposits in relation to Tertiary stocks and gravity contours, Colorado. (From: G. J. Neuburg. et al., U.S. Geol. Surv. Circular 704.)

intermontane belt of north-central British Columbia (Monger and Church, 1977; Cann and Godwin, 1980). These interfingering flows and tuffs occur as roof pendants within a calc-alkaline granitic pluton and are intruded by porphyritic stocks and dykes (Gabrielse et al., 1977; Cann, 1976; Monger, 1977). The pendant rocks show zones of quartz-sericite, pyrite, propylitic and zeolitic alteration. Of these, only the quartz-sericite-pyrite zone is known to be directly related to mineralisation (Cann and Godwin, 1980), and the molybdenite occurs in limonite-filled fractures in the central and more intense part of the alteration. Other minerals are pyrite, chalcopyrite, and magnetite and hematite. The intrusive rocks surrounding the pendant and the cross-cutting dykes do not contain significant amounts of sulphides, and thus seem later than the main stage of mineralisation. Using K-Ar and Rb-Sr methods, Cann and Godwin (1980) dated the pendant volcanic rocks and the mineralisation at 204-190 Ma and 180 Ma, respectively. Thus the mineralisation represent a late phase of the cooling of the rocks.

2.5.2 The vein-type molybdenite mineralisation

McLeod et al. (1988) have reported the occurrence of Sn-W-Mo-bearing sheeted veins in the Mount Douglas Granite, southwestern New Brunswick. Orebodies of the polymetallic Sn-W-Mo type occur at Mount Pleasant (Ruitenberg, 1967,1972; Kooiman et al., 1986) and the Burnt Hill W deposit. According to McLeod et al. (1988), these sheeted veins contain extensive low-grade Sn-W-Mo systems. The

early phase of the granite, which is coarse to medium grained and seriate represents the slowly cooled carapace of the intrusion. The late phases, which are medium to fine grained, equigranular, or porphyritic, were accompanied by repeated and widespread fracturing of the carapace and injection of the mineralising fluids.

Molybdenite mineralisation associated with granitic pegmatite and quartzo-feldspathic veins has been reported from several localities. A typical example is the Preissac-Lacorne molybdenite deposit in the Albitibi area of Quebec, Canada (Norman, 1945; T. Mulja, pers. comm.). The host rock is peraluminous granite (calc-alkaline) and is itself mineralised with disseminated molybdenite. The concentration of Mo increases toward the margins of the intrusive body. Pegmatitic veins at this contact are particularly Mo-rich.

2.5.3 Other types of Mo mineralisation

The remaining types of Mo deposit are of minor importance and are economically important only where Mo is associated with highly valued minerals.

Konnerup-Madsen (1979) documented the existence of a Oxtamorphosed low-grade molybdenite deposit in Vest-Agder, southern Norway. It occurs in amphibolitic horizons in high-grade granitic gneiss in the southernmost part of the Precambrian shield, with pyrite, chalcopyrite and pyrrhotite.

Mo is usually recovered as a by-product in the Bedded Sandstone-type Uranium deposits. The Mo occurs in phases like jordisite (amorphous MoS_2) and ilsemanite ($Mo_3O_8.nH_2O$, also amorphous), and is probably derived from the leaching of enriched black shales (Jensen and Bateman, 1981). Examples of such deposits are found in Arizona, Utah, Colorado, New Mexico, Wyoming, South Dakota, and Texas.

CHAPTER THREE

REGIONAL GEOLOGY

3.1 INTRODUCTION

This chapter reviews the geologic and tectonic setting of the Younger Granites of Nigeria and describes the basement geology around the Kigom complex. The newer basalt that overlie parts of the basement and the Younger Granites but that are absent in the Kigom complex also are described, and their whole-rock geochemistry is discussed.

3.2 GEOLOGICAL SETTING

The Nigerian Basement complex consists of 4 main rock units (McCurry, 1976): the Older Metasediments consisting of quartzites, marble, basic and calcareous schists, biotite and hornblende gniesses (2500 ± 200 Ma); the Younger Metasediments consisting of phyllites, schists and interbedded volcanics (1000 ± 200 Ma); the Older Granites (650 ± 150 Ma) whose intrusion during the Pan-African Orogeny (750 ± 100 Ma) was preceded by deformation, metamorphism, migmitisation and reactivation of pre-existing rocks. Of these, the migmatised pre-existing rocks and the Older Granites are the basement to the Younger Granite complexes, the metasediments being absent from this part of the country.

3.3 TECTONIC SETTING

The Nigerian Younger Granite Complexes form part of a chain of intrusions along the 9th meridian, extending from the Niger Republic to the margin of the middle Benue Trough (Fig. 1). This chain is structurally controlled by the existing Pan-African trends within the 'Basement' and continues southward to South Africa along the zone of inferred initial crustal separation of the African and South American continents (Jacobson et al., 1958; Turner, 1976; Bowden and Jones, 1978). These intrusive complexes are thus located along a zone of pronounced continental uplift followed by mid-plate magmatism, suggesting that they represent a failed attempt to rupture the continent along this major lineament (Olade, 1980; Imeopkaria, 1985).

The intrusions are mostly preceded by ring fracturing followed by cauldron subsidence. The initial stage was marked by the outpouring of lavas and pyroclastic ejecta of rhyolitic composition, each complex, in most cases, representing a volcanic centre through which the ring dykes later intruded (van Breemen et al., 1977).

Magmatism began in the north of the Younger Granite Province in the early Triassic (about 200 Ma) and ended in the south in the Late Jurassic (about 140 Ma). For example, using whole-rock Rb-Sr isochron studies, van Breemen and Bowden (1973) and Bowden et al. (1976) confirmed a sequential age trend of 290-330 Ma for the southern Niger Complexes through 174 Ma for the

Liruei Complex in the north of the Younger Granite Province to a 154 Ma for the Sara-Fier complex in the south. This progressive younging southward is reflected in the overlapping of some of the centres of the ring complexes (e.g., the Ningi, Shokobo, Jos-Bukuru, and the Sara-Fier complexes), a phenomenon attributed to the migration of the magmatic foci due to a thermal anomaly in the mantle (Bowden, 1982).

The volcanic rocks and the later granitic intrusions were emplaced into a mixed assemblage of gneisses and migmatites that were deformed or redeformed during the Pan African orogeny (700 ± 150 Ma) and Older Granites that were emplaced and probably also deformed during the orogeny. The contact of these 'basement' rocks with outer units of the granitic plutons are steep, as the latter stand out with high relief.

The Kigom complex belongs to the central complexes of the Younger Granite Province. It has sharp contacts with the closest Younger Granite complex, Ganawuri complex (Fig. 1), but certainly belongs to a different centre.

3.4 GEOLOGICAL AND GEOCHEMICAL CHARACTERISTICS

Both the peralkaline and peraluminous granites occur in the Younger granite province. In many complexes (e.g., Tibchi and the Ririwai) both types of granite occur together. Generally, the northern complexes are more peralkaline than the southern complexes. Among the northern complexes, there is, however, no

definite pattern of occurrence; for example, whereas the peralkaline granites are located within the central part of the Ririwai and are in fact the last part of the complex to consolidate, they represent the marginal phases of the Tibchi complex. Complexes that consist entirely of peralkaline or peraluminous rocks do exist; for example, the Kigom complex is peralkaline, and the Jos-Bukuru complex is peraluminous.

In bulk composition, the complexes are granitic, but the peralkaline granites are poor in Al, Mg, and Ca compared with the peraluminous granites. The peralkaline granites typically have higher Fe_2O_3/FeO ratios and enrichments of trace elements such as Zr and Y (Olade, 1980; Imeokparia, 1985). These pattern of enrichments compare closely with those of typical A-type granites of Whalen et al. (1987). Mo, and W are generally not enriched, as only traces of these elements have been reported to be associated with the tin mineralisation. Data from the peraluminous Ganawuri complex, for example, show a whole-rock abundance of only 2-4 ppm (Table 3).

3.5 The Kigom Basement Rocks

The basement to the Kigom complex consists mainly of low-lying medium-grained migmatite and gniesses with N-S trending pegmatite and sulphide-rich dolerite dykes. The mafic bands of the migmatite consist mainly of biotite, with minor amounts of muscovite (Plate 2). Garnet is also a common occurrence in both

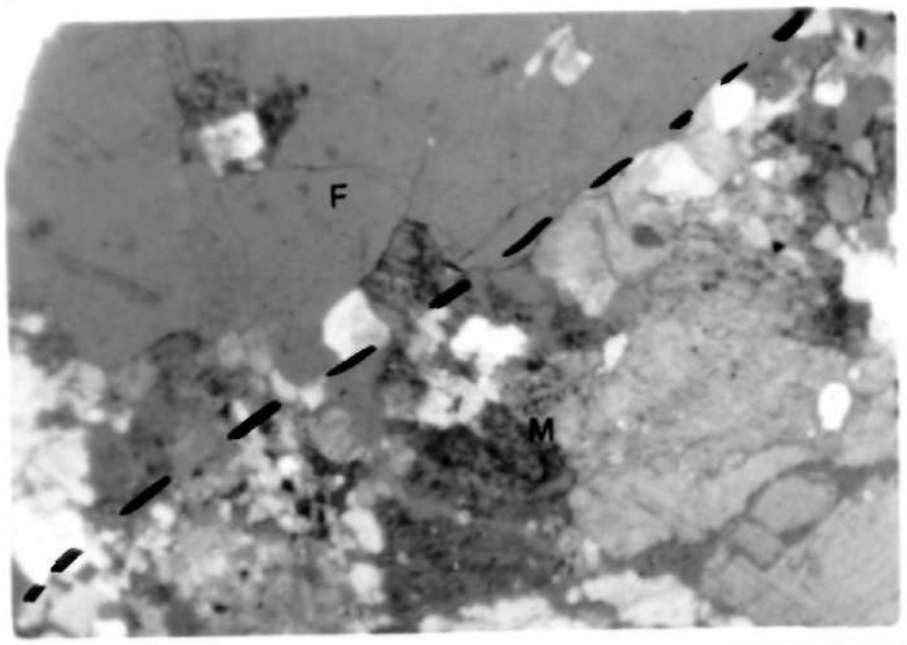
felsic and mafic bands. This composition is diagnostic of rocks that have undergone recrystallisation and "metamorphic differentiation" characteristic of migmatite genesis.

Whole-rock chemical data on the migmatite (Table 4) indicate that they are granodioritic in composition with normative Or+Ab+Q > 75% in which Ab>Q>Or, and normative An of 8.34%. Compared to the composition of the average continental crust, they are enriched in Al_2O_3, Na_2O, K_2O, Ba, Mo, Zr, Rb, Y, Sn, Li, F, and Th but are relatively depleted in TiO_2, CaO, MgO, MnO, P_2O_5, Sr, and V. There are abundances of 9.90%, 1.47%, 1.23%, and 0.19%, respectively, of normative Hy, Mt, Il, and Ap (Table 4).

Compared with the tin-mineralised and tin-barren pegmatite within migmatite from southwestern Nigeria (Matheis et al., 1982), the granitic pegmatite dykes in the basement of the study area show similar trends of enrichment in Ba, Sr, Rb, and Pb. Sn and Nb are, however, relatively depleted. Mo and W are not enriched beyond the normal crustal value (Table 5).

The sulphide-rich dolerite dyke is greenish and fine grained and consists of orthopyroxene, plagioclase, and biotite. The sulphides: pyrite and chalcopyrite, are poikilitic having inclusions of plagioclase. They also occur as inclusions in the pyroxenes (Plate 3) indicating that they are among the last of the minerals to crystallise. The whole-rock geochemistry shows that the dolerite is Fe- and Mg-rich having a total Fe content of 14.20% Fe_2O_3 and Mg content of 8.47% MgO but is silica undersaturated; 45% SiO_2 (Table 6). In bulk composition, it shows normative: Ab,

A



B

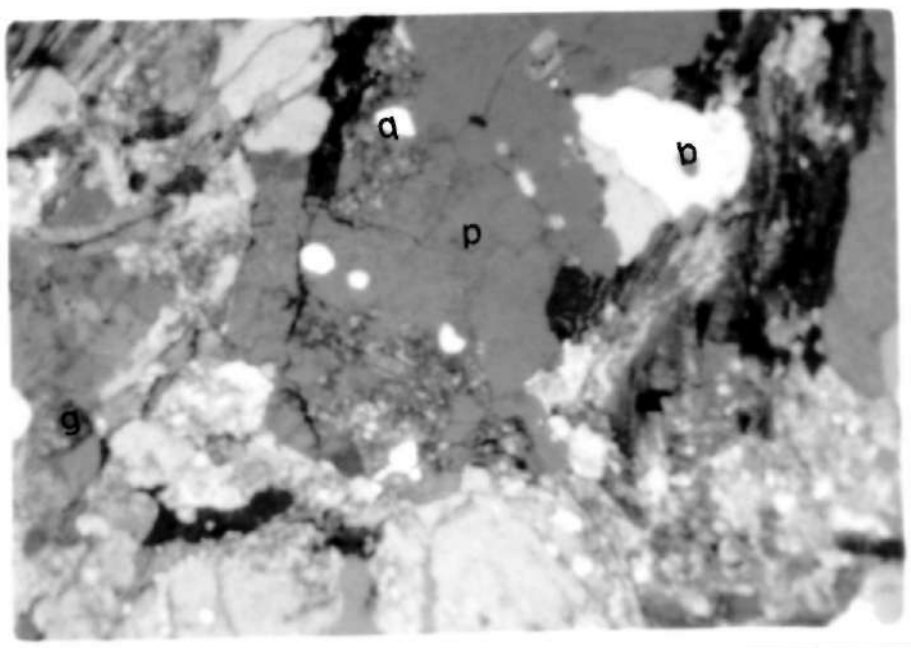


Plate 2. Photomicrograph of the basement migmatite showing:
A) the boundary between the felsic and the mafic bands and
B) the mafic bands. Note the occurrence of inclusions of quartz in perthite of the felsic band, and of biotite and garnet in the mafic band. Magnification x5. Cross polars

Table 3. Whole-rock geochemical analyses of some of the Nigerian Younger Granite complexes

		1	2	3	4	5
SiO_2	wt%	74.91	73.93	76.00	75.56	74.52
TiO_2		0.09	0.18	0.10	0.09	0.05
Al_2O_3		12.97	12.60	14.00	11.51	13.70
Fe_2O_3		0.64	0.35	0.70	2.30	1.23
FeO		0.93	2.17	0.90	0.80	0.29
MnO		0.02	0.02	0.01	0.05	0.01
MgO		0.07	<0.01	0.03	0.04	0.07
CaO		0.47	0.66	0.53	0.16	0.50
Na_2O		4.46	4.00	2.96	5.64	4.20
K_2O		4.43	4.50	4.50	4.01	4.05
P_2O_5		0.01	0.02	trace	trace	trace
Total		99.00	98.44	99.73	100.16	98.62
trace elements (ppm)						
Ba		34	170	57	21	80
Sr		4	39	7	3	3
Nb		130	71	160	634	150
Rb		1022	231	844	1160	800
Zr		90	248	207	1900	200
Y		290	99	268	425	211
Th		60	38	61	257	61
U		-	4	-	-	-
Sn		90	5	64	14	26
W		2500	2	674	-	133
Mo		-	4	-	-	-
Cu		-	125	-	-	-
Li		317	27	230	400	180
F		8200	2190	8520	10800	4860

1 ore-bearing biotite granite, Tibchi complex (Ike, 1979)
2 *hornblende-biotite granite, Ganawuri complex (this study)*
3 ore-bearing biotite granite, Afu complex (Imeokparia, 1982)
4 peralkaline granite, Buji complex (Imeokparia, 1985)
5 ore-bearing biotite granite, Liruei complex (Imeokparia, 1985).

Table 4. Average geochemical composition of the basement migmatite around the Kigom complex

Oxides wt%	1	2
SiO_2	66.53	61.9
TiO_2	0.86	0.8
Al_2O_3	15.30	15.6
Fe_2O_3	1.37	2.6
FeO	4.54	3.9
MnO	0.08	0.1
MgO	1.69	3.1
CaO	1.76	5.7
Na_2O	3.52	3.1
K_2O	3.20	2.9
P_2O_5	0.09	0.3
L.O.I	0.73	-
Total	99.77	99.28
normative composition (moles %)		
Q	23.79	14.88
Ab	32.25	28.26
Or	19.35	17.40
An	8.34	20.40
C	3.42	-
Mt	1.47	2.76
Il	1.23	0.11
Ap	0.19	0.64
Hy	9.90	10.50
trace elements (ppm)		
Ba	583.00	425.00
Nb	12.00	20.00
Zr	237.00	165.00
Y	36.00	33.00
Sr	265.00	375.00
Rb	170.00	90.00
Pb	20.00	13.00
Th	20.00	7.20
U	2.00	1.80
Cu	74.00	55.00
Zn	78.00	70.00
Mo	7.00	1.50
Sn	1.00	2.00
Be	0.80	2.80
Li	59.00	20.00
F	1200.00	625.00
As	2.00	1.80
Ag	0.10	0.07
V	87.00	135.00

1 basement migmatite around Kigom
2 average crustal abundance (Mason and Moore, 1982).

Table 5. Geochemical analyses of pegmatite in the basement migmatite of the study area compared with pegmatite elsewhere in Nigeria

Oxides wt%	1	2	3	4
SiO_2	68.19	76.10	76.20	76.20
TiO_2	0.02	0.05	0.03	0.04
Al_2O_3	17.68	15.30	14.10	14.30
Fe_2O_3	0.35	1.50	0.81	0.50
FeO	0.34	nd	nd	nd
MnO	<0.01	0.08	0.09	0.02
MgO	<0.01	0.35	0.19	0.18
CaO	0.94	0.34	0.36	0.44
Na_2O	3.13	0.48	5.00	3.70
K_2O	8.57	6.70	1.40	3.60
P_2O_5	0.02	0.12	0.14	0.14
L.O.I	0.63	1.80	1.10	0.77
Total	99.74	102.82	99.42	99.89
trace elements (ppm)				
Nb	1.00	107.00	74.00	46.00
Zr	12.00	158.00	203.00	183.00
Y	7.00	53.00	52.00	47.00
Sr	543.00	38.00	16.00	14.00
Rb	108.00	383.00	241.00	204.00
Pb	93.00	nd	nd	nd
Th	1.00	nd	nd	nd
U	1.00	nd	nd	nd
Cu	62.00	nd	nd	nd
Zn	91.00	nd	nd	nd
Mo	1.00	nd	nd	nd
Sn	1.00	40.00	22.00	5.00
Be	0.90	15.00	22.00	<5.00
Li	4.00	63.00	96.00	47.00
F	120.00	nd	nd	nd
As	5.00	nd	nd	nd
Ag	0.10	nd	nd	nd
V	13.00	nd	nd	nd

nd not determined

1 N-S trending pegmatite within the migmatite west of Kigom
2 Tin-mineralised Ijero tabular pegmatite from the basement of southwestern Nigeria (Mathies et al., 1982).
3 Ijero tin-productive massive pegmatite (Mathies et al., 1982).
4 Ijero tin-barren massive pegmatite (Mathies et al., 1982).

20.42%; An, 26.27%; Di, 22.43%; Ol, 17.46%; Or, 4.90%; Ne, 0.82%; Mt, 3.80%; Il, 3.18%; and Ap, 0.75%. This composition corresponds most closely to that of alkali basalt (Table 6). The dolerites also plot on the K_2O+Na_2O vs SiO_2 diagram in the region of alkali basalt (Fig. 7) The dolerites are, however, enriched in Y, Zn, Cu, W, and Nb. Mo is not enriched.

3.6 THE NEWER BASALT

The Cenozoic "newer basalt", so designated to distinguish them from the earlier mostly weathered "older basalt" (Plate 4a), are greenish in colour and fine grained and porphyritic, having phenocrysts of plagioclase set in a groundmass of olivine, pyroxene and plagioclase (Plate 4b). Magnetite is present in minor amounts. None of the minerals show preferred orientation as would be expected if flowage had accompanied crystallisation. The olivine crystals are rimmed by orthopyroxene, indicating a reaction relationship between olivine and magma.

In bulk composition, the basalt are silica undersaturated (Table 6). They are relatively enriched in FeO, K_2O, Na_2O, and MgO compared with the alkali basalt composition of Macdonald (1968) (Table 6). The newer basalt also show relative enrichments in trace elements like Sr, Y, Nb, Rb, Li and Zr, but have low values of Sn, Ba, F, and Li compared with those of the dolerite dykes (Table 5). Like in the dolerites, Mo is not enriched.

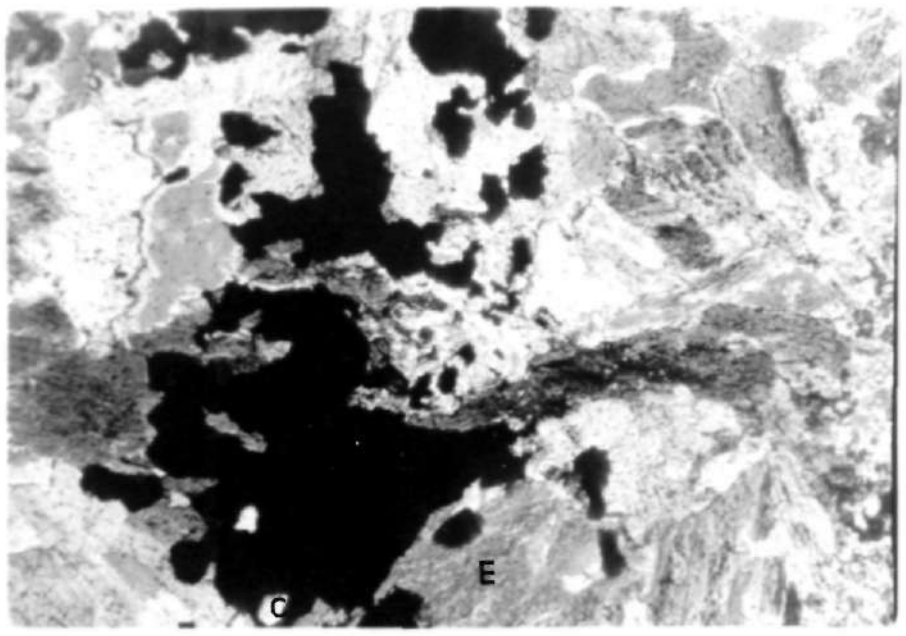


Plate 3. Photomicrograph of a sample of the dolerite dyke in the basement migmatite of the study area. The isotropic minerals are pyrite and chalcopyrite. Note the inclusion of plagioclase in the pyrite crystals and the pyrite crystals in pyroxene. Magnification X10.

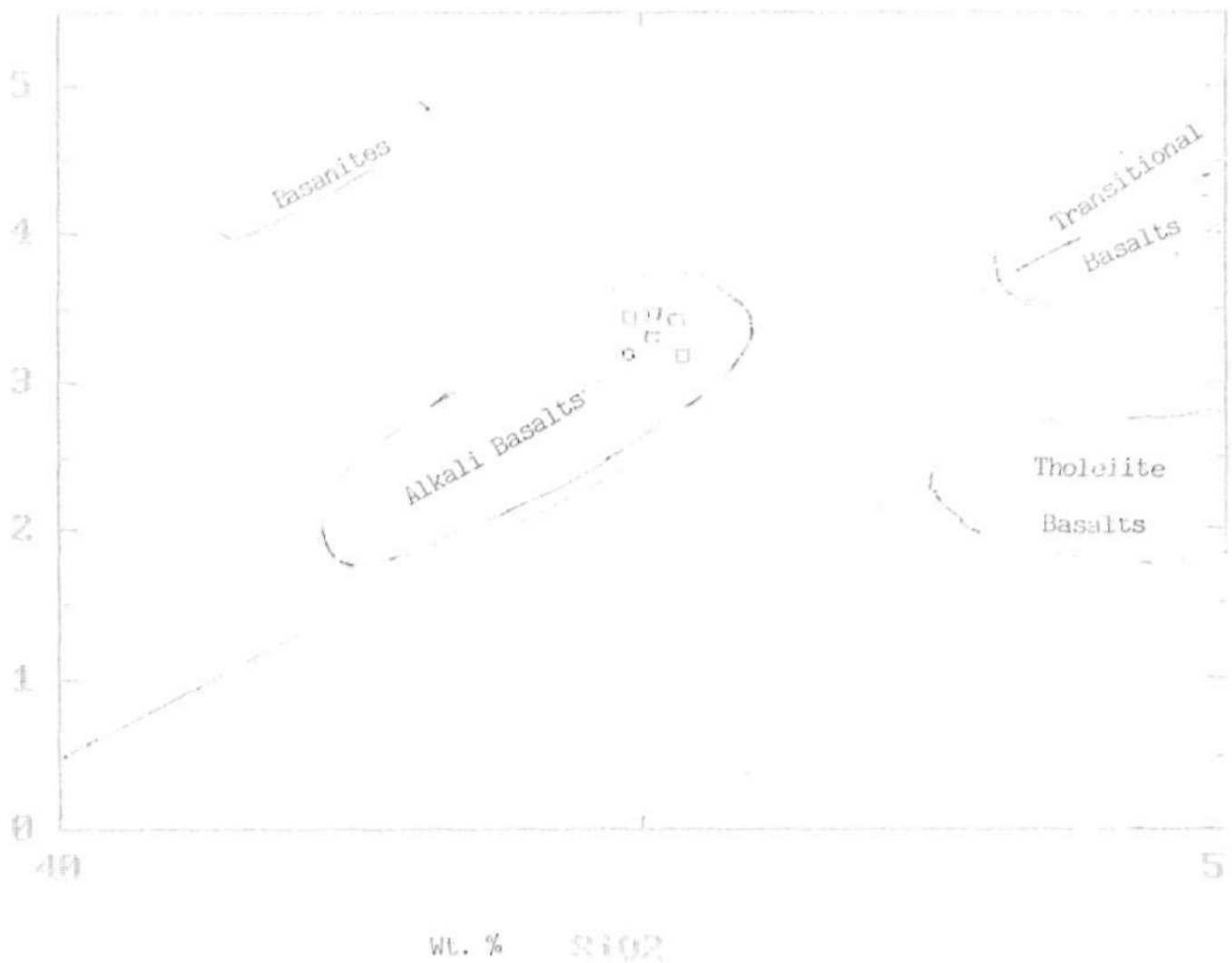


Figure 7. $Na_2O + K_2O$ versus SiO_2 plot for the dolerite dyke. The dolerite plot in the region of alkali basalt of Staudigel et al., 1984.

The basalt contains normative nepheline, albite, diopside, and olivine of 7.08, 20.83, 17.15, and 22.83 moles %, respectively, (Table 6). The basalt thus plots on the Ne-Fo-Di-Ab subtetrahedron of the normative basalt tetrahedron of Yoder and Tilley (1962). The presence of more than 5% normative nepheline (Hess, 1989), indicates that the basalt is basanitic in composition. Normative anorthite, orthoclase, magnetite, ilmenite and apatite are also present with abundances of 17.68%, 8.9%, 1.2%, 1.18%, respectively.



Plate 4a. Photograph of part of the weathered older basalt east of the Kigom complex being excavated for alluvial tin.

A



B

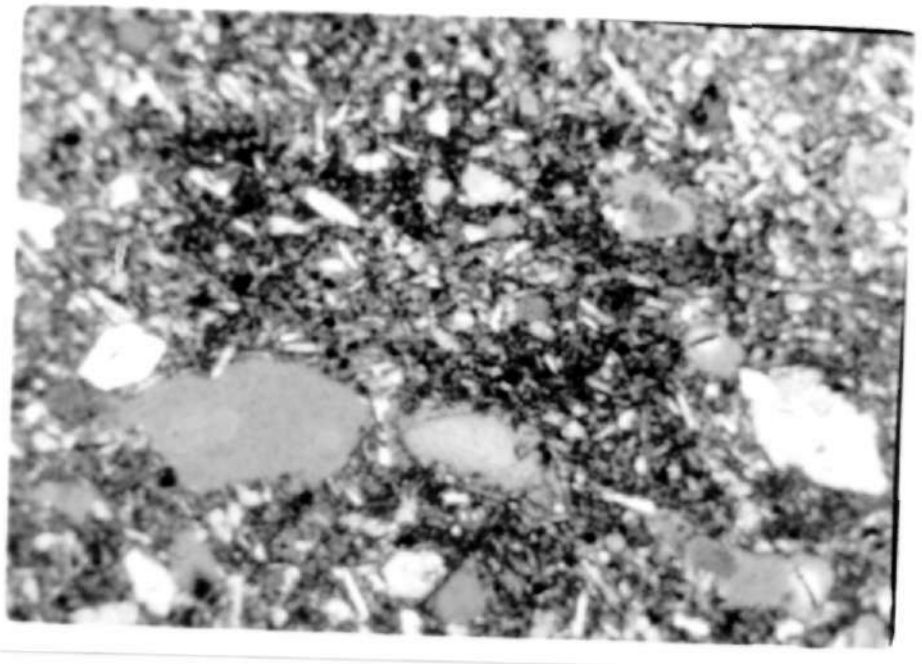


Plate 4b A) Basalt crater typical of the newer basalt in the study area. B) Photomicrograph of the newer basalt. Note the porphyritic texture of the rock and the olivine-pyroxene relationship. Magnification x5.

Table 6. Geochemical analyses of dolerite dykes in the basement migmatite and of the newer basalt of the study area compared with compositions of an alkaline basalt of Macdonald, 1968.

	dolerite dyke	alkali basalt	newer basalt
SiO_2 wt%	45.36	45.4	47.37
TiO_2	2.23	3.0	2.23
Al_2O_3	14.18	14.7	14.22
Fe_2O_3	3.68	4.41	1.20
FeO	10.63	9.2	10.48
MnO	0.25	-	0.16
MgO	8.47	7.8	9.74
CaO	11.14	0.5	8.71
Na_2O	2.37	3.0	3.67
K_2O	0.81	1.0	1.52
P_2O_5	0.34	-	0.57
L.O.I	0.70	-	0.07
Total	99.47	99.01	100.01
Normative compositions (moles %)			
Q	-	-	-
Ab	20.42	20.24	20.83
An	26.27	24.20	17.66
Or	4.90	6.03	8.89
Di	22.43	23.20	17.15
Ol	17.46	13.32	22.83
Mt	3.80	4.38	1.30
Il	3.18	4.27	3.08
Ap	0.73	-	1.18
Ne	0.82	4.38	7.08
Trace elements (ppm)			
Nb	25.00	nd	53.00
Zr	135.00	nd	207.00
Y	26.00	nd	47.00
Sr	414.00	nd	689.00
Ba	662.00	nd	492.00
Rb	33.00	nd	41.00
Pb	20.00	nd	44.00
Th	7.00	nd	7.00
U	2.00	nd	5.00
Sn	41.00	nd	1.00
Cu	27.00	nd	56.00
Zn	209.00	nd	92.00
W	8.00	nd	7.00
Be	1.80	nd	0.70
As	6.00	nd	2.00
Ag	0.20	nd	0.10
Li	15.00	nd	4.00
F	1300.00	nd	500.00
Mo	1.00	nd	2.00

nd not determined

CHAPTER FOUR

FIELD OCCURRENCE AND PETROGRAPHY

4.1 INTRODUCTION

This chapter describes the outcrop pattern, mode of occurrence, and petrography of the rocks of the Kigom Complex and the associated dykes. For these purposes, the alkali amphiboles associated with the Kigom are referred to as arfvedsonite and riebeckite. The chemical compositions of the amphiboles will be discussed in chapter six.

4.2 FIELD OCCURRENCE

Geographically, the Kigom (Fig. 8) stands prominently as a cupola. It's contacts are near-vertical with the basement to the north, south and west, and with hornblende granites of the Ganawuri Complex to the southeast. Unlike the other complexes in the Province (Jacobson et al., 1958), the Kigom complex is not associated with the early volcanic rocks and does not show enclaves of basement within it, suggesting that the emplacement of the Complex was not preceded by ring fracturing and cauldron subsidence. Thus the complex is exposed in a mass of rock that is structurally and petrologically distinct.

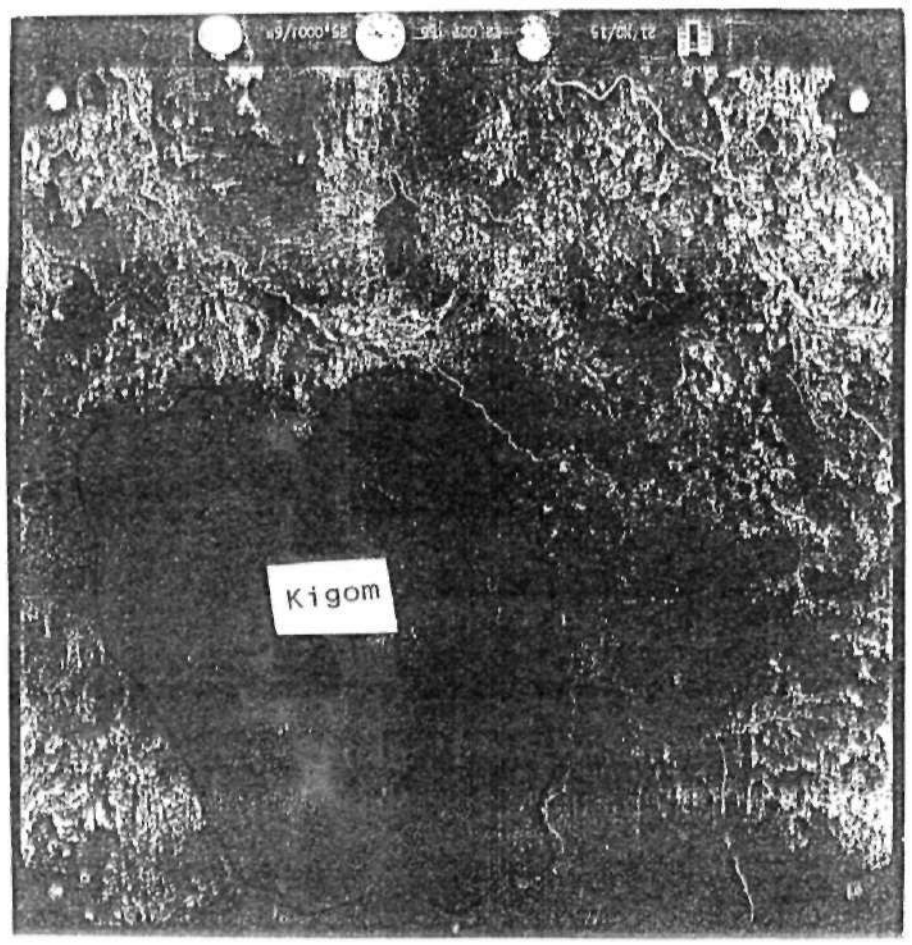


Figure 8. Aerial photo of the Kigom and the surrounding rocks.

The Kigom Complex comprises of four categories of granitic rocks; 1) the aegirine microgranite to the west, 2) the arfvedsonite granite to the northwest, 3) the riebeckite granite to the east, northeast and south, and 4) riebeckite-aegirine granite in the central sector (Fig. 9, see appendix).

The aegirine microgranites occupy the lowest altitudes and have a gradational lithological contact with the riebeckite-aegirine granites and the arfvedsonite granites, and a steep intrusive contact with the basement migmatite to the west. The aegirine microgranites commonly have pods of fayalite and quartz that vary from 3 to 15 cm across; the pods increasing in size towards the contact with the basement in the direction of slower cooling rate and decreasing temperature of crystallisation. The outcrops of the riebeckite-aegirine granite and those of the arfvedsonite granites are mostly in the form of ridges, with occasional peaks. Rhyolitic dykes up to 30 cm in width occupy NW-SE-trending fractures at the topmost part of the outcrops. In addition to these dykes, the arfvedsonite granites also host pegmatite dykes occupying NW-SE-trending fractures. The eastern part of the riebeckite granites is relatively low-lying, whereas the northern part is in the form of ridges with individual peaks. Molybdenite mineralisation is associated exclusively with the riebeckite granite unit. A felsic dyke was also encountered within one of the adit of the ore zone.

The rhyolitic dykes consist of several parts; a) the core of rhyolite consisting only of white bands of the host rock and

green bands of rhyolite near the contact of the dyke with the host rock, and c) the chilled margin of the dyke (Plate 5).

The interlamination at the contact is interpreted to result from shearing of the host rocks at the initiation of intrusion of the dyke, indicating that the fractures opened more than once during the intrusion of the dyke.

Associated with these granites are fractures trending NW-SE (oldest), N-S, and NE-SW (youngest). The most prominent of these are the NW-SE and the N-S fractures (Fig. 10). Of these, only the former is mineralised serving as hosts to the pegmatites and rhyolites. The fractures reflect a regional control, as they tend to coincide with those of the surrounding basement (Fig. 2).

4.3 PETROGRAPHY

Macroscopic and microscopic descriptions of the granites of the Kigom Complex and the associated dykes will be given in turn.

4.3.1 The aegirine microgranite

The aegirine microgranite is leucocratic, fine grained and porphyritic. The rock has distinctive pods of fayalite and quartz. The phenocrysts are crystals of quartz, and perthite set in a groundmass of quartz, perthite, and aegirine.

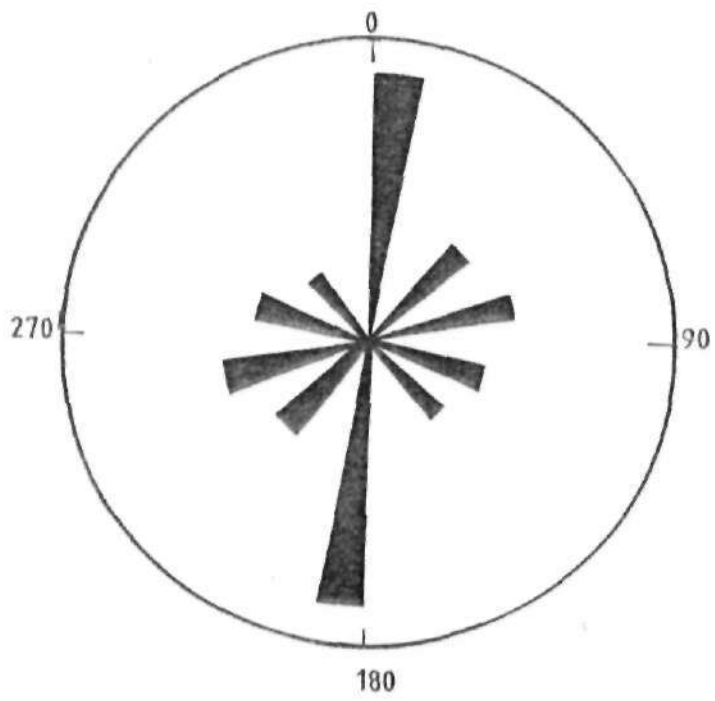


Figure 10. Rose diagram of the joints on the Kigom complex

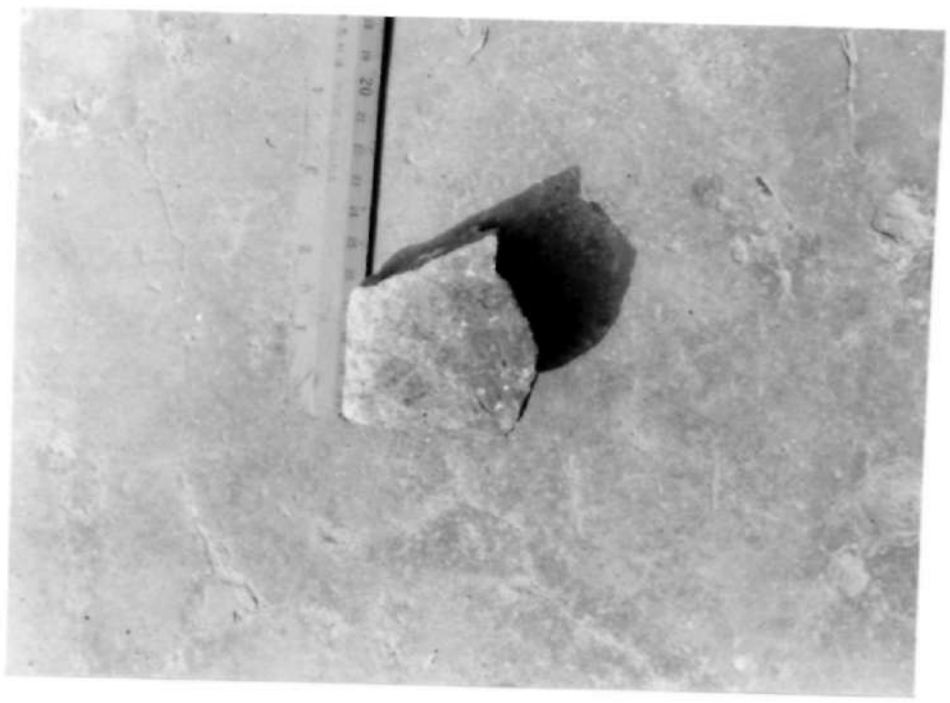


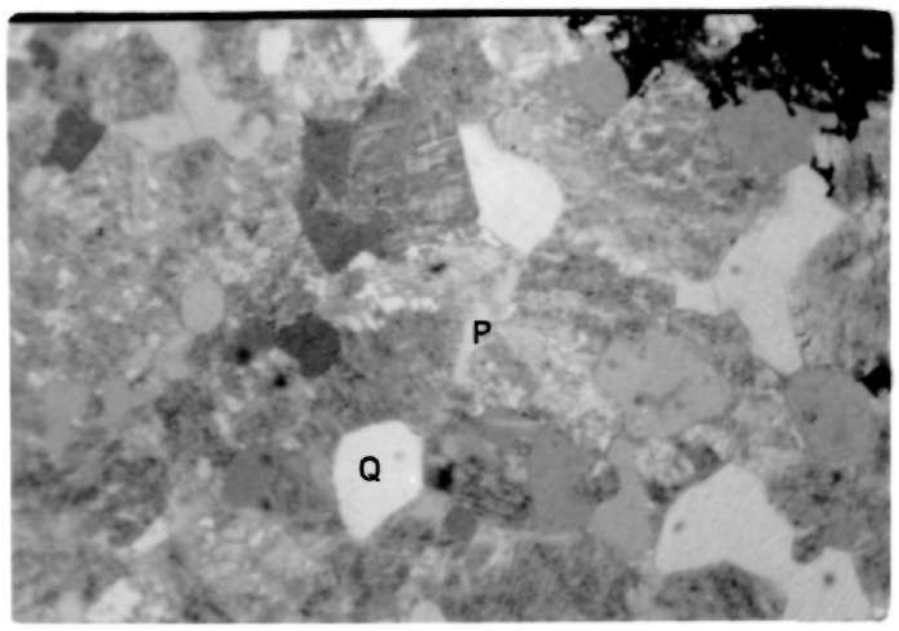
Plate 5. A photograph of a sample of the rhyolite dyke.

The essential minerals are quartz, perthite and aegirine, whereas the minor and accessory minerals consist of fluorite, zircon and hematite. Quartz (20% by volume) also is present in two generations, as euhedral and poikilitic crystals containing inclusions of perthite, and as small subhedral crystals (Plate 6) of hydrothermal origin. Perthite (60% by volume) present as small euhedral crystals with intergrowth of albite and orthoclase, are the most abundant mineral (Plate 6). The aegirine forms fine prismatic crystals with blunt terminations against quartz and perthite. The crystals are in many cases partly altered along cleavage planes to hematite (Plate 6). Hematite also is present as small crystals within the rock.

The pods in the rock consists essentially of euhedral crystals of quartz and fayalite. The fayalite is altered along cracks to hematite (Plate 7). These minerals have thin chilled margins with the microgranite, suggesting that crystallisation began with them. The loss of heat and volatiles to the surrounding basement migmatite combined with increased activity of $f(O_2)$ led to the change in crystallisation path such that feldspars and aegirine also could crystallise. If so, the microgranites then constitute the first of the intruding magma to crystallise, and this was under a more reducing environment.

The hematitisation of aegirine and the crystallisation of hydrothermal quartz were related to later hydrothermal fluid which metasomatically altered the rocks of the Kigom complex.

A



B

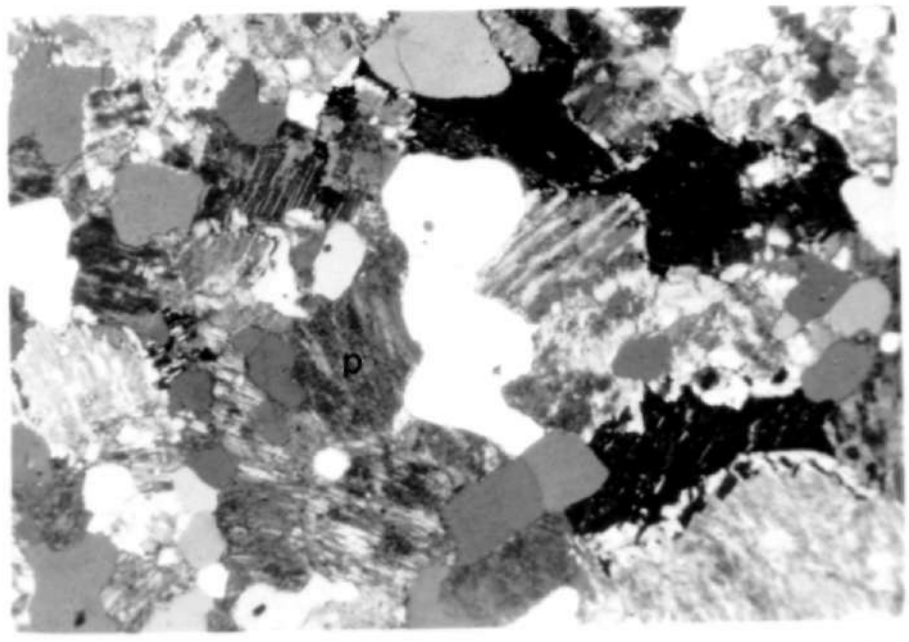
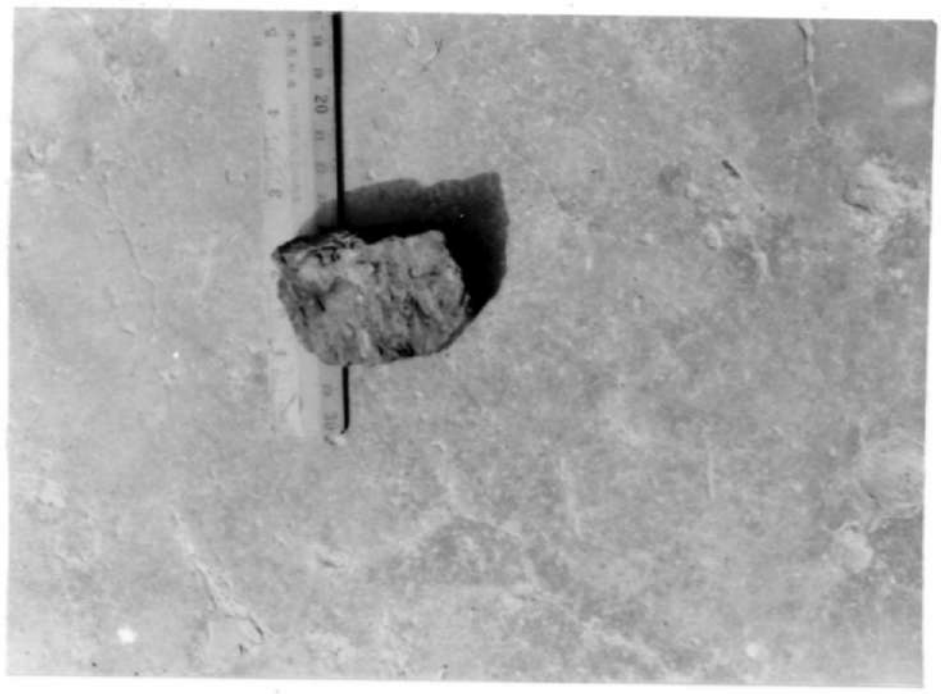


Plate 6. Photomicrograph of the aegirine microgranite showing: A) perthite (p) and quartz (q) crystals, magnification x5, B) microcline (p) and aegirine (a), magnification x10.

A



B



Plate 7. A) Photograph of the fayalite crystal

B) Photomicrograph of the fayalite crystals, magnification x5.

4.3.2 The arfvedsonite granite

The arfvedsonite granite is leucocratic, coarse grained and porphyritic (Plate 8). The phenocrysts are crystals of perthite and arfvedsonite set in a groundmass of quartz, and, perthite with minor amounts of zircon, fluorite, thorite, and astrophyllite.

Quartz (20% by volume) is present in two generations; large euhedral crystals, occasionally involved in graphic intergrowths with perthite, and as small subhedral crystals in the groundmass and as inclusions in arfvedsonite and perthite (Plate 9). Perthite (60%, by volume) shows regular intergrowths of albite and orthoclase. The volume of albite is generally small, the perthite being almost entirely orthoclase (Plate 9). The arfvedsonite (15%, by volume) occur as prismatic crystals with blunt terminations against quartz and perthite. The arfvedsonite crystals commonly have inclusions of primary quartz; along their contact there is deposition of astrophyllite (Plate 10). Astrophyllite also occurs along cleavage planes of arfvedsonite and perthite.

Zircon is common as small colourless prismatic crystals among the feldspars. The characteristic tetragonal shape of thorite clearly distinguishes this mineral from zircon with which it shares similar pleochroic colours. Thorite crystals show darker colours in plane-polarised light and have relatively low relief compared to that of zircon. Thorite crystals are commonly associated with the second-generation quartz and are, like zircon, secondary minerals whose crystallisation is related to the hydrothermal fluids or at

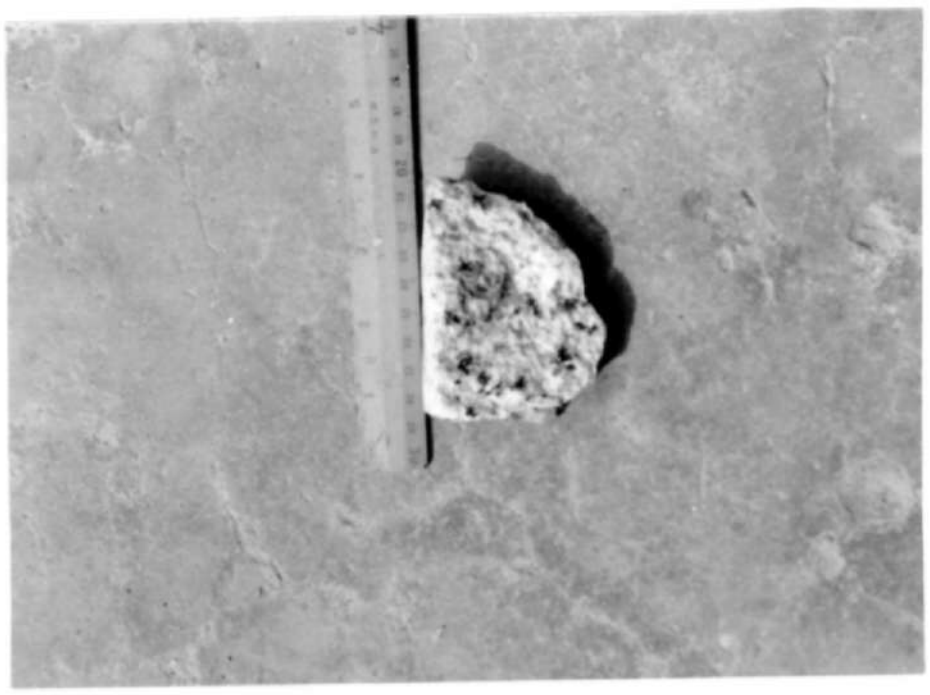
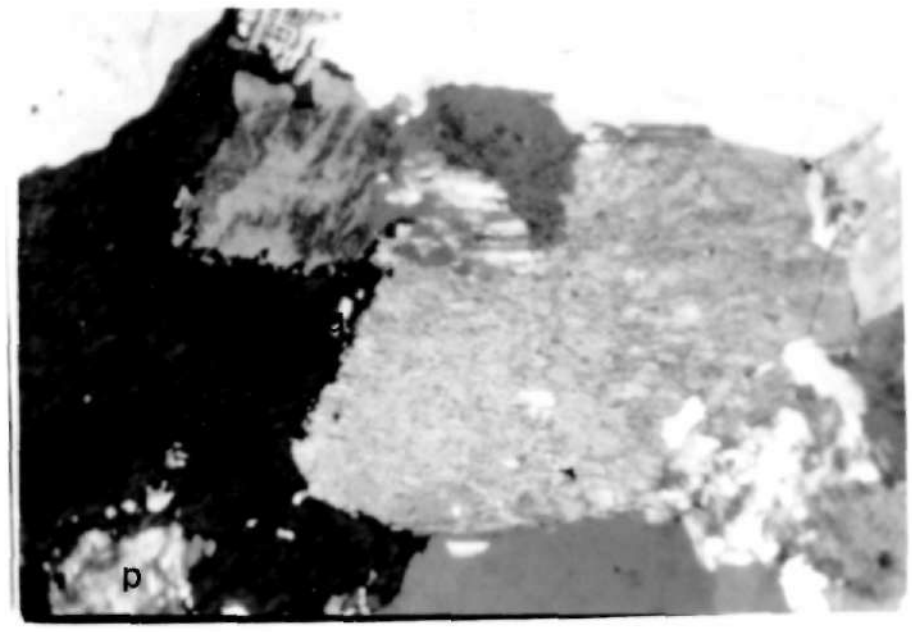


Plate 8. Photograph of a sample of the arfvedsonite granite. Note the porphyritic coarse-grained texture of the rock.

A



B

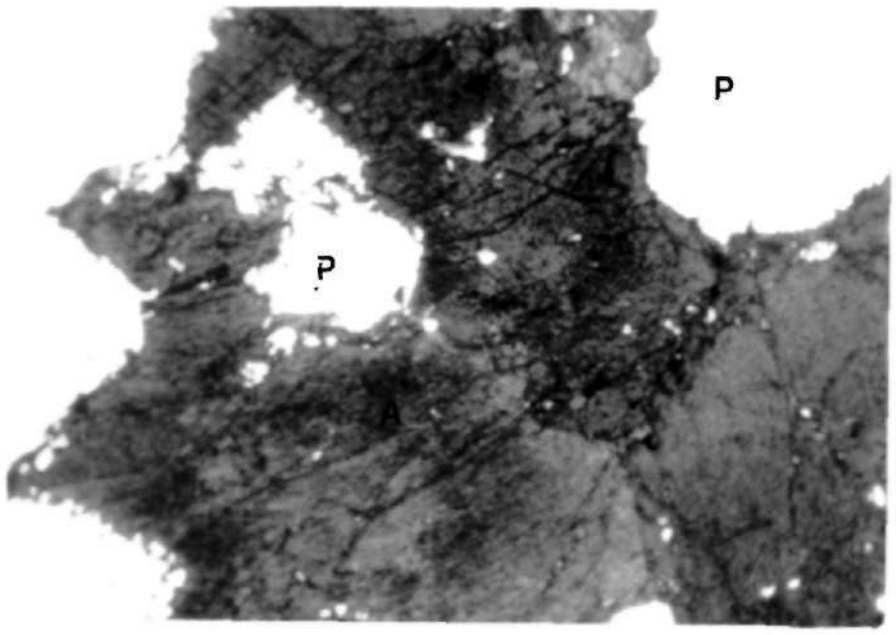
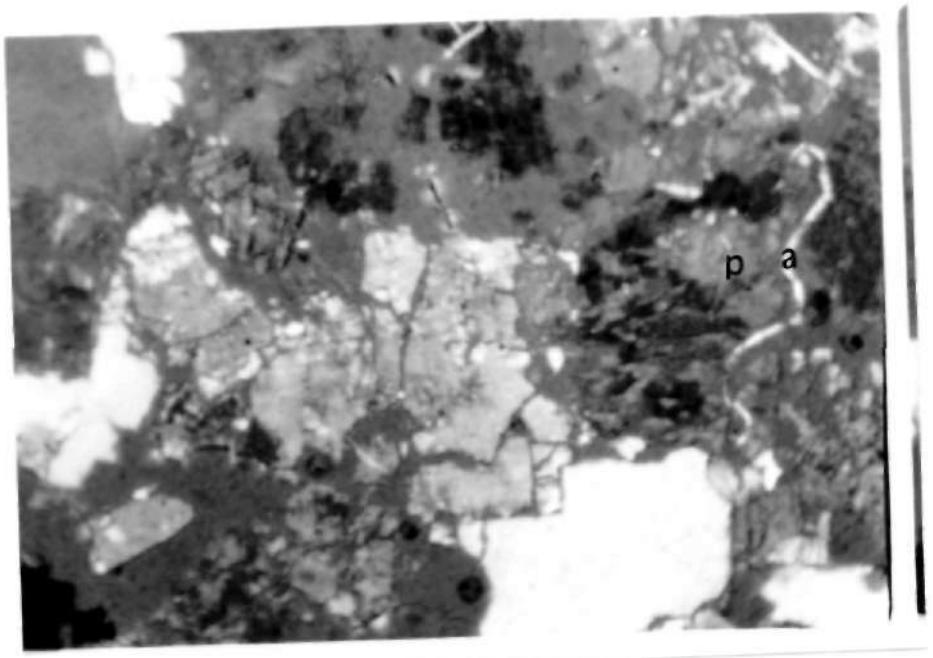


Plate 9. Photomicrograph of the arfvedsonite granite showing: A) the inclusion of quartz (q) and perthite (p) in arfvedsonite crystals, B) the modified texture of perthites (p) close to the arfvedsonites. Magnification, x5. *Cross polars*



AHMADU BELLO UNIVERSITY
KASHIM IBRAHIM LIBRARY

Plate 10. Photomicrograph of the arfvedsonite granite showing fine micaceous looking astrophyllite (a) in perthite (p). Magnification, x5. Cross polars

least the late stage-magmatic crystallisation.

4.3.3 The riebeckite granite

The riebeckite granite is leucocratic, medium grained and porphyritic. The phenocrysts are quartz, white perthite and riebeckite set in a groundmass consisting of fine-grained quartz, and orthoclase perthite and accessory minerals which include fluorite, zircon, astrophyllite, and, occasionally, biotite and magnetite. The riebeckite is distributed in dark-coloured irregularly shaped patches or aggregates interstitial to the other leucocratic minerals. The absence of discrete grains of albite indicates that the rock is hypersolvus.

In the perthite crystals (55% by volume), the albitic domains are polysynthetically twinned whereas the orthoclase is cloudy due to turbidity (Plate 11) resulting from metasomatic alteration of an alkali-rich fluid into the system. Close to the riebeckite, the perthite is enriched in K-feldspar. This modification may reflect the local removal of Na, consumed in the late growth of sodic amphibole. If so, the close association of texturally modified perthite to riebeckite suggests that the ion exchange was most active in contact regions between these two minerals. Quartz crystals (25% by volume) belong to two generations; an earlier nonpoikilitic subhedral crystals that are usually smaller in size(0.5 to 1 mm) than the latter poikilitic euhedral crystals (2 to 4 mm, in size), which have inclusions of

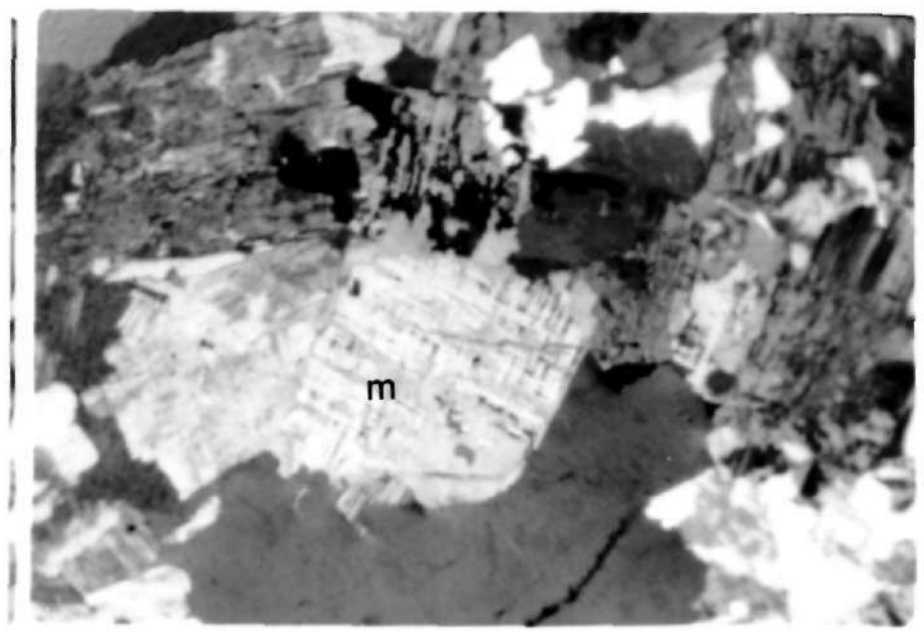


Plate 11. Photomicrograph of the riebeckite granite showing microcline (m). Magnification, x5. Cross polars

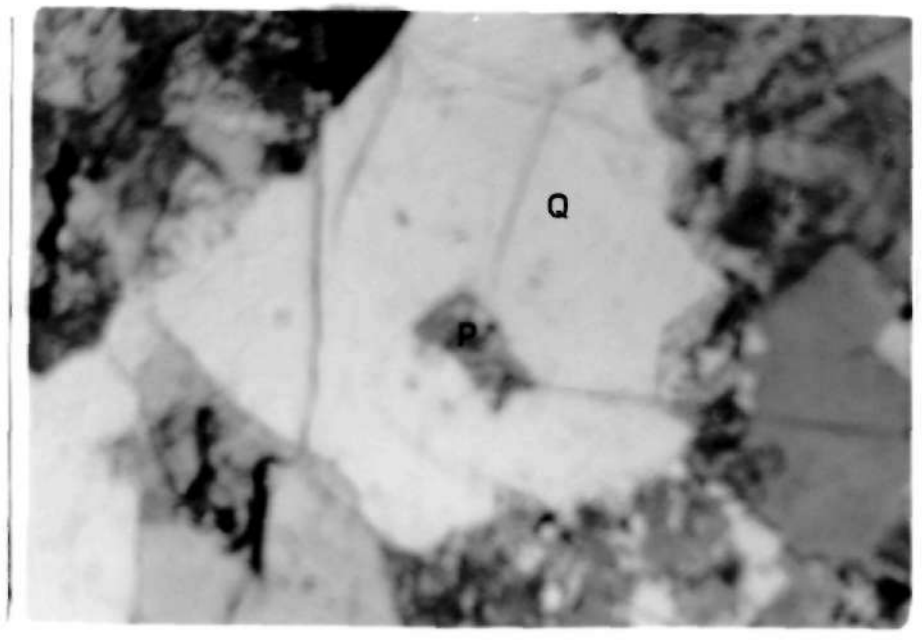


Plate 12. Photomicrograph of parts of the riebeckite granite showing inclusions of perthite (p) in the later quartz (q). Magnification, x10. Cross polars

the earlier quartz, and of riebeckite, perthite and zircon (Plate 12). The included perthites are only marginally modified, indicating that the growth of second qaurtz came before the modification of the perthite near the riebeckite. Whereas the first generation quartz is attributed to crystallisation from the magma, the second is related to crystallisation from a hydrothermal fluid. Such quartz, probably, is one of the latest minerals to crystallise. Riebeckite (15% by volume) is present as large poikilitic crystals (Plate 13) that enclose some crystals of perthite. Along the contact with the oikocrysts, the pleochroism of the amphibole is modified. This is considered a result of later reaction of the hydrothermal fluid with the sodic amphibole. This texture is typical of amphiboles formed at late-stage magmatic or hydrothermal (subsolidus) stage. Ike et al. (1985) have documented similar textures in amphiboles of the Tibchi Complex to the north of Kigom and have related them to deuteric adjustments. In some of the samples, the riebeckite crystals are modified along cleavage planes and at margins to aegirine and biotite, respectively. This may result from an oxidation reaction, also attributable to a circulating hydrothermal fluid. Euhedral crystals of zircon and fluorite (Plate 14) are common, whereas fine crystals of astrophyllite are presentin the rock as late minerals deposited along cleavages in perthite and riebeckite. Small grains of magnetite are among the accessories.

At the ore zone, at the contact of the riebeckite granite with the basement migmatite, the riebeckite granites show the same

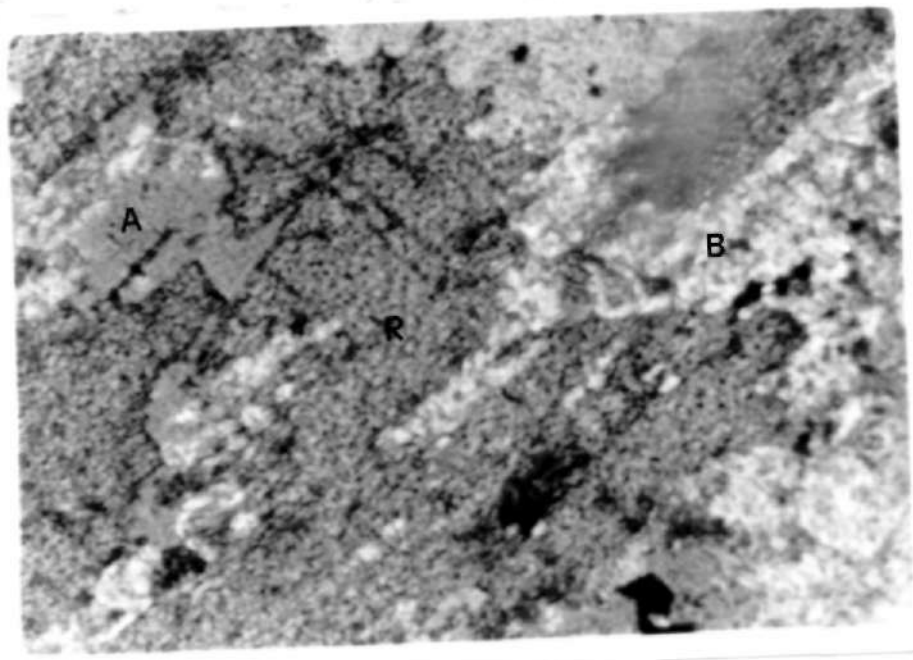


Plate 13. Photomicrograph of riebeckite (R) crystals in riebeckite granite. Note the alteration into biotite (b) and aegirine (a). Magnification, x5. Cross polars

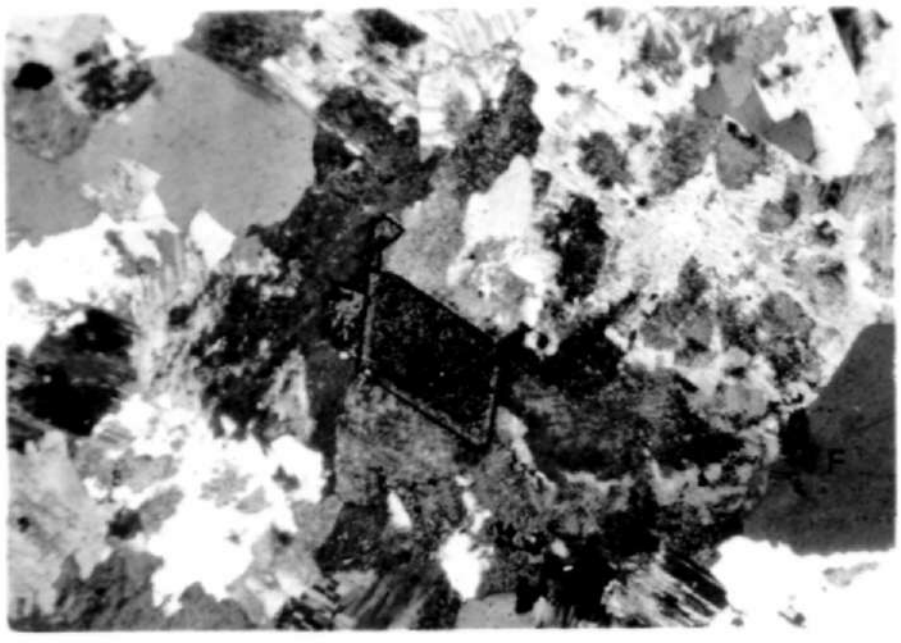


Plate 14. Photomicrograph of riebeckite granite showing euhedral crystals of zircon (z) and flourite (F, right corner). Magnification, x5. Cross polars

petrographic characteristics, except for the presence of molybdenite as one of the essential minerals. The molybdenite is present as irregular flakes with finger-like protrusions into the adjacent perthitic feldspar which is being replaced. Some of the pethites that could not be completely replaced occur in the molybdenite as inclusions. The molybdenite crystals vary from 3 to 15 mm across and may attain 20 mm in some samples.

4.3.4 The riebeckite-aegirine-biotite granite

The riebeckite-aegirine-biotite granite is leucocratic, medium to coarse grained and porphyritic. The phenocrysts of quartz and perthite are set in a groundmass of quartz, perthite, aegirine, biotite, and riebeckite, with fluorite, zircon, and astrophyllite occurring as accessory minerals. The mafic minerals are mainly fine grained and oriented in the groundmass. This is commonly the case at the contact with the riebeckite granites, where needles of aegirine are most abundant. Toward the centre of the Kigom, however, biotite becomes common, and aegirine less common.

Like the riebeckite granite, quartz crystals (20% by volume) in the riebeckite-aegirine-biotite granite grew in two generations; as large euhedral crystals having straight grain boundaries with perthite, and as small subhedral crystals occurring as inclusions in perthite, riebeckite and aegirine. Perthite crystals (60% by volume of the rock) show characteristic twinned

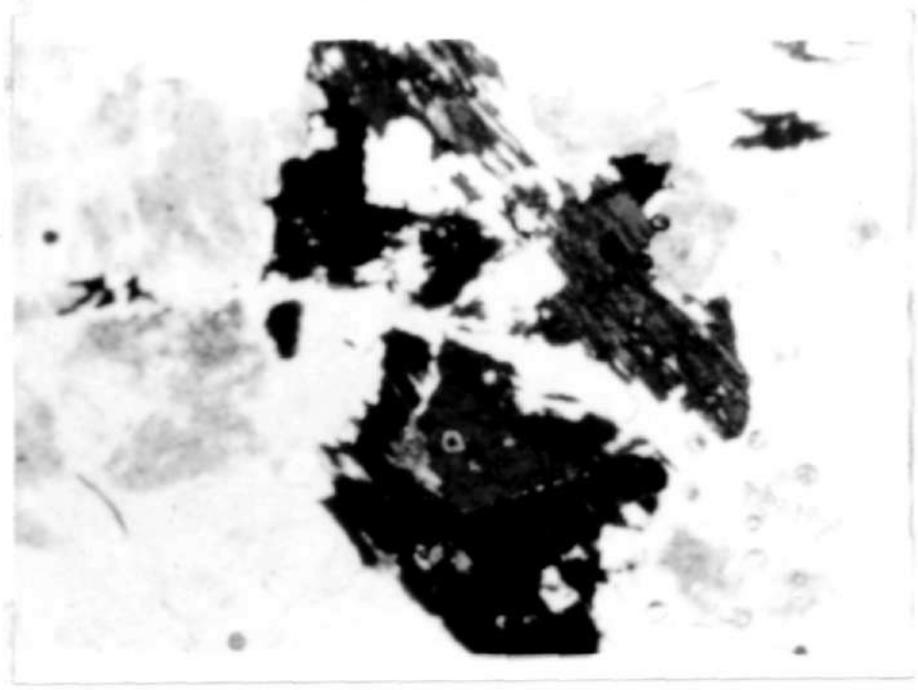
albite surrounding and veining an orthoclase-rich core. Fine crystals of astrophyllite have crystallised along cleavage planes of some of the perthite crystals. The riebeckite crystals (15% by volume), are poikilitic and contains quartz, zircon, and perthite. The pleochroism of the amphibole is modified along the contact with the oikocrysts. Nearly all the crystals of riebeckite have been converted to aegirine, and locally to biotite, along their margins and cleavage planes (Plate 15). Unlike the alteration in the riebeckite granites; the aegirine, here considered to be secondary, is so prominent to constitute an essential mineral in most parts of the rock. In the centre of the granite, however, biotite, also secondary, becomes more common relative to aegirine. These alteration characteristics are related to a alkali-rich hydrothermal fluid in which the fluid had long reaction time with the subsolidus minerals resulting in a K^{+}-for-Na^{+} ion exchange and an oxidation to form magnetite and aegirine.

Euhedral crystals of fluorite are in contact with the second-generation quartz. Thorites, identified by their tetragonal shape, high relief, dark brown colour and marked polarisation colours, are present as a group of radiating needles.

4.3.5 The Pegmatite Dyke

The pegmatite is leucocratic, medium grained and evenly textured. The essential minerals are quartz and orthoclase perthite with arfvedsonite present in minor amounts. Quartz crystals (26%,

A



B

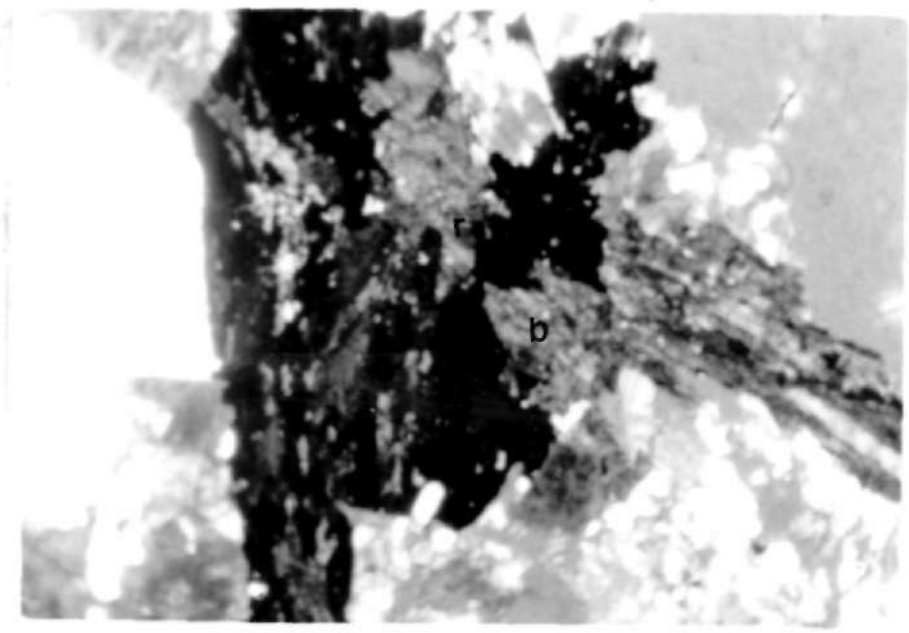
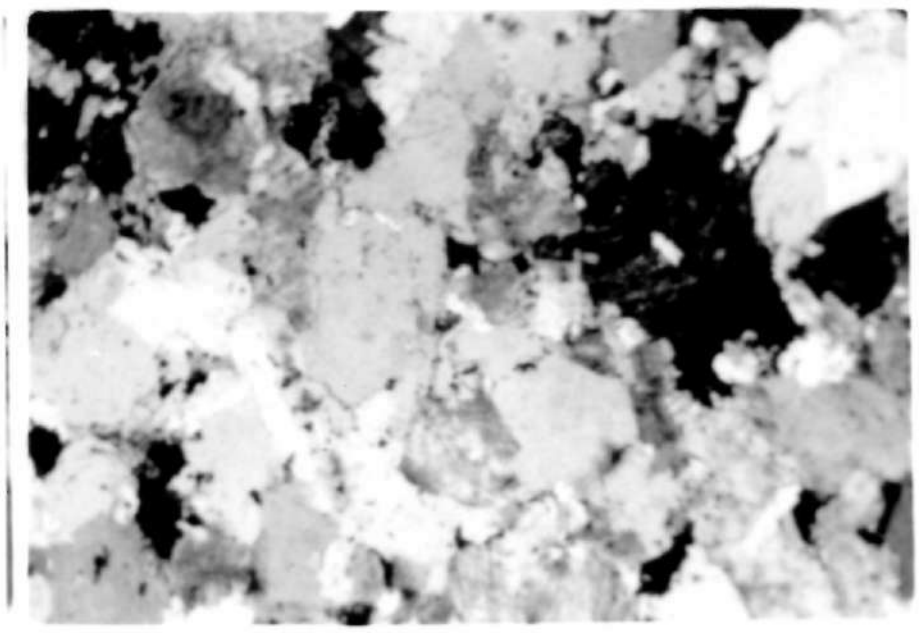


Plate 15. Photomicrograph of the *riebeckite-aegirine-biotite* granite showing altered riebeckite in: A) plane polarised light and B) cross-polars (aegirine (a); biotite (b); riebeckite (r)). Magnification, x5.

A



B

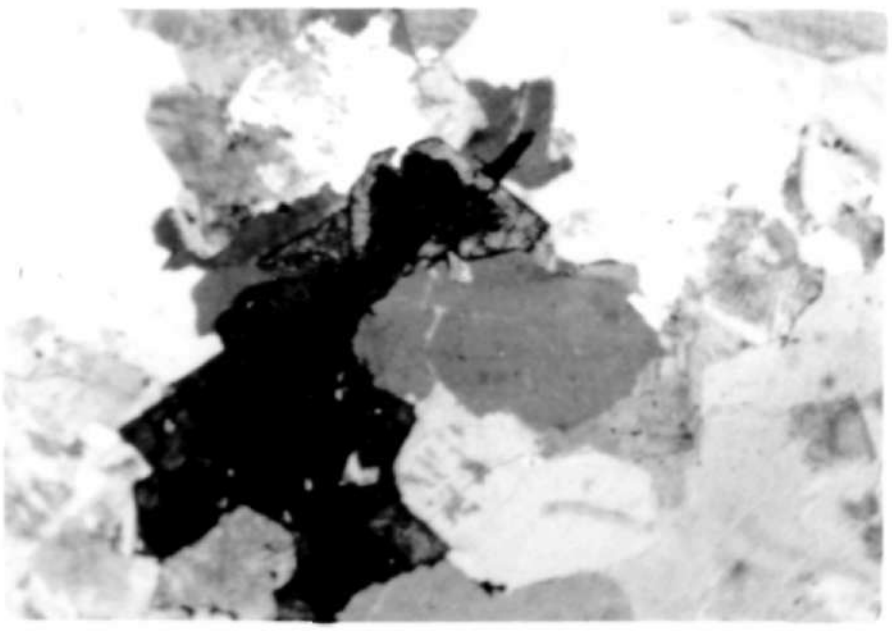
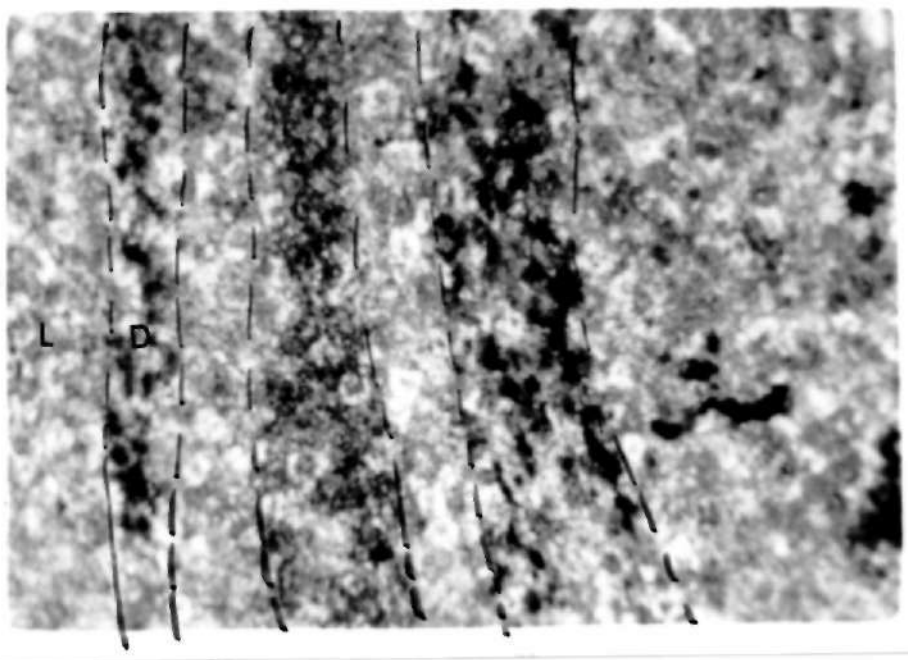


Plate 16. Photomicrograph of the felsic dyke. A) magnification, x5; B) magnification, x10. Note the rimmed zircon (z) in B). Plane light.

A



B

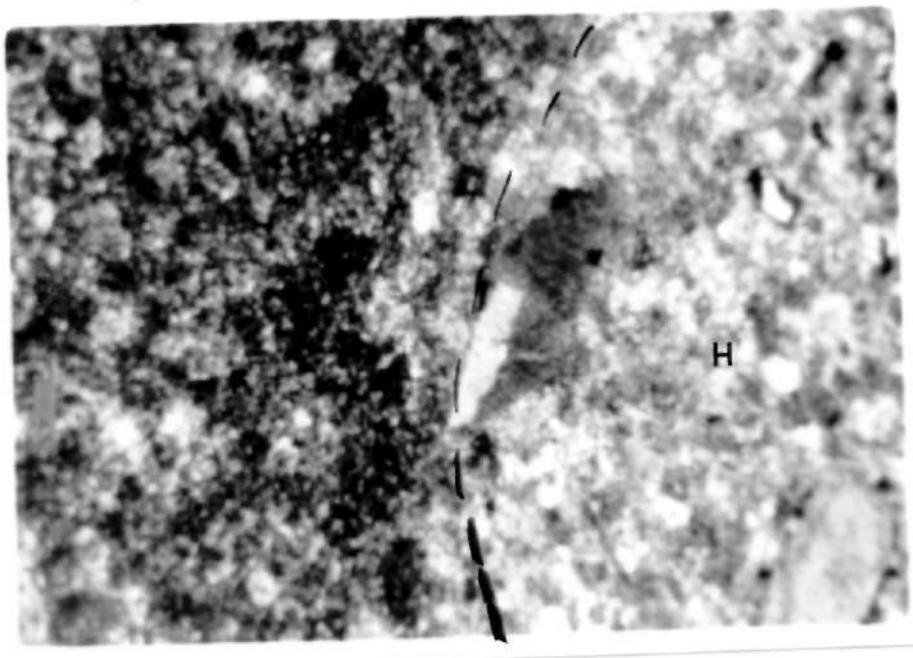


Plate 17. Photomicrograph of the rhyolite dyke in the study area showing: A) the light (L) and dark (D) bands, B) the contact with host rock (H). Magnification, x5. Cross polars.

by volume) are euhedral in shape and are commonly associated with perthite and arfvedsonite. The orthoclase perthite is turbid and poikilitic having inclusions of rounded grains of an earlier generation of perthite, most likely those of the arfvedsonite granite; the host rock. With respect to the opening of fractures, there is no evidence of shearing or cataclasis, as is the case of the intrusion of the rhyolite dyke. The presence of arfvedsonite is consistent with intrusion shortly before the final consolidation of the arfvedsonite granite.

4.3.6 The felsic dyke

The felsic dyke is a fine-grained dark-coloured rock consisting of perthites (70% by volume), zircon (20% by volume), and quartz (8% by volume). The zircon is rimmed and, in some crystals it has inclusions of perthite (Plate 16), indicating that perthites were among the first to crystallise.

4.3.7 The rhyolitic Dyke

The rhyolite dyke is light green and has a trachytic texture. The rock is fine grained and porphyritic. The phenocrysts of K-feldspar are set in an aphanitic groundmass.

In thin section, the phenocrysts contain subhedral crystals of quartz. The groundmass consists of fine prismatic crystals of pyroxene and orthoclase with a few grains of fayalite. These

minerals have some parallel alignment thus imparting a flow texture to the rock. The sheared part of the dyke consists of fine alternating bands of light and dark minerals (Plate 17). Each of the bands is separated by thin lines that divide them into different structural units. The light bands consist of feldspars and quartz whereas the dark bank consists of olivine and pyroxene. Close to the contact with the dark band, the quartz in the light band contains inclusions; the quartz representing late-stage crystallisations.

At the contact with the host rocks, recrystallised quartz and microcline become important (Plate 17). The quartz crystals are poikilitic and contain inclusions of subhedral crystals of quartz belonging to the intruded rock. Fayalite and aegirine also are present but are not oriented in any particular direction. Crystals of riebeckite or arfvedsonite close to the contact with the dyke have been partly altered, and astrophyllite is also deposited within cleavage planes of perthites in the host rock.

The above description does indicate that the opening of the fractures was preceded by cataclasis prior to the intrusion of the dyke.

4.4 MINERAL PARAGENESIS

The petrography of the Kigom granites indicates that the minerals are related to both the magma and hydrothermal fluids. Three stages of crystallisation can be recognised: the early and

late magmatic stage, the early hydrothermal stage and the late hydrothermal stage.

The early magmatic minerals are the euhedral crystals of quartz and fayalite associated with the microgranites, whereas the late magmatic minerals include the K-feldspars typically now exsolved into a perthitic intergrowth, the subhedral quartz crystals present mainly in the groundmass but also occurring as small inclusions in perthite and amphibole, the phenocrysts of quartz and magnetite present in very minor amounts in the rocks, and zircon. The early hydrothermal minerals are the bulk of the amphibole: the riebeckite and the arfvedsonite probably began to crystallise in the melt but completed their crystallisation at the subsolidus i.e., early hydrothermal stage. This involved the local removal of Na^{+} from the earlier crystallised perthite close to the amphibole resulting in the presence of modified exsolution texture of the perthite. During the late hydrothermal stage, oxidation and reduction reactions were dominant. The oxidation phase involved;

a) the replacement of the amphibole by aegirine and biotite, as is the case with the riebeckite and the riebeckite-aegirine granites, and the deposition of astrophyllite along cleavage planes of perthite and amphibole.
b) the alteration of the albitic portions of perthite to orthoclase - a process that involves the exchange of K^{+} in the hydrothermal fluids for Na^{+} in the albitic perthite.

c) the replacement of aegirine by hematite within the aegirine microgranites

d) the crystallisation of quartz in all rock units and those accompanying the MoS_2 mineralisation in the ore zone: a process involving the breakdown of the earlier crystallised silicates

e) the crystallisation of fluorite, and thorite which are present as accessories.

The reduction phase involved the crystallisation of sulphide minerals such as molybdenite, pyrite, chalcopyrite, and galena. At this stage all the F and the OH must have been used up such that the stage is more of reducing that oxidising favouring the concentration of sulphides. This phase is localised and the fluid tends to be structurally controlled along the contact of the riebeckite granites with both the basement and the riebeckite granites and the riebeckite-aegirine granites. The fact that these sulphide-bearing minerals are interstitial to perthite and actually replaces it does indicate that they were deposited by a chemically active fluid of a low pH/Eh.

These mineral assemblages are typical of strongly peralkaline granites that have undergone sodic metasomatism or albitisation (e.g., Abaa, 1991; Whalen et al., 1987).

CHAPTER FIVE

MINERALISATION

5.1 INTRODUCTION

This chapter describes the mode of occurrence and ore petrography of molybdenite and associated mineralisations, and discusses their petrogenetic implications.

5.2 MODE OF OCCURRENCE

The mineralisation is located at the contact between the riebeckite and riebeckite-aegirine granites of the Kigom on one hand, and the basement migmatite on the other hand. Mineralisation involves the formation of the sulphides molybdenite, pyrite, chalcopyrite, sphalerite, galena, helvite and bornite.

The sulphides occur disseminated. Sampling of the adits made by the Fidelity Mining Syndicates in 1958 (Plate 18) indicates that, using the abundance of the dominant sulphides, the mineralisation has a zoned distribution: a pyrite zone enclosing a molybdenite zone. The pyrite zone occurs within the arfvedsonite-riebeckite granites of the Kigom close to the contact with the basement and forms the outer shell of the mineralisation. It also has minor amounts of chalcopyrite and sphalerite. In this zone, molybdenite, helvite and bornite are absent.



Plate 18a. Photograph of part of the adit by the Fidelity mining syndicate



Plate 18b. The abandoned treatment site for the molybdenite mine.

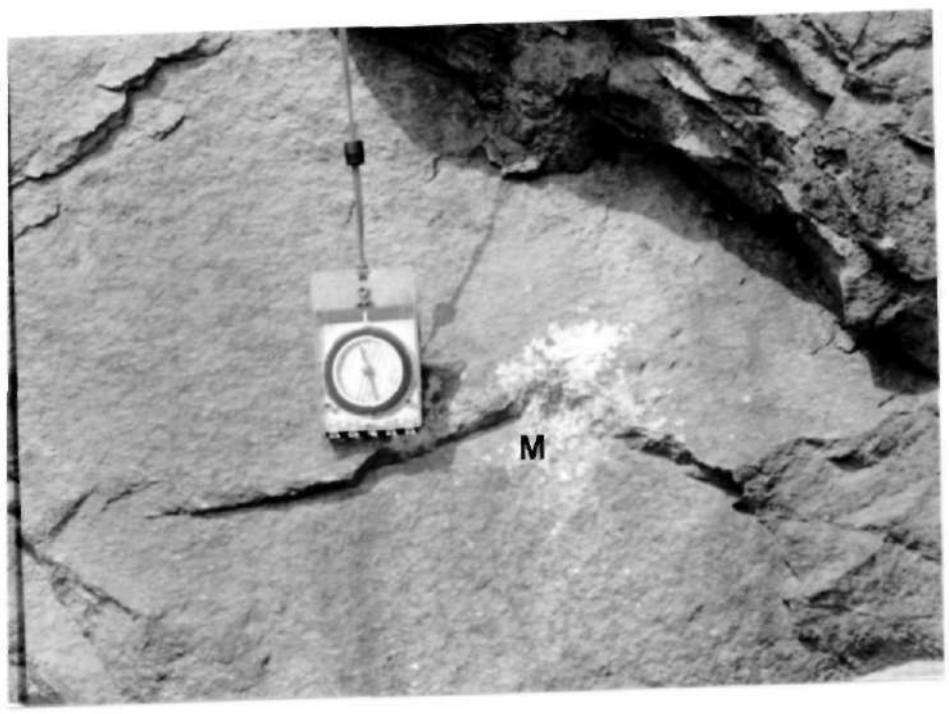
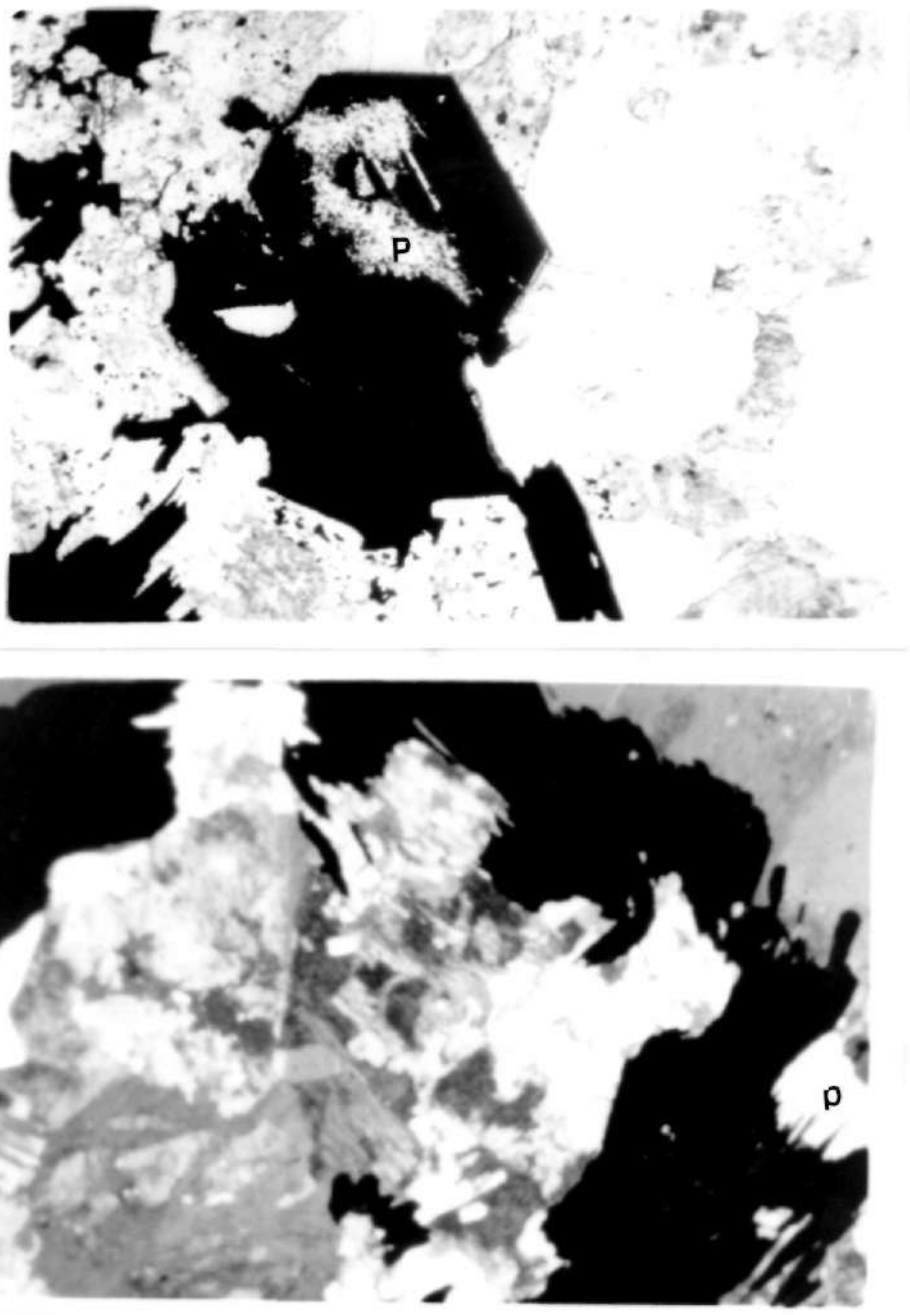


Plate 19. Photograph of the molybdenite zone showing the disseminated mineralisation (m).

sulphides	pyrite zone	molybdenite zone
molybdenite		
sphalerite		
pyrite		
chalcopyrite		
covellite		
bornite		
helvite		
galena		

Figure 11. Pattern of distribution of the sulphide mineralisation at the ore zone of the Kigom complex.

Associated with molybdenite are small crystals of covellite, identified by its characteristic blue colour and trigonal shape. The covellite occur at the margins and as inclusions within molybdenite and within fractures and cleavage planes of quartz and perthite close to molybdenite. Euhedral crystals of helvite identified by their honey colour, greenish pleochroism and cubic (octahedral) shape, are found in association with molybdenite. Helvite occurs as discrete and distinct grains such that there is no sign of overgrowth between it and molybdenite (Plate 24) indicating that both minerals had simultaneous growth. A few grains of galena occurring as euhedral crystals with characteristic cubic shape and complete isotropism in reflected light occur in association with molybdenite. Like helvite, galena occurs as isolated grains with no sign of overgrowth indicating that it was deposited about the same time with molybdenite. The brownish tint of sphalerite clearly distinguishes it from molybdenite. Perthites within this zone have had the albitic portions modified to orthoclase (Plate 25). As a result of prolonged interaction of the solutions, the perthites become modified and begin to grow into amphibole with characteristic bluish colour (Plate 25) indicating that the perthites have undergone textural and mineralogical modifications. Aegirine is not common within the ore zone. Where present, the aegirine overlies quartz and perthite crystals but is overlaid by molybdenite crystals. This textural relationship indicates that the alteration to aegirine was most likely complete before the deposition of the

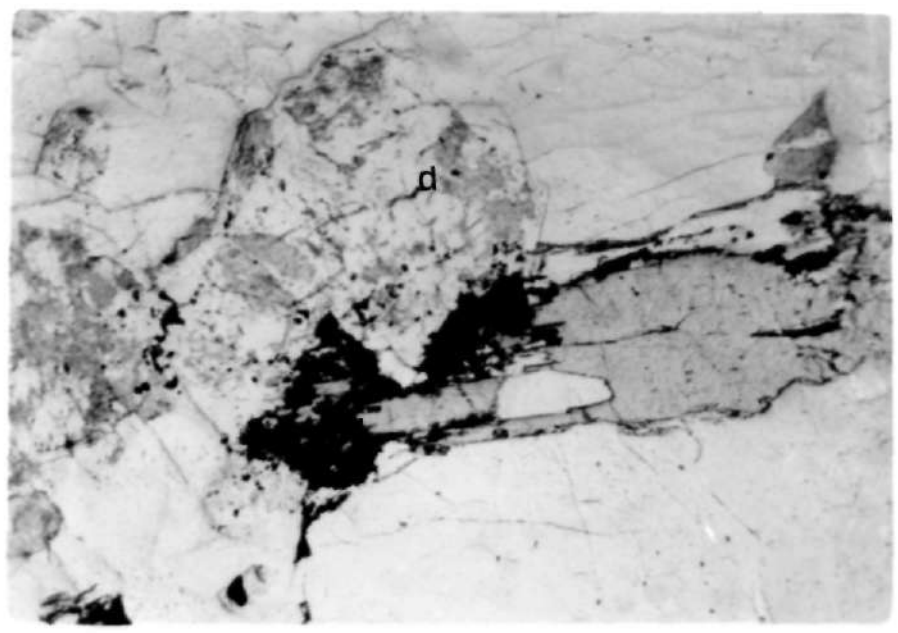


A

B

Plate 20. Photomicrograph of the ore zone showing molybdenite (isotropic, transmitted light): A) occurring both as trigonal crystals (T) and as flakes (F), and having inclusions of perthite (P), B) growing and replacing perthites. Magnification, x5. Cross polars.

A



B

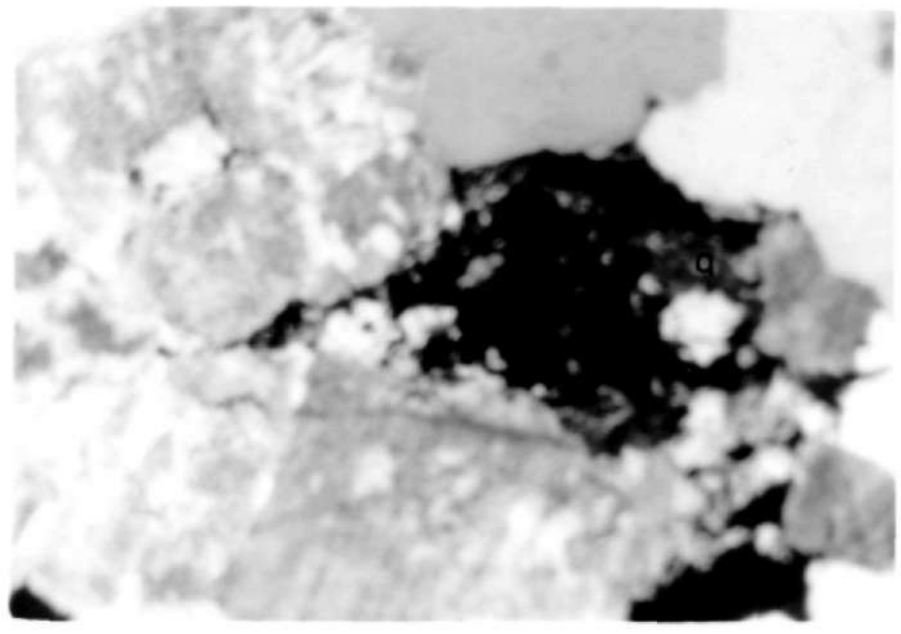
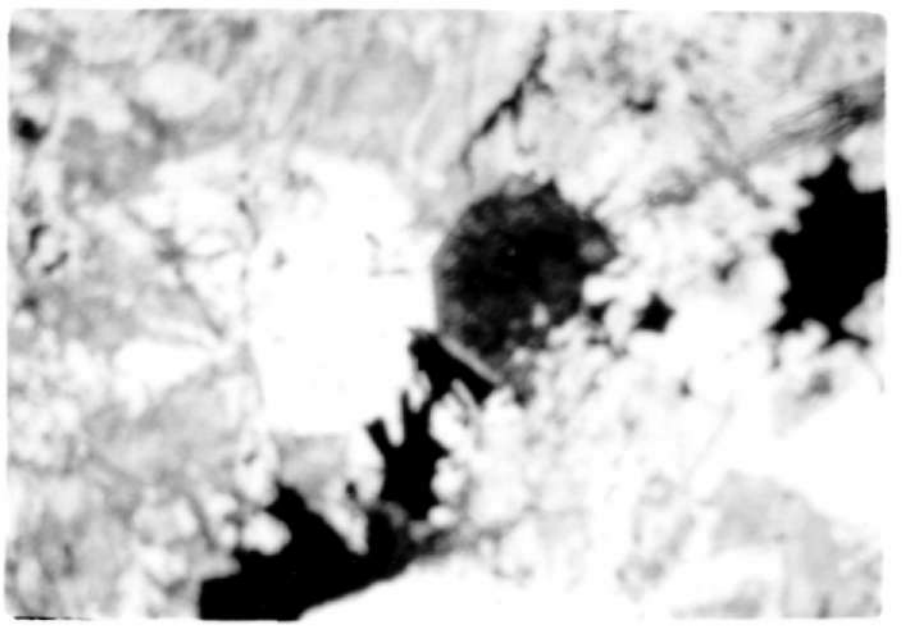


Plate 21. Photomicrograph of the ore zone showing altered perthite (A) and amphibole (B) to biotite (b). Magnification, x5. *Cross polars.*



Plate 22. Photomicrograph of the ore zone showing the growth of astrophyllite (a) along planes of perthite (P). Crossed polars. Magnification, x5.

A



B

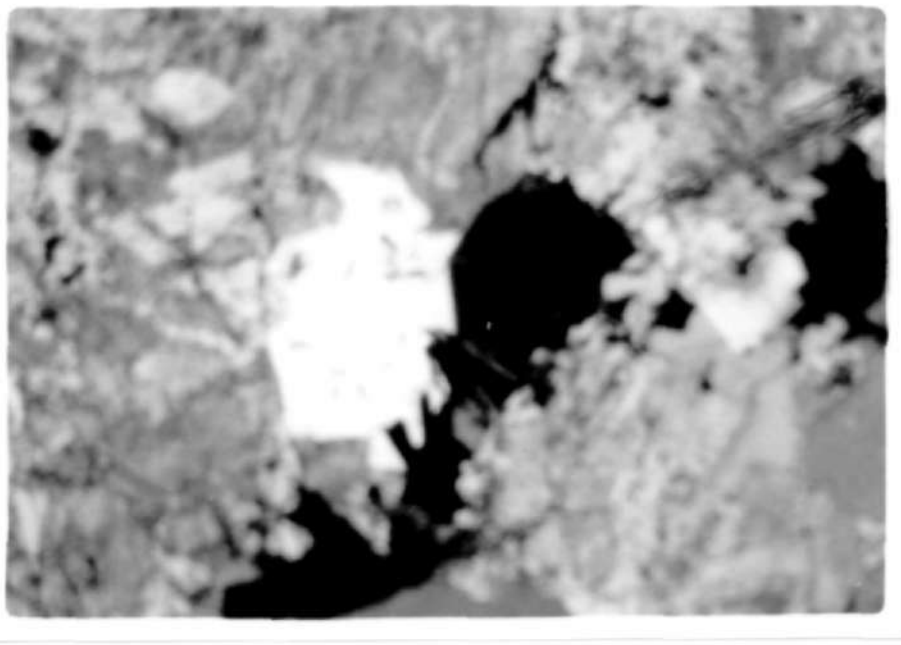
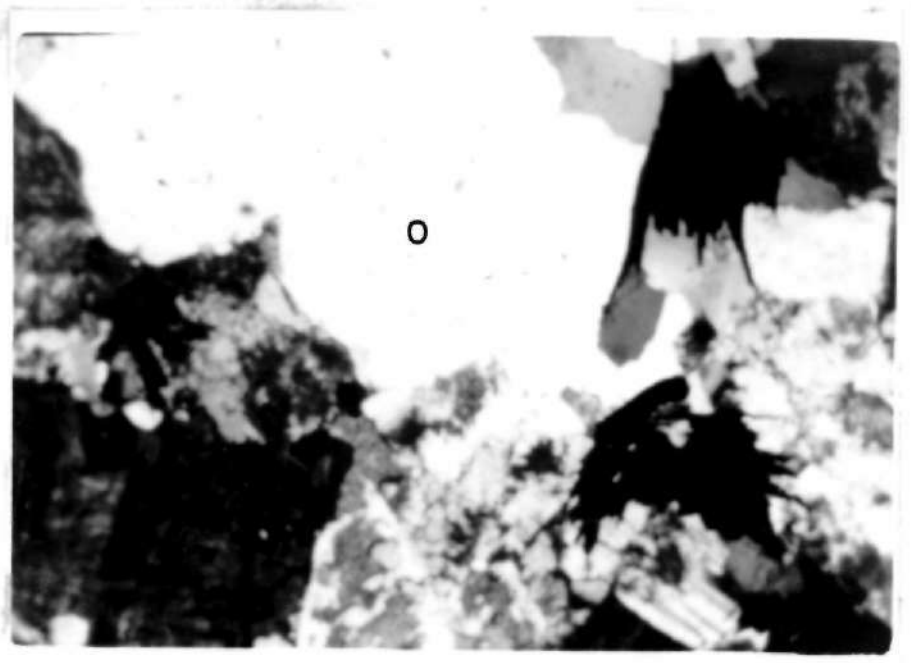


Plate 23. Photomicrograph of part of the ore zone showing the contact relationship between helvite (octahedral) (H) and molybdenite (f). A) plane polarised light, B) cross polars. Magnification, x5.

A



B

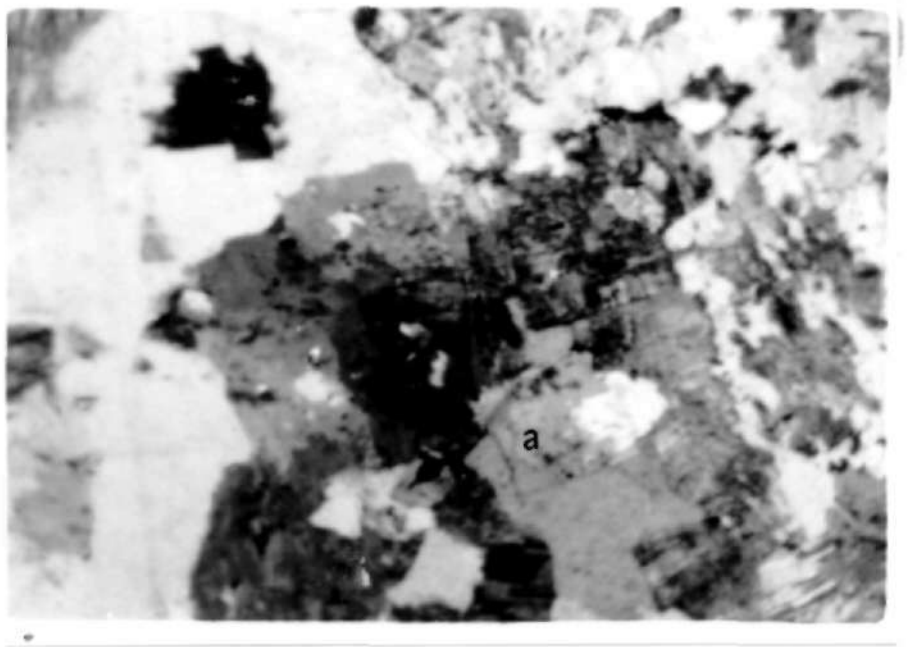


Plate 24. Photomicrograph of altered perthites in the ore zone. A) first stage alteration to orthoclase (O), and B) second stage alteration to amphibole? Cross polars. Magnification, x5.

molybdenite crystals. Euhedral crystals of white quartz overlie perthite crystals indicating that the mineralisation was accompanied by degradation of silicate minerals in the process of alkali metasomatism.

Within the pyrite zone, similar alteration characteristics are common, though less abundant; the perthites show modified exsolution textures, and the amphiboles and perthites are altered to biotite, and silicification also is common. Thus in terms of textural modifications and silicate mineralogy, this zone is similar to the molybdenite zone. Molybdenite is, however, absent while pyrite and chalcopyrite are abundant. Sphalerite occurring with brownish tint co-exists with the pyrite and chalcopyrite.

These features indicate that the deposition of the ore minerals was preceded by the introduction of a chemically active fluid related to the last phases of the alkali-rich siliceuos hydrothermal fluid that permeated the entire rock of the Kigom complex. The ore zone so far exposed is not a vein structure. There are no major fractures and there is no evidence of any linkage with the late rhyolitic intrusions elsewhere within the Kigom complex as there are no such rocks at the ore zone. The poikilitic texture of the ore minerals is suggestive of the fact that the deposition of the ore minerals is related to a reaction of the fluid with perthite resulting in its replacement. The longer the reaction time the better the porosity created by the fluid for the deposition of MoS_2. Crystallisation of MoS_2 was most likely preceded by a drop in temperature and in $f(O_2)$ or an increase in $f(S_2)$ of the solution

(i.e., the environment changed from being H_2O and F saturated (oxidising) to a S^{2-} saturated fluid (reducing)). The presence of Cu-bearing minerals like chalcopyrite suggests that the sulphides were crystallised at low temperatures, between 150 to 300 °C as Cu-bearing minerals associated with hydrothermal fluids are known to have been deposited at low temperatures. Smith et al. (1980) has shown, experimentally, that the crystallisation of Mo is enhanced at low temperatures of 300 °C.

CHAPTER SIX

GEOCHEMISTRY

6.1 INTRODUCTION

Forty samples representing the various rock units of the Kigom Complex were analysed. The averages of the geochemical data are presented in Tables 7-11 and the results are discussed below. In addition, representative grains of riebeckite, arfvedsonite, biotite, astrophyllite, and aegirine from ten representative samples from the rock units of the study area were analysed using the electron microprobe. The composition of the minerals and their recalculated formulas are presented in Table 11-16 and discussed below. The composition and degree of Al-Si order of coexisting feldspars in perthite in these samples were determined by x-ray diffraction (powder method). The bulk of the data is presented in the appendix.

Major and minor elements, electron-microprobe and x-ray diffraction analyses were carried out at the Department of Geological Sciences, McGill University, Montreal. The trace element data were provided by the ACME Analytical Laboratories Limited, Vancouver, British Columbia.

6.2 ANALYTICAL METHODS

The abundances of the major elements, and the elements Ni, Cr, V, Ba, Cu, Zn, and Co, were determined by the x-ray fluorescence technique on fused beads prepared from ignited samples using a 1:5 die. The samples were fused with lithium tetraborate following the procedure of Norrish and Chappell (1967). Matrix correction was done using a-correction factors. The abundace of FeO was determined using ammonium metavanadate titration. The detection limit for the major elements was 0.01%. For Cr, the detection limits were 15 ppm, and for the rest of the elements 10 ppm. The abundances of the elements Nb, Zr, Y, Sr, Rb, Th, Pb, and U were determined using pressed powder pellets for XRF, as described by Jenkins and Van Gelder (1968): matrix correction was by Kβ-comption scatter from Rh X-ray tube, whereas the abundances of Mo, W, Be, Li, Sn, As, and Ag were determined using ICP Spectography as described by Thompson and Walsh (1983). The abundance of F was determined using an ion-selective electrode and a standard addition technique.

The electron microprobe used is equipped with four automated wavelength-dispersion spectrometers, and an energy-dispersion system (EDS). The analyses were carried out under the following conditions: accelerating voltage, 15 kV; beam current, 15 nA; spot size, 8 μm; counting time, 100 seconds for F, 50 for Cl, 25 seconds for the others. A variety of mineral and metal standards were used: diopside for the determination of Ca, Si, and Mg;

orthoclase for K, and Al; vandium for Cl; fluorite for F; andradite for Fe; albite for Na; titanite for Ti; and Mn-bearing ilmenite for Mn.

The powder-diffraction patterns were recorded with a Guinier-Hagg focusing camera ($CuK\alpha_1$ radiation). The diffraction maxima were corrected by reference to a synthetic spinel (a = 8.0833 Å at room temperature), indexed, and used as input for the program of Appleman and Evans (1973). The refined unit-cell parameters were used to infer degree of Al-Si order and composition (in terms of N_{Or}).

6.3 WHOLE-ROCK GEOCHEMISTRY

6.3.1 The Major Oxides

All the rock units of the Kigom complex have characteristically high abundances of SiO_2, K_2O, Na_2O, Al_2O_3 and low values of MgO, MnO, CaO, and Cr_2O_3 (Table 7). Among the samples analysed, SiO_2 is most enriched in the aegirine microgranite with 76.9 wt%, and least enriched in the riebeckite granites with 75.0 wt%. The arfvedsonite granite has higher abundance of K_2O with 4.51 wt%, whereas the riebeckite-aegirine-biotite granite has higher values of Na_2O with 4.70 wt%. TiO_2 abundance is highest in the aegirine microgranite with 0.11 wt% and least in the riebeckite-aegirine-biotite granite and the arfvedsonite granite with 0.08 wt%. Al_2O_3 is more enriched in the aegirine microgranite with 12.18

Table 7. Average whole-rock major oxides composition of the major rock units of the Kigom complex.

Oxides wt%	1	2	3	4	5	6	7
SiO_2	76.93	76.14	74.97	75.46	73.16	71.38	73.81
TiO_2	0.11	0.08	0.10	0.08	0.27	0.07	0.26
Al_2O_3	12.18	11.87	11.79	11.61	12.07	12.34	12.40
Fe_2O_3	0.85	1.03	1.85	1.82	1.86	1.96	1.24
FeO	0.35	1.23	1.34	1.38	1.99	0.91	1.58
MnO	<0.01	0.01	0.02	0.02	0.07	0.05	0.06
MgO	<0.01	<0.01	<0.01	<0.01	tr	0.16	0.20
CaO	0.01	<0.01	0.06	0.01	0.50	0.17	0.75
Na_2O	4.06	4.51	4.53	4.70	4.57	7.17	4.07
K_2O	4.31	4.31	4.26	4.20	4.79	4.17	4.65
P_2O_5	0.01	0.01	0.01	0.01	0.02	0.01	0.04
L.O.I	0.72	0.27	0.54	0.29	0.02	0.12	-
Total	99.53	99.47	99.48	99.58	99.32	98.51	99.34
normative compositions (moles %)							
Ap	0.02	0.02	0.02	0.02	0.05	-	0.09
Il	0.16	0.11	0.14	0.11	0.51	0.13	0.37
Mt	0.60	0.73	1.52	0.82	1.27	-	1.32
Or	26.01	25.87	25.69	25.22	28.30	24.64	28.01
Ab	37.24	39.96	40.00	39.18	35.41	40.25	37.26
An	-0.02	-0.07	nd	-0.02	-	-	1.87
Di	nd	nd	0.18	nd	1.90	-	1.33
Hy	0.00	1.35	0.91	1.54	1.61	2.05	1.24
Ac	0.00	0.95	1.22	2.97	2.85	5.67	-
C	0.94	0.26	nd	0.01	-	-	-
Q	34.84	31.04	30.32	30.14	27.36	22.11	28.51
Fl	-	-	-	-	0.12	0.24	-
Ns	-	-	-	-	-	3.25	-
Total	99.79	100.24	100.00	100.00	100.00	100.00	100.00
Na+K/Al	1.01	1.02	1.02	1.06			
Al/Na+K+Ca	0.99	0.98	0.94	0.97			

1 aegirine microgranite (fayalite-bearing)
2 arfvedsonite granite
3 riebeckite granite
4 riebeckite-aegirine (-biotite) granite
5 arfvedsonite granite of the Sha-Kaleri complex (Jacobson et al., 1958)
6 albite riebeckitic arfvedsonite granite of the Liruei complex (Black, 1963)
7 typical A-type granite composition of Whalen et al. (1987)

Table 8. Average whole-rock major oxides composition of the ore zone of the Kigom complex.

Oxides (wt %)	1	2	3	4	5
SiO_2	76.45	75.59	76.15	75.65	75.71
TiO_2	0.18	0.15	0.14	0.12	0.17
Al_2O_3	10.88	11.33	11.02	10.96	10.94
Fe_2O_3	0.51	0.99	0.83	1.42	0.90
FeO	2.00	2.16	2.41	2.01	2.43
MnO	0.02	0.02	0.02	0.01	0.02
MgO	<0.01	<0.01	<0.01	<0.01	<0.01
CaO	0.06	0.11	0.10	0.13	0.11
Na_2O	5.03	4.59	4.60	4.57	4.55
K_2O	2.53	4.08	3.76	4.26	4.29
P_2O_5	0.01	0.01	0.10	<0.01	0.02
L.O.I	0.24	0.24	0.22	0.32	0.29
Total	97.91	99.27	99.35	99.45	99.35
normative compositions (moles%)					
Ap	0.02	0.02	0.21	nd	0.04
Il	0.26	0.21	0.20	0.17	0.24
Mt	0.33	nd	nd	nd	nd
Or	15.44	24.59	22.67	25.67	25.84
Ab	45.90	38.49	38.71	35.35	35.04
An	nd	nd	-0.16	-0.00	nd
Di	0.19	0.39	nd	0.52	0.34
Hy	2.66	3.04	3.64	2.76	3.46
Ac	0.60	2.82	2.36	4.04	2.56
C	nd	nd	0.06	nd	nd
Q	34.61	30.44	32.16	31.05	31.45
Ns	nd	nd	0.15	0.44	1.03
Total	100.00	100.00	100.00	100.00	100.00
Na+K/Al	1.01	1.06	1.06	1.11	1.11
Al/Na+K+Ca	0.98	0.93	0.93	0.89	0.89

Arrow indicates sample path: from the outer through the inner zone of mineralisation

1 the outer pyrite zone
2 granite at the ore zone (least mineralised)
3 " "
4 " "
5 granite at the ore zone (richly mineralised)
note the generally decreasing trend of Na_2O, and the increasing K_2O towards the richly mineralised granite.
low totals are due to trace element enrichment

Table 9. Average whole-rock major oxides composition of the Dykes associated with the Kigom complex.

Oxides (wt %)	1	2	3
SiO_2	75.51	66.21	73.13
TiO_2	0.14	0.04	0.32
Al_2O_3	12.20	19.23	11.20
Fe_2O_3	1.88	0.61	1.34
FeO	1.01	nd	2.69
MnO	0.03	nd	0.03
MgO	nd	nd	<0.01
CaO	0.02	nd	0.11
Na_2O	3.62	7.22	2.03
K_2O	4.46	5.24	3.92
P_2O_5	0.01	0.01	0.05
L.O.I	0.98	0.78	0.33
Total	99.86	99.32	96.20
Normative composition (moles%)			
Ap	0.02	0.02	0.12
Il	0.20	nd	0.51
Mt	2.02	nd	1.59
Or	27.09	30.37	26.37
Ab	33.42	63.60	20.75
An	0.03	-0.06	0.25
Hy	0.11	nd	3.23
C	1.58	1.83	0.06
Q	35.53	3.81	47.13
Hm	nd	0.42	
Ru	nd	0.03	
Total	100.00	100.00	100.00

nd absent
1 rhyolitic dyke associated with both the arfvedsonite granite and the riebeckite aegirine biotite granite
2 pegmatite associated with the arfvedsonite granite
3 felsic dyke intrusive into the mineralised zone

Table 10. Whole-rock trace element composition of the Kigom complex and the ore zone (in ppm).

Elements	1	2	3	4	5	6	7	8	9
Nb	208	118	74	79	950	329	289	212	318
Zr	530	457	512	588	7134	589	971	714	739
Y	52	35	13	21	894	174	192	179	148
Sr	4	1	4	2	43	3	2	3	3
Rb	176	299	330	290	400	296	274	280	323
Pb	8	12	10	17	18	102	111	856	98
Th	34	34	22	27	131	55	59	43	77
U	4	5	nd	4	35	10	9	nd	6
Co	nd	nd	nd	nd	nd	nd	nd	nd	nd
Cu	33	125	22	85	372	174	287	528	62
Zn	79	285	442	402	498	874	528	856	411
Mo	1	2	1	1	2	5	12	85	2760
W	4	2	6	4	3	2	4	2	2
Li	48	137	216	111	22	95	121	111	93
F	560	960	1100	1220	1400	1690	1430	1720	1860
Sn	1	7	11	10	30	13	14	10	17
Ag	3	0.1	2	0.2	10.6	4	2	2	2
As	2	2	2	2	4	2	2	5	2
Be	3.9	6.9	5.8	7.3	25	3.1	3.6	3	2.4
Ba	4	1	7	1	32	1	2	1	5
Ni	1	10	7	10	22	10	9	11	10
Cr	28	33	29	30	43	31	34	32	32
V	1	1	1	1	2	1	1	1	1
ratios									
Rb/Sr	44	299	82.5	145	9.3	99	137	93	108
Rb/Ba	44	299	47.2	290	12.5	296	137	280	65
Zr/Y	10	13	39.4	28	8	4	5	4	5
Zr/TiO_2	0.5	0.6	0.1	0.1	4	0.4	0.7	0.6	0.4

nd absent (beyond detection limit)
1 aegirine microgranite (fayalite-bearing)
2 arfvedsonite granite
3 riebeckite granite
4 riebeckite-aegirine (-biotite) granite
5 the outer pyrite zone
6 granite at the ore zone (least mineralised)
7 " "
8 " "
9 granite at the ore zone (richly mineralised)

Table 11. Whole-rock trace element analyses of the Dykes associated with the Kigom complex

Elements (ppm)	1	2	3
Nb	224	110	3885
Zr	1024	527	38200
Y	31	26	1899
Sr	2	2	61
Rb	226	263	1041
Pb	18	48	13
Th	32	36	1821
U	3	4	159
Co	nd	3	27
Cu	26	72	70
Zn	213	14	712
Mo	1	1	5
W	2	5	6
Li	83	4	63
F	600	60	1260
Sn	11	2	94
Ag	0.2	0.7	0.2
As	2	4	2
Be	5.5	4.2	12.9
Ba	32	14	28
Ni	12	3	28
V	1	1	6
Cr	28	17	44
Ratios			
Rb/Sr	113.00	131.50	17.06
Rb/Ba	7.06	18.79	37.18
Zr/Y	33.03	22.00	20.12
Zr/TiO_2	0.73	1.43	11.94

nd not determined (below detection limit)
1 rhyolitic dyke associated with both the arfvedsonite granite and the riebeckite aegirine biotite granite
2 pegmatite associated with the arfvedsonite granite
3 felsic dyke intrusive into the mineralised zone

wt% as compared to 11.61-11.87 wt% in the others. $Fe_{(total)}$ is most enriched in the riebeckite granite and in the riebeckite-aegirine-biotite granite. CaO is generally depleted and is in fact absent from most of the samples. The riebeckite granite has the highest abundance of 0.06 wt%. The abundance of CaO follows the path of increasing F in the rock. This is related to the formation of fluorite which may be late. The concentration of Mg is below the detection limit. MnO also is very low with 0.02 wt% in most samples. The distribution of the major oxides, thus, indicates the enrichment patterns displayed in figures 12-14: the aegirine microgranite in SiO_2, Al_2O_3, and TiO_2; the riebeckite granite in CaO and Fe_2O_3; the arfvedsonite granite in K_2O; the riebeckite-aegirine-biotite granite in Na_2O and MnO. According to the abundances of the major oxides the Kigom granites have crystallised from a very evolved magma.

The molar sum Na_2O+K_2O exceeds Al_2O_3 in all cases (Table 7). Following the classification of Shand (1951), the sampes of Kigom granites are all peralkaline (Fig. 15). Each granite-type, however, has isolated regions of concentration indicating that the crystallising magma underwent some degree of differentiation. The granites also have molecular $Al_2O_3/(CaO+Na_2O+K_2O)$ ratios that are below 1.0 and compare with those of A-type granites of Whalen et al. (1987). A plot of the A/CNK ratios versus those of NK/A (Fig. 16) indicate an interesting pattern of peralkalinity: the fayalite-aegirine microgranites plot in the weakly peralkaline zone; the arfvedsonite granites slightly below the microgranites; the

riebeckite and the riebeckite-aegirine-biotite granites in the centre of the peralkaline field; and the ore zone (see below) plots at the extreme right of the peralkaline field. This trend of peralkalinity follows the path of consolidation of the magma, and latter in the crystallisation process, the degree of metasomatism resulting from the influx of an alkali-rich fluid: the fayalite-granite being the first to crystallise was least affected; the arfvedsonite granite, the riebeckite granite, the riebeckite-aegirine-biotite granites and the ore zone followed in turn. The Fe_2O_3/FeO ratios is higher in the Kigom granites relative to those for the average A-type granite and thus show the presence of normative acmite which varies from 0% in the aegirine microgranite to as high as 2.97% in the riebeckite-aegirine-biotite granite (Table 8).

In terms of bulk composition, all the granites have normative Q + Or + Ab > 93 % in which Ab > Q > Or (Table 7). This is typical of peralkaline granites that have crystallised from F-rich magma and latter-alkali-metasomatism (e.g., Martin and Bowden, 1981; Whalen et al., 1987). An is absent in these rocks. On the Q-Or-Ab triangular diagram (Fig. 17), all the granites plot in the alkali feldspar-rich region with a shift towards the Q-Ab axis. The Kigom granites all plot on the Or-Ab axis of the Or-Ab-An triangular diagram (Fig. 18) and are in the lower half of the Or-Ab axis indicating that the coexisting feldspars in perthite, in general, have more albite than orthoclase as reflected in the normative calculations of the granites. Using the Q-Or-Ab

triangular diagram of Luth et al. (1964), the aegirine microgranite plots on the 1 kbar minimum while the riebeckite granite, the arfvedsonite granite, riebeckite-aegirine-biotite granite plot between the 1 and 2 kbar minima (Fig. 17). Hess (1989) interpreted such shifts in minimum to be due to increasing water pressure and feldspathic compositions. This indicates that the initial magma of the Kigom which consolidated as the aegirine microgranite was water saturated. The high F-content in the melt displaced the minimum towards the increasingly feldspathic and sodic compositions about which condition the arfvedsonite granite, and mostly the riebeckite and riebeckite-aegirine-biotite granite consolidated. The plots of the granites fit the Q-Ab-Or plot for fluorine-bearing granites of Manning (1982) with 1-2 wt% F and excess water at 1 kbar (Fig. 17). The abundance of fluorine is, thus, partly responsible for the shift towards albite, since the addition of fluorine lowers the viscosity and crystallisation temperature and shifts the isobaric minimum towards albite-richer compositions in the water-saturated granitic melts (e.g., Kovalenko,1973; Manning, 1982). Similar results have been reported from the peralkaline granites of the Ririwai complex of the Younger Granites of Nigeria (e.g., Martin and Bowden, 1981). Compared with the average composition of perlakaline granites from some complexes in the Younger granite Province (Table 7), the Kigom granites are enriched in SiO_2 and depleted in MnO, MgO, and CaO. Such composition (Whalen et al., 1987), is typical of strongly evolved peralkaline granites.

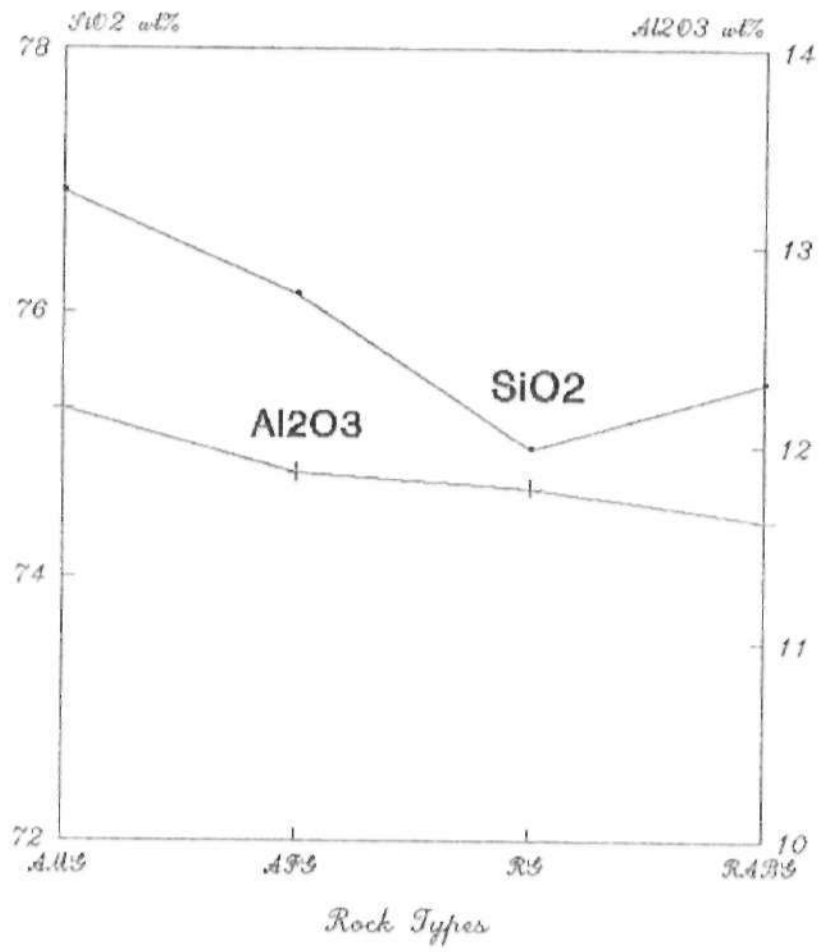


Figure 12. SiO_2 and Al_2O_3 Distribution plot for the Kigom granites. AMG aegirine microgranite, AFG arfvedsonite granite RG riebeckite granite, RABG riebeckite-aegirine-biotite granite.

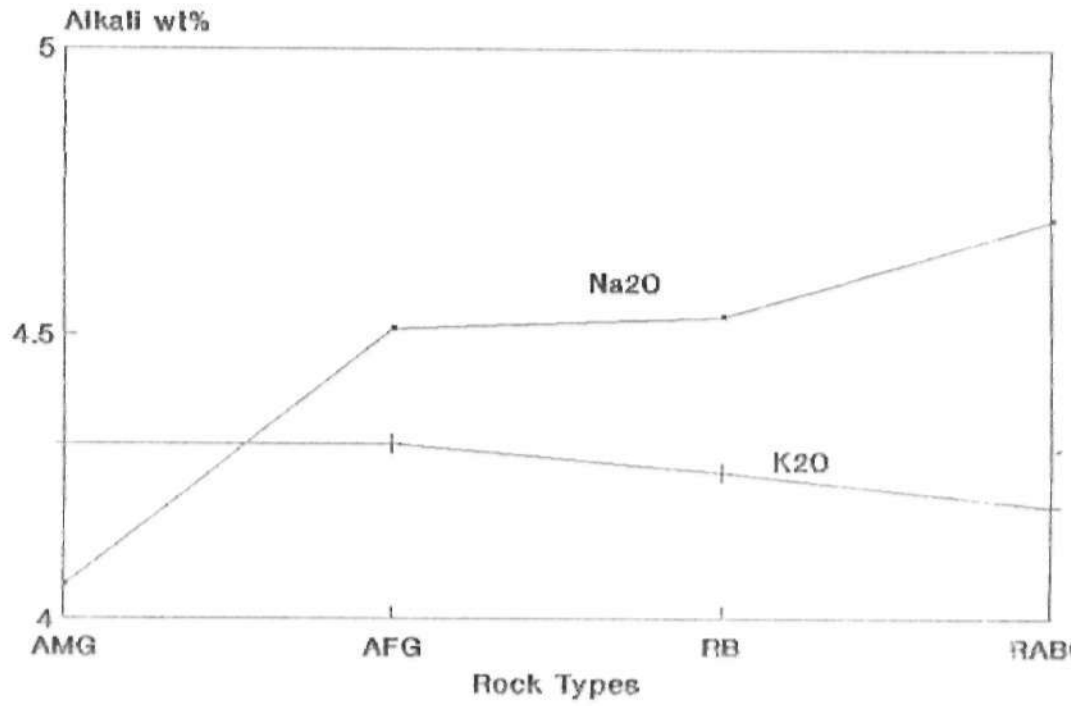


Figure 13. Na_2O and K_2O Distribution plot for the Kigom granites Note the Na_2O increases towards the riebeckite-aegirine-biotite granite following the path of consolidation AMG aegirine microgranite, AFG arfvedsonite granite RG riebeckite granite, RABG riebeckite-aegirine-biotite granite.

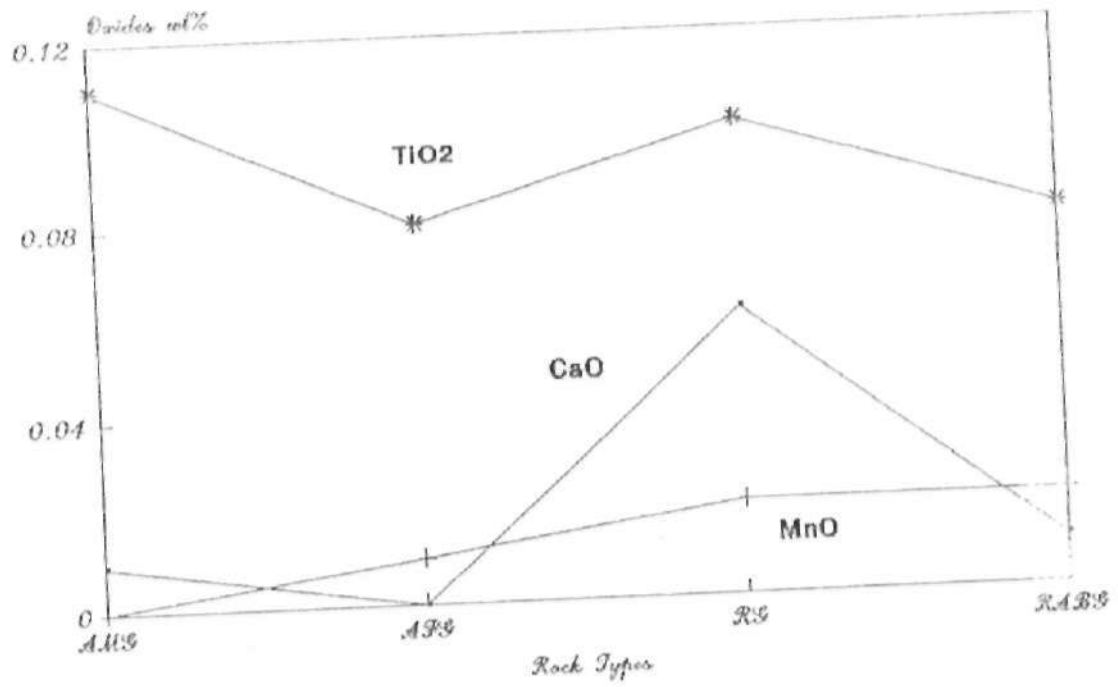


Figure 14. CaO, TiO_2, and MnO Distribution plot for the Kigom granites. AMG aegirine microgranite, AFG arfvedsonite granite, RG riebeckite granite, RABG riebeckite-aegirine-biotite granite.

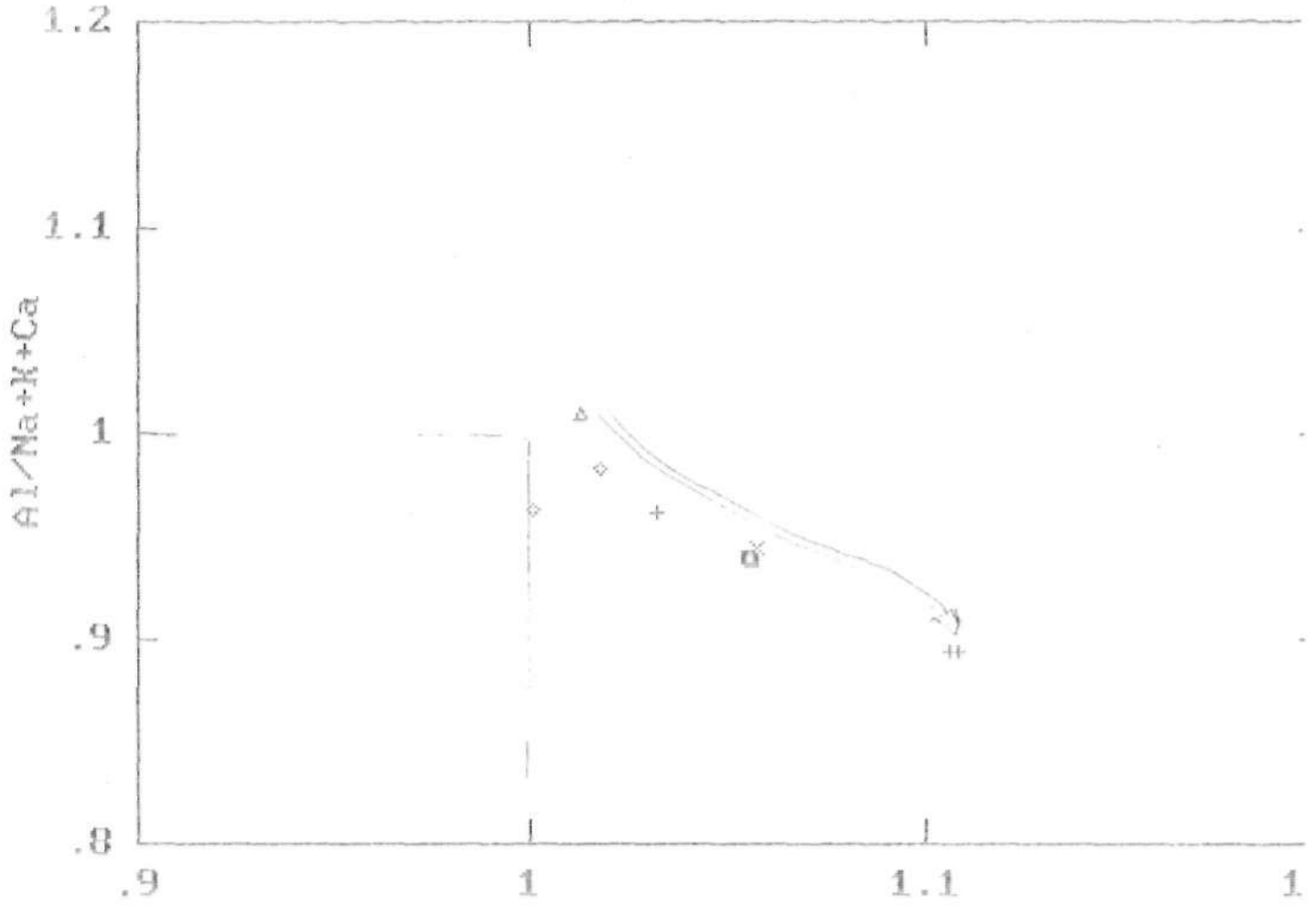


Figure 16. Alumina saturation and alkali saturation plot for the Kigom granites. Note the interestingly increasing peralkalinity from the aegirine microgranite to the ore zone in the riebeckite granite. Triangle, aegirine microgranite; star, arfvedsonite granite; square, riebeckite-aegirine granite; multiple, riebeckite-aegirine-biotite granite; cross, ore zone of riebeckite granite.

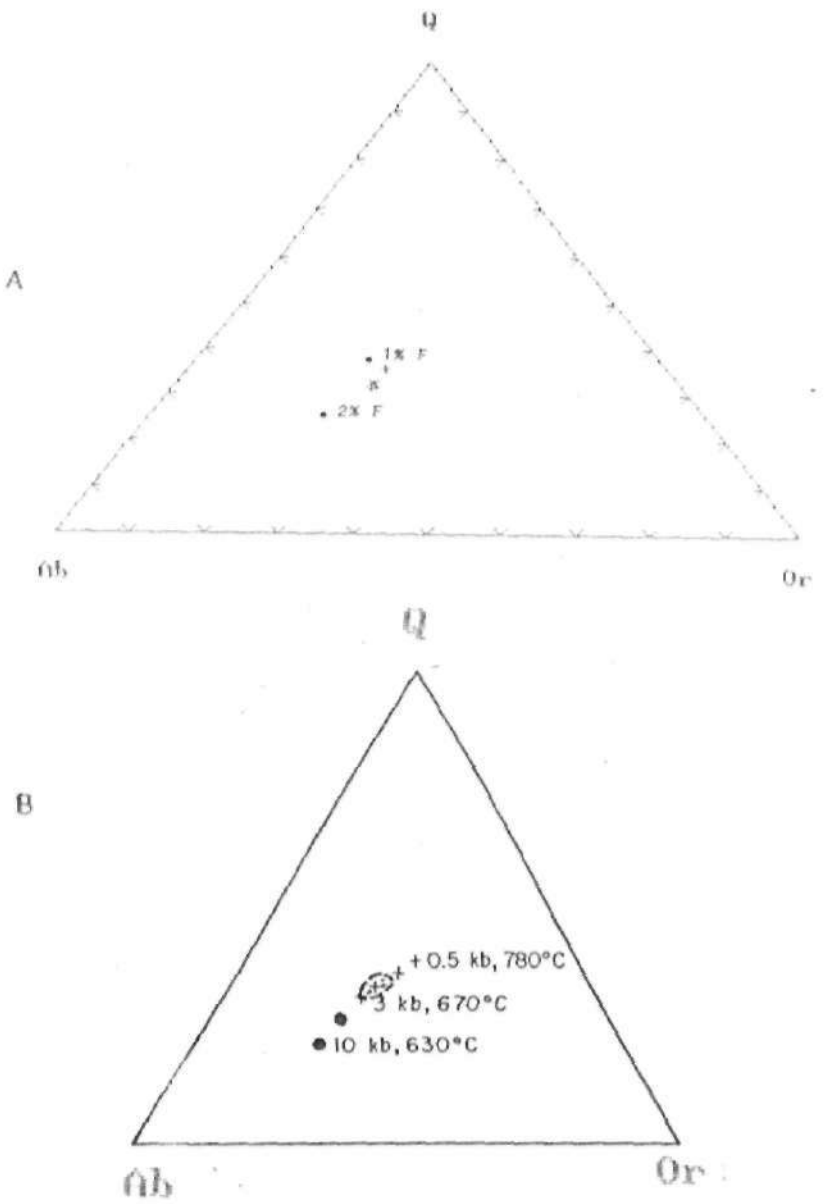


Figure 17. Q-Ab-Or triangular plot for the Kigom granites compared against (A) the F-bearing systems of Manning (1982) and (B) the minima in granite system for water pressures of Luth et al., 1964. Note the shift of the plots towards the albite-end as the system becomes more F-rich. Cross, fayalite-bearing aegirine microgranite; multiple, arfvedsonite granite; square, riebeckite granite; star, riebeckite-aegirine granite; triangle, riebeckite-aegirine-biotite granite.

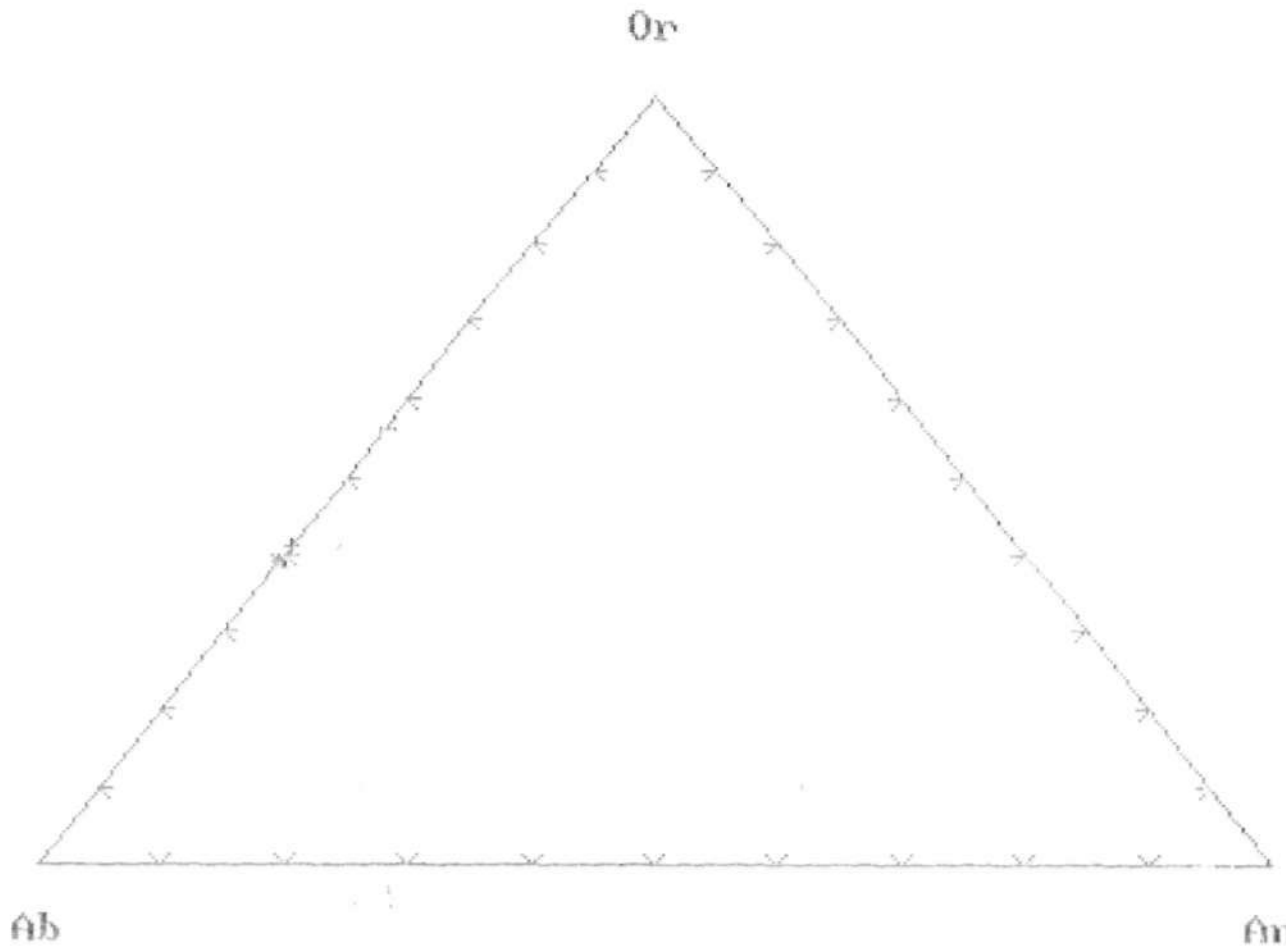


Figure 18. Or-Ab-An triangular plot of the Kigom granites. Notice that the plots of the granites are on the first-half of Ab-Or axis indicating that the granites generally have more albites than orthoclase in the co-existing feldspars in perthite.

KASHIM IBRAHIM LIBRARY
RECEIVED
April 1994
ZARIA, NIGERIA
Ahmadu Bello University

4330883

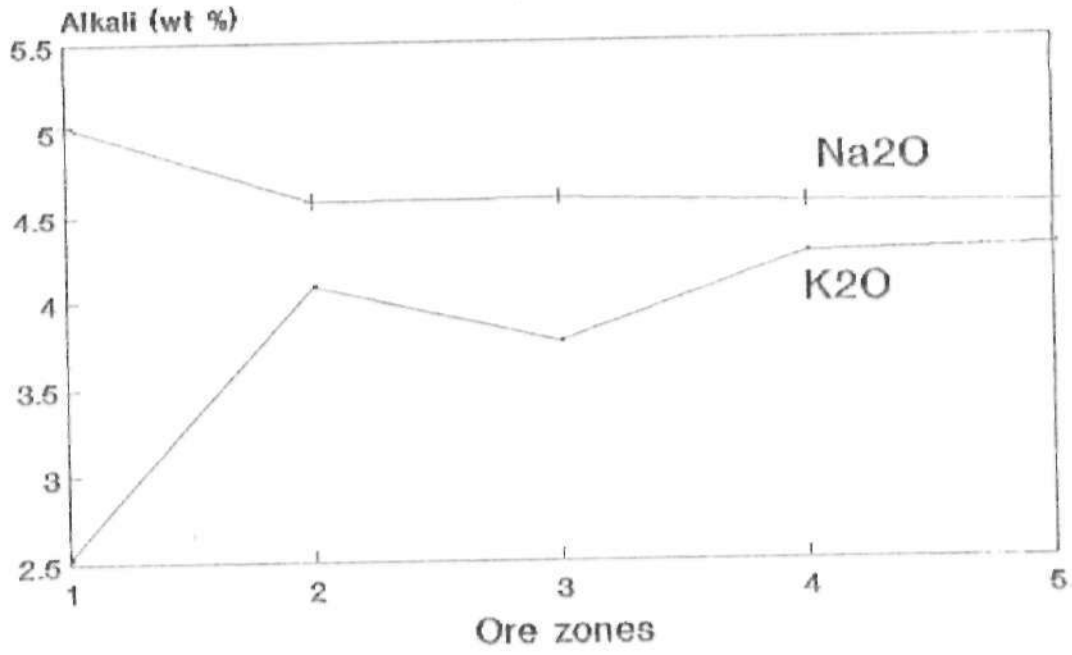


Figure 19. Alkali distribution plot for the ore zones.

Refer to Table 8 for identification

The rhyolitic dyke associated with the Kigom complex shows similar major element composition to that of the Kigom granites with the exception of Na_2O which is lower (Table 9) most likely because of the absence of alkali metasomatism in the rock. In bulk composition, the rhyolite compares most closely to that of alkali-rich rhyolite, but are trachytic in texture. The rhyolite has normative Q + Or + Ab > 90% with 2.02% Mt, 1.58% C, 0.11% Hy, 0.2% Il and 0.03 Di (Table 9). The pegmatite dyke, however, show higher values of K_2O and lower values of SiO_2. They have normative Or + Ab > 93% with normative Q of only 3.81% (Table 9).

The ore zone is enriched in TiO_2 wt%, FeO wt%, CaO and SiO_2 wt% compared with those of the riebeckite granites: increasing, respectively, from 0.10 to 0.17 wt%, 1.34 to 2.43 wt%, 0.06 to 0.13 wt% and from 74.97 to 76.45 wt %. Al_2O_3 and Fe_2O_3 are slightly depleted (Tables 7-8). The low values of the ore zone in Al_2O_3 resulted in the higher NK/A, and lower A/CNK ratios compared to the other granites of the Kigom complex (Fig 16), whereas the relatively higher SiO_2 indicates that some degree of silicification was involved in the metasomatism. Within the ore zone, K_2O generally increases from the outer to the inner zones, whereas Na_2O shows a reverse trend (Fig. 19). These increases are related to the deposition of astrophyllite and pyrite in the zone. The other major oxides show similar compositions to those of the riebeckite granite.

The felsic dyke at the ore zone shows very interesting composition. Compared with the granites of the Kigom complex, TiO_2

and FeO are enriched but Al_2O_3, Na_2O, CaO and SiO_2 are depleted (Table 9). In terms of bulk composition, the dyke is granitic with normative Q + Or + Ab > 90 % in which Q>Or>Ab (Table 9).

6.3.2 *The Trace Elements*

The granites of the Kigom complex generally have high values of Nb, Cu, Zn, Zr, Th, U, Rb, F and Y (Table 10, Figs. 20-26). Whereas Nb and Y are most enriched in the aegirine microgranite (208 and 52 ppm, respectively) they are least enriched in the riebeckite granite (79 and 21 ppm). Cu and Cr are most enriched in the arfvedsonite granite. The riebeckite granite has the highest values of Zn, Rb and Li, whereas the riebeckite-aegirine-biotite granite is more enriched in F and Be. Th and U show no particular trend. Sr and Co are depleted. The Kigom granites, apart the zone of mineralisation, have low values of 1-2 ppm Mo. The content of Sn in the rocks increases from 1 ppm in the aegirine microgranite, 7 ppm in the arfvedsonite granite to 11 ppm in the riebeckite granite; the riebeckite-aegirine-biotite granite has 10 ppm. W follows the same pattern as Sn, but not not so much enriched.

These trends are indicative of magmatic enrichments that follow the path of consolidation: the first to consolidate, the least enriched. The Kigom granites all plot close at the Rb-end of the Ba-Rb-Sr triangular diagram (Fig. 26) in a region of the topaz-bearing granites of Haapala (1977a), described as late-stage granites.

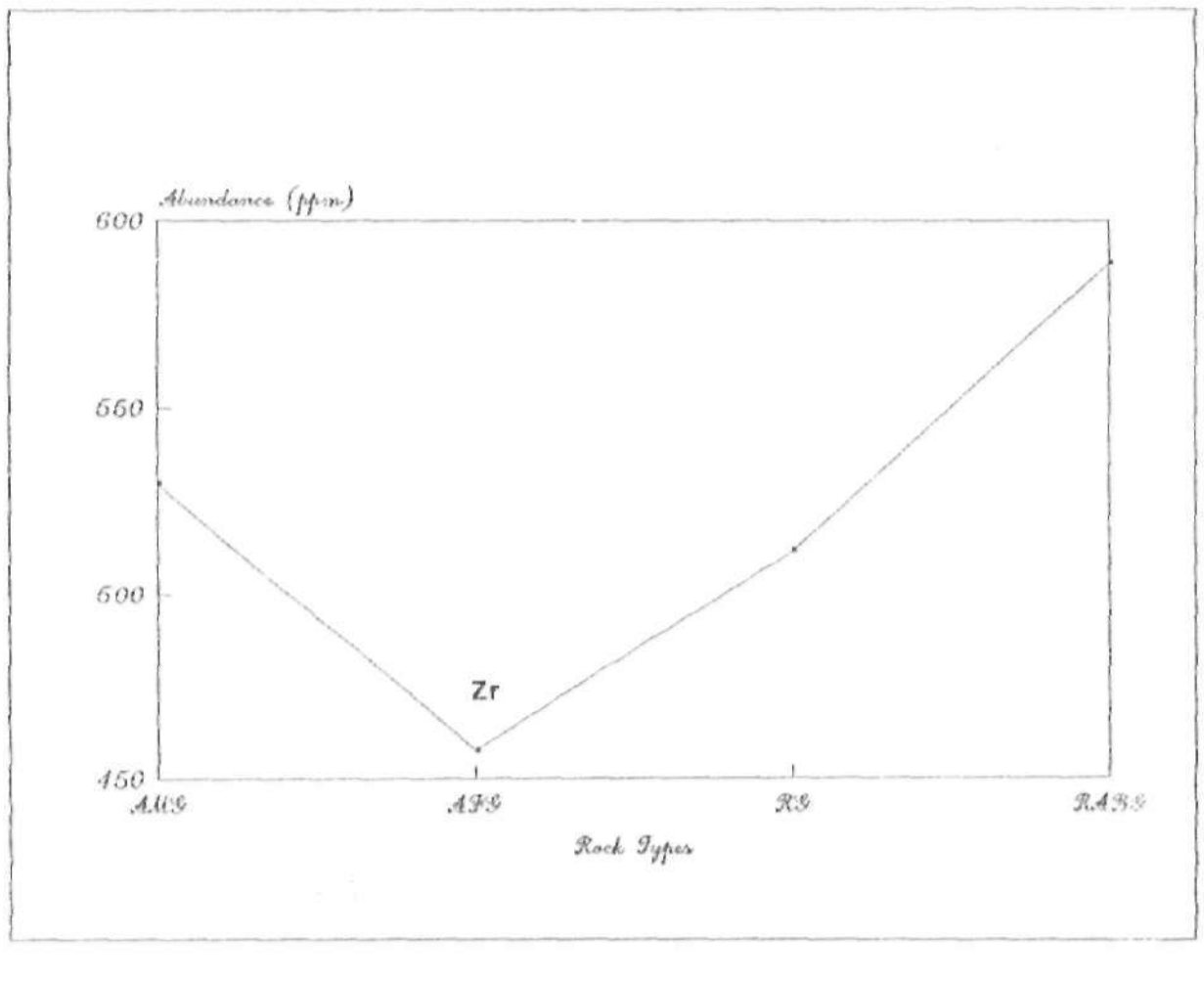


Figure 20. The distribution of Zr in the granites of the Kigom complex.

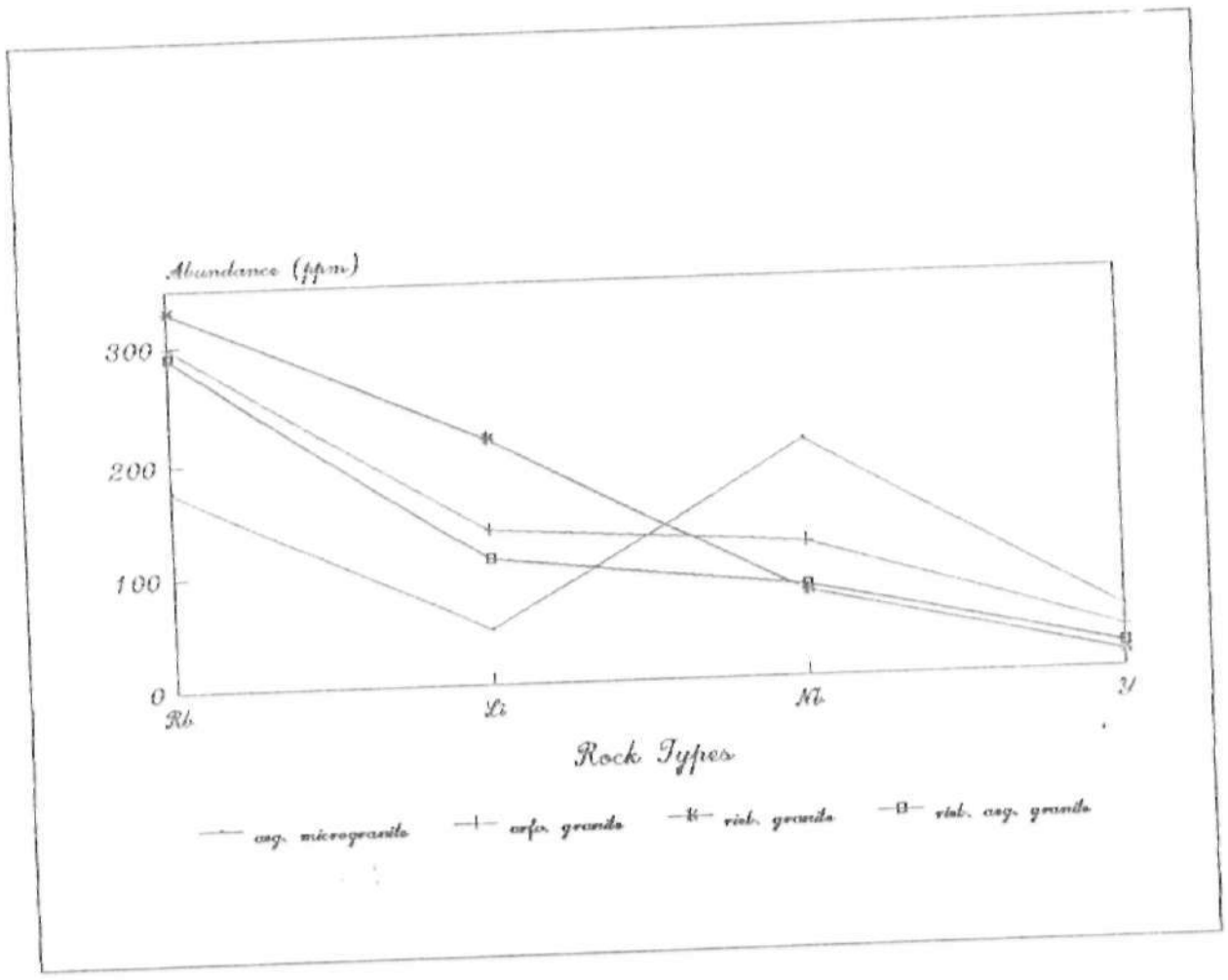


Figure 21. Distribution plot for the trace elements Rb, Li, Zn, Nb and Y in the granites of the Kigom complex.

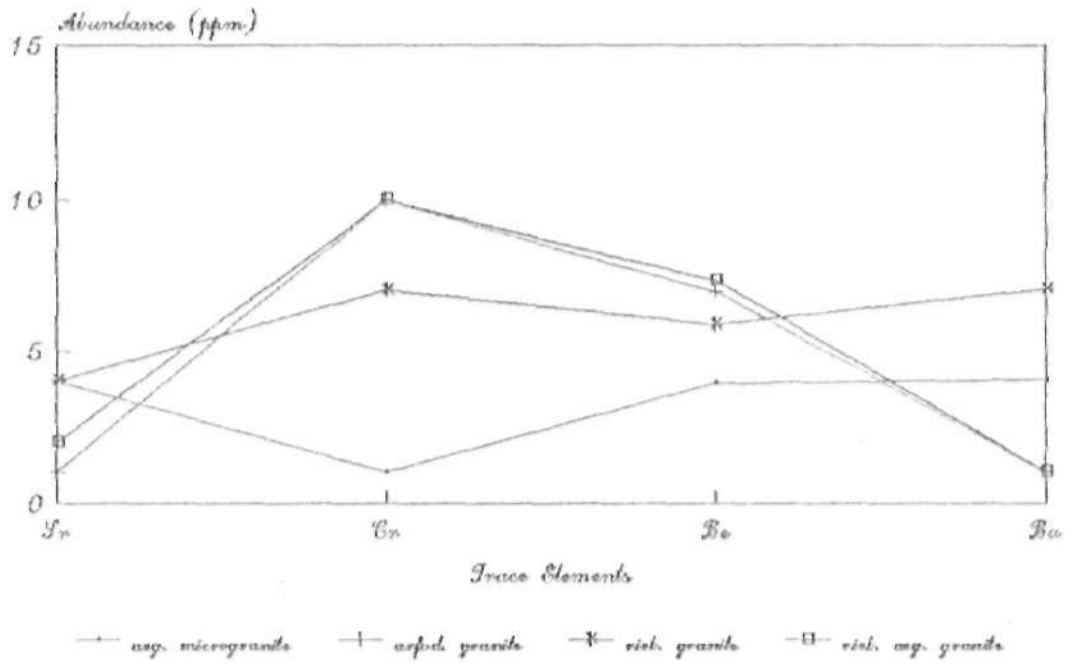


Figure 22. Distribution plot for trace elements Sr, Cr, Be and Ba in the granites of the Kigom complex.

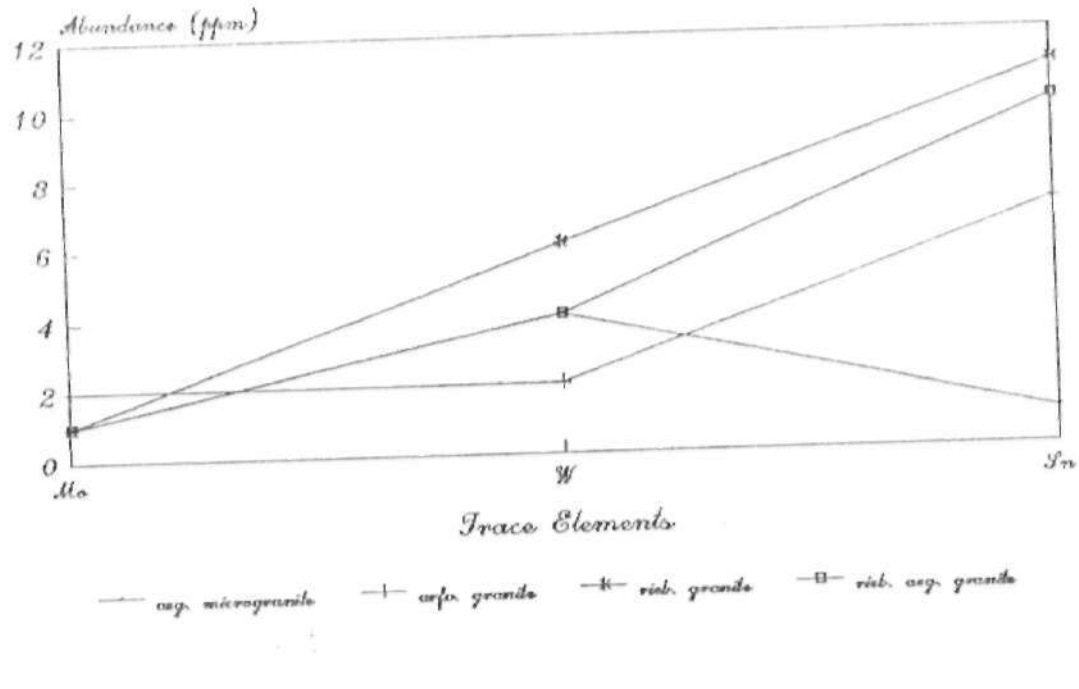


Figure 23. Distribution plot for the trace elements: Mo, W and Sn in the granites of the Kigom complex.

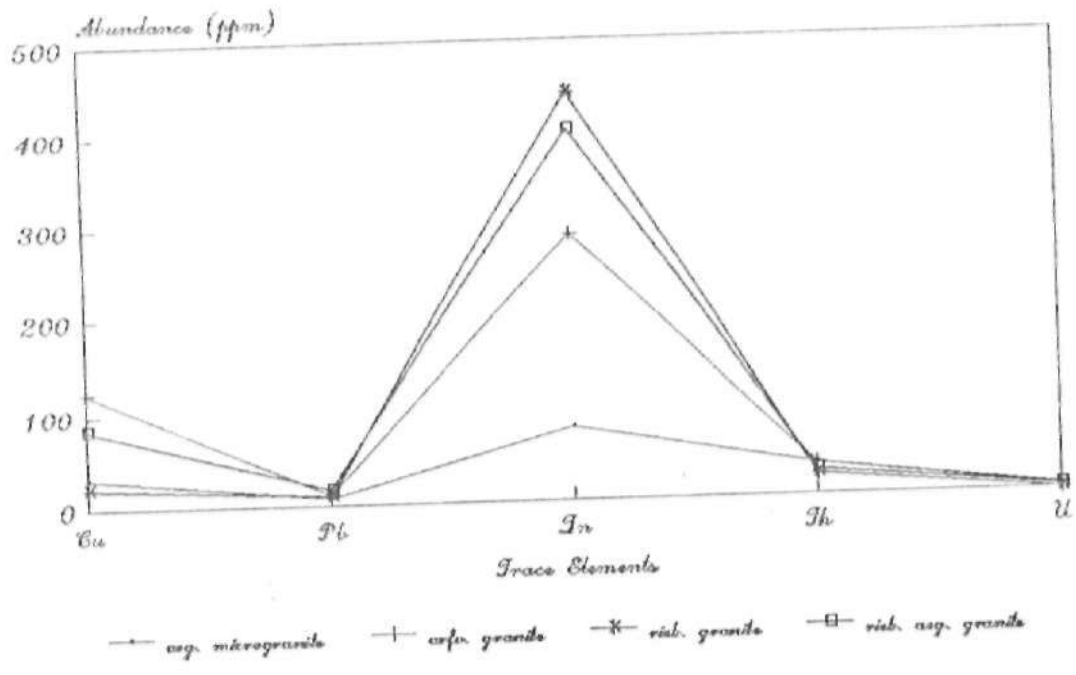


Figure 24. The distribution of Cu, Pb, Th, and U in the Kigom granites.

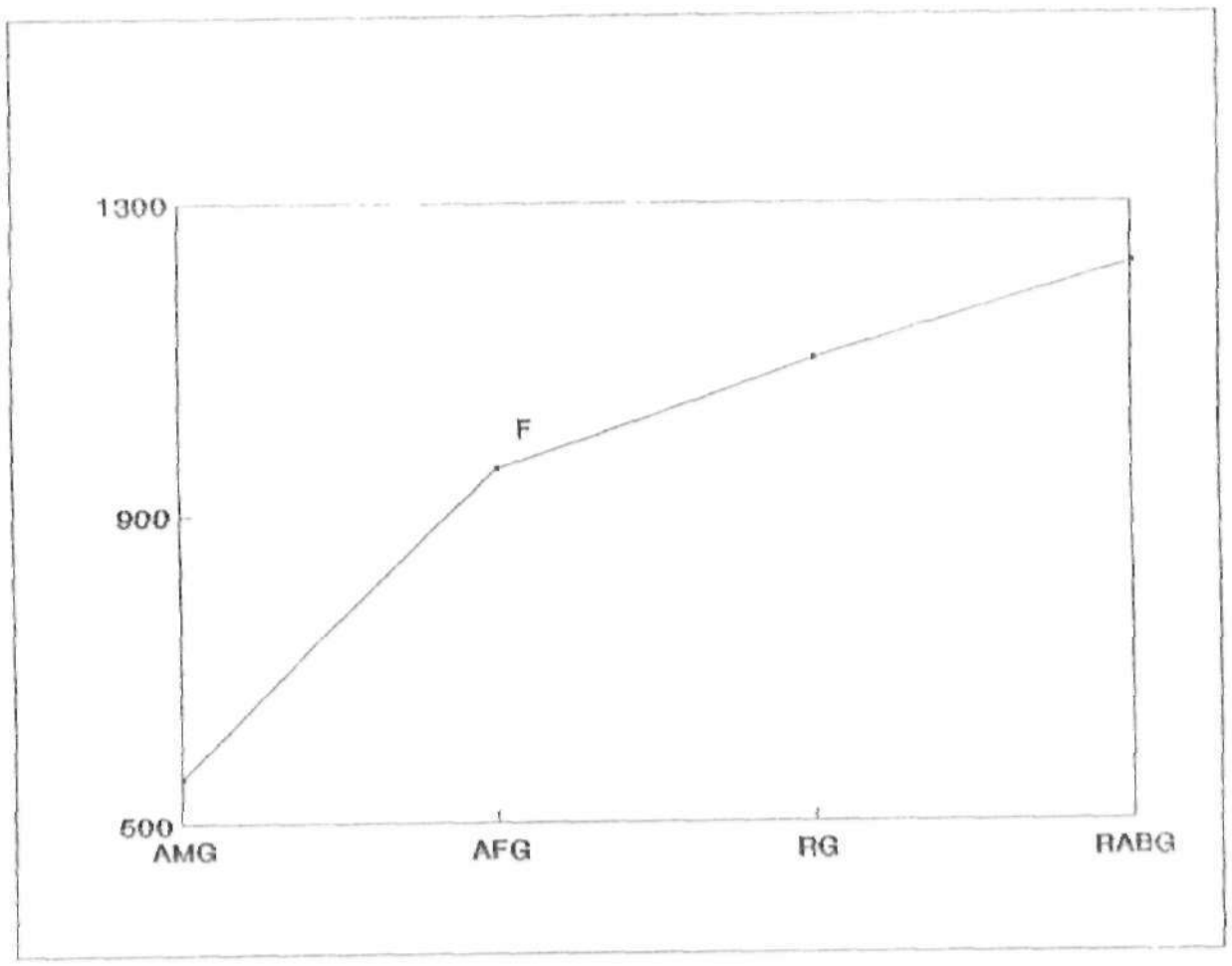


Figure 25. Distribution plot for F in the granites of the Kigom complex. Note the increasing F from the aegirine microgranite to the riebeckite-aegirine-biotite granite.

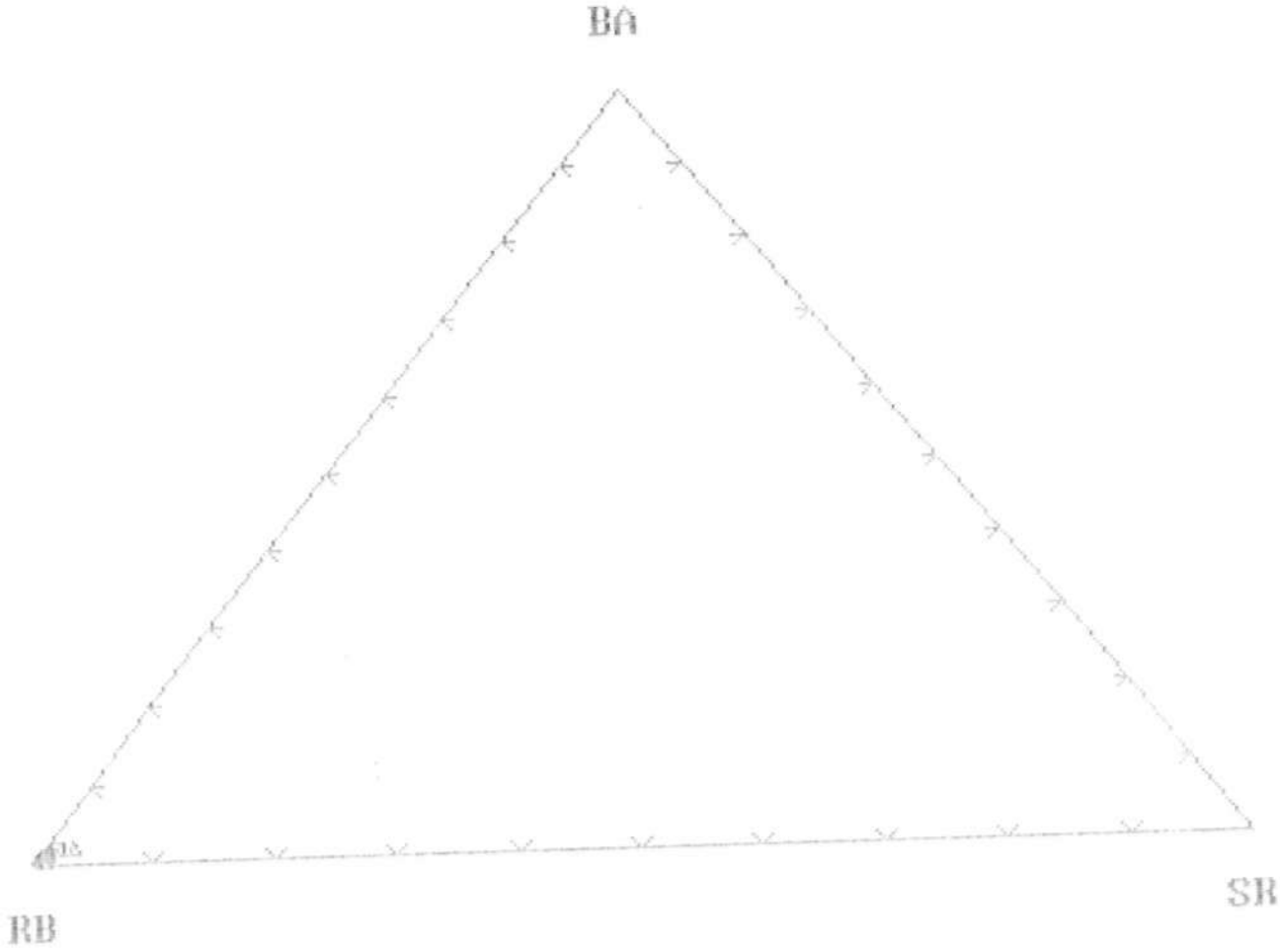


Figure 26. Ba-Rb-Sr triangular plot for the granites of the Kigom complex.

The ore zone of the Kigom is rather strikingly enriched in the trace elements: Pb, Cu, Mo, Zn, Zr, Th, U, Y, Nb, and Be (Table 10, Figs. 27-32), compared to the other parts of the Kigom. The enrichment reflects the zoning of the mineralisation into the pyrite zone and the molybdenite zone. Pb increases from 18 ppm in the pyrite zone to as high as 3.48% in the molybdenite zone (Fig. 27). This is due mainly to the presence of galena. Mo increases from 2 ppm in the pyrite zone through 12-85 ppm at the edges of the molybdenite zone to 0.28% in the center; Mo typically shows a steep gradient in mineralised plutons (e.g., Bright, 1974) (Fig. 28). Th is highest in the pyrite zone with 131 ppm, but varies between 22 and 77 ppm (Fig. 29) in the molybdenite zone. Zr has a similar distribution, varying from 739 to 1393 ppm in the molybdenite zone to 7134 ppm in the pyrite zone (Fig 30). Y ranges from 148-369 ppm in the molybdenite zone to 894 ppm in the pyrite zone. Nb is most enriched in the pyrite zone, with 950 ppm; it varies from 289 ppm to 329 ppm in the molybdenite zone (Fig. 31). Cu increases from 372 ppm in the pyrite zone to 461 ppm in the molybdenite zone. Zn and U show similar trend to that of Cu (Fig 29). W does not show any preferential enrichment having an abundance of 2-4 ppm. Sn, Bi, As and, to some extent, Li, are enriched in the molybdenite zone (17, 143, 16 and 1860 ppm, respectively, Fig. 32). Sr, Co and Ba are depleted in both zones. Be, 24.5 ppm, is very high at the pyrite zone close to the contact with the basement. It has low values of 2.5 ppm in the molybdenite zone. Thus, the pyrite zone typically shows higher values of Zr, Th, Nb, and Be, whereas the molybdenite

zone is richer in Mo, Cu, Zn, U, and Pb; mostly chalcophile elements. The felsic dyke at the ore zone is the most enriched part of the Kigom complex in Zr, Nb, Y, Rb, Th, and U, with abundances of 3.82%, 3885ppm, 1899 ppm, 1041 ppm, 1829 ppm, and 159 ppm, respectively (Table 11). This enrichment may be related to the abundance of zircon which is the main accessory mineral at the margin and to the concentration of alkali-bearing minerals in the rocks. Zircon is a known to be a good host to many of the above-named elements (Elande et al., 1978). The alkali (K_2O/Na_2O) ratio is high (1.91). This is probably responsible for the high Rb values. Sn is also most enriched in the dyke with an abundance of 94 ppm (Table 11). Compared with the compositions of the pyrite zone of the ore zone, Mo and W also are slighly enriched, both having an abundance of 6 ppm (Table 11).

Though with relatively high values compared with those in the basement, the pegmatite dyke of the Kigom complex does not show any relative enrichments in trace elements compared to those of the host rocks (Table 11). The rhyolite dyke, however, is enriched in Zr, Nb, Rb, Zn and Be (Table 11). The content of Zr, 1024 ppm, is higher than those for the granites. Pb, Cu, Zn, Y, Mo and Cr are relatively depleted.

The high concentration of high field strength elements such as Ti, Zr, Y and Nb, and the low values of low-field-strength elements such as Ba and Sr in the Kigom granites are indicative of a late stage in the fractionation/differentiation sequence. Compared with average A-type granites, the enrichment of the Kigom

rocks in elements like Zr (>500 ppm), Nb(>25 ppm), Y (>60 ppm), and Th (>15 ppm) coupled with a high Rb/Sr ratio is typical of peralkaline suites (Bowden, 1985; Abaa and Omada, 1990). The high values of Zr suggests that the granites represent magmas that have crystallised from shallow subvolcanic intrusions and suffered subsolidus recrystallisation. They are also typical of peralkaline granites (Whalen et al., 1987) and tin-barren granites (Cf; Olade, 1980) to which class the Kigom granites belong. Mo-rich granitic systems, like those of Kigom, are known to be typically Rb-rich but Sr-poor. A typical example is the Climax Mo deposit, which is associated with peralkaline granites (Westra and Keith, 1981).

These geochemical signatures indicate that all samples of the Kigom granites are closely related and evolved from the same parental magma which, however, differentiated during crystallisation.

Compared with the Bordvika granites which share similar tectonic and petrological characteristics (Gyeti and Schonwandt, 1979), the Kigom granites are more enriched in Nb, Zr, Y, Rb, Th, F, U and V, but are depleted in Ba and Sr. These enrichments are reflected in the very high Rb/Sr, Rb/Ba, Zr/Y, Zr/TiO_2 and F/Zr ratios (Table 10), indicating that the Kigom represents highly differentiated shallow-level granites.

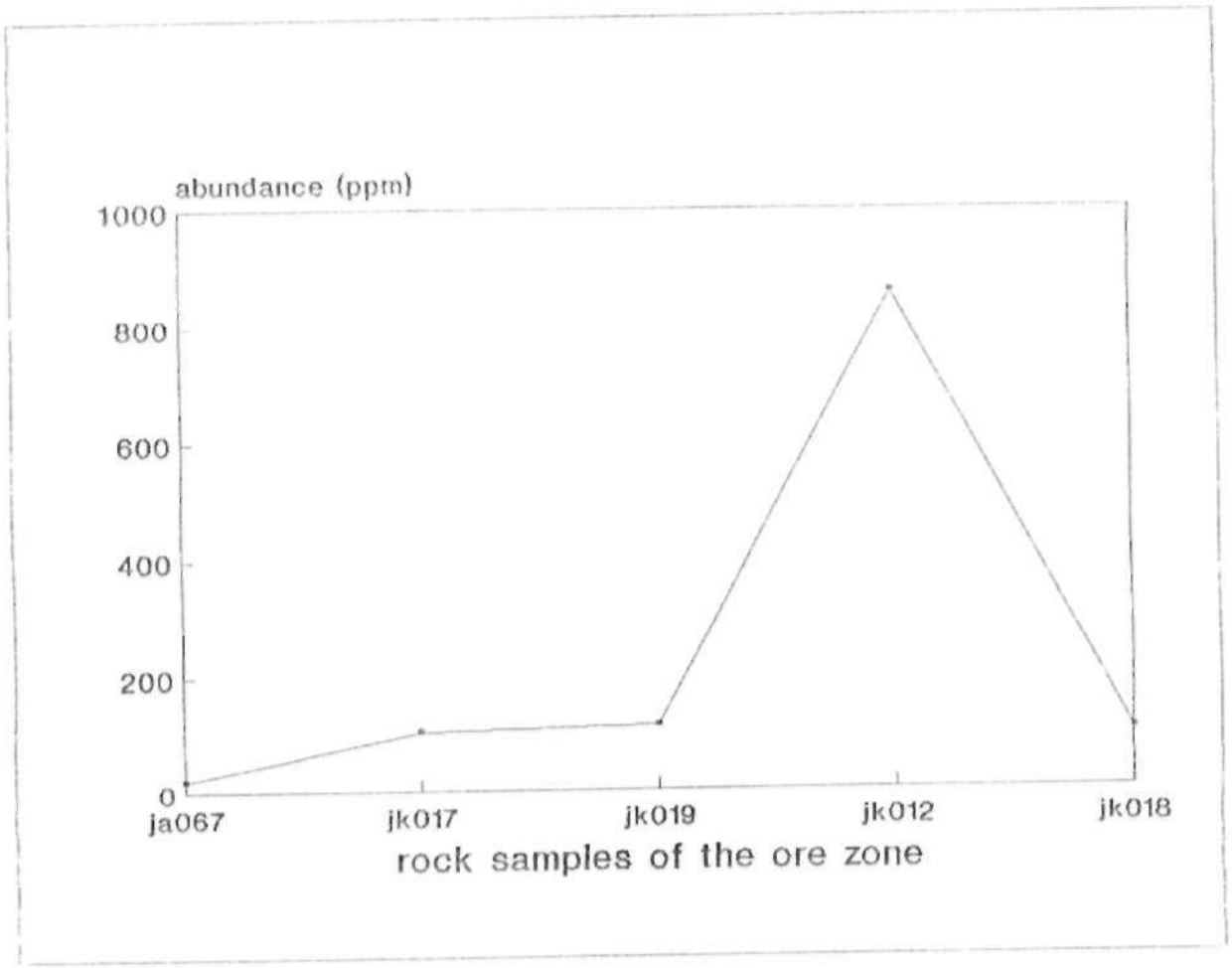


Figure 27. Distribution plot for Pb in the ore zone of the riebeckite granite.

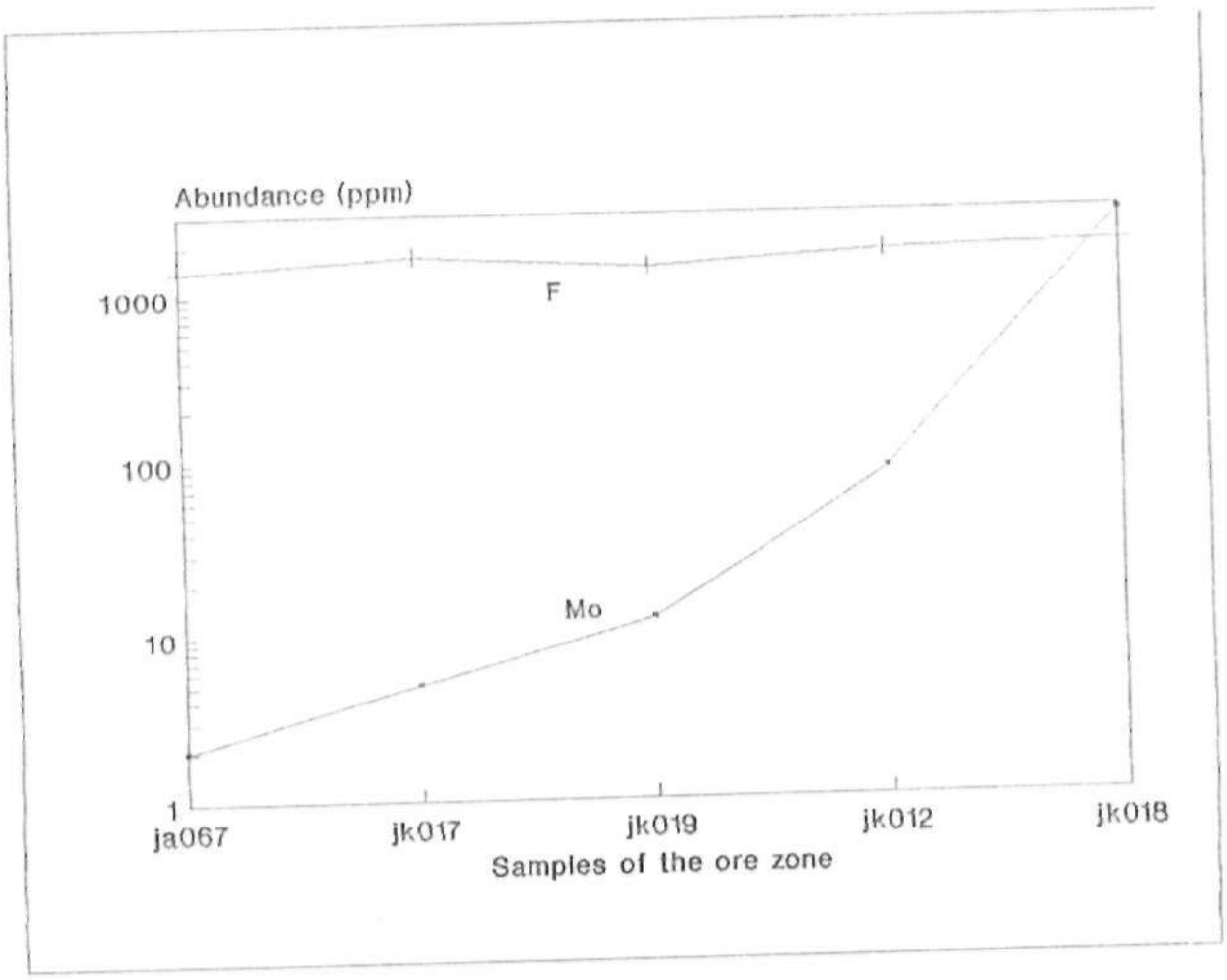


Figure 28. Distribution plot for F and Mo in the ore zone of the riebeckite granite.

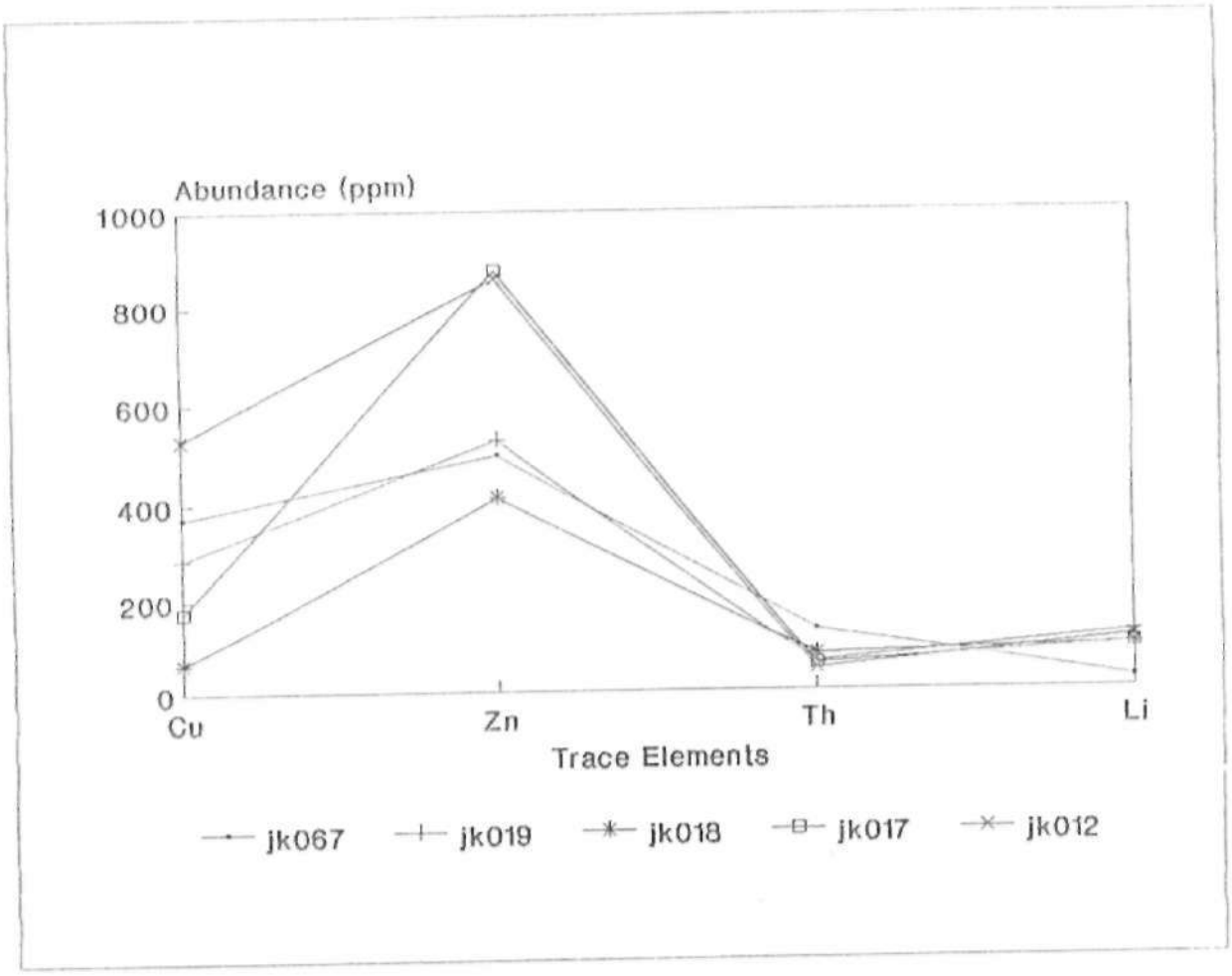


Figure 29. Distribution plot for the trace elements: Cu, Zn, Th and Li for the ore zone of the riebeckite granite.

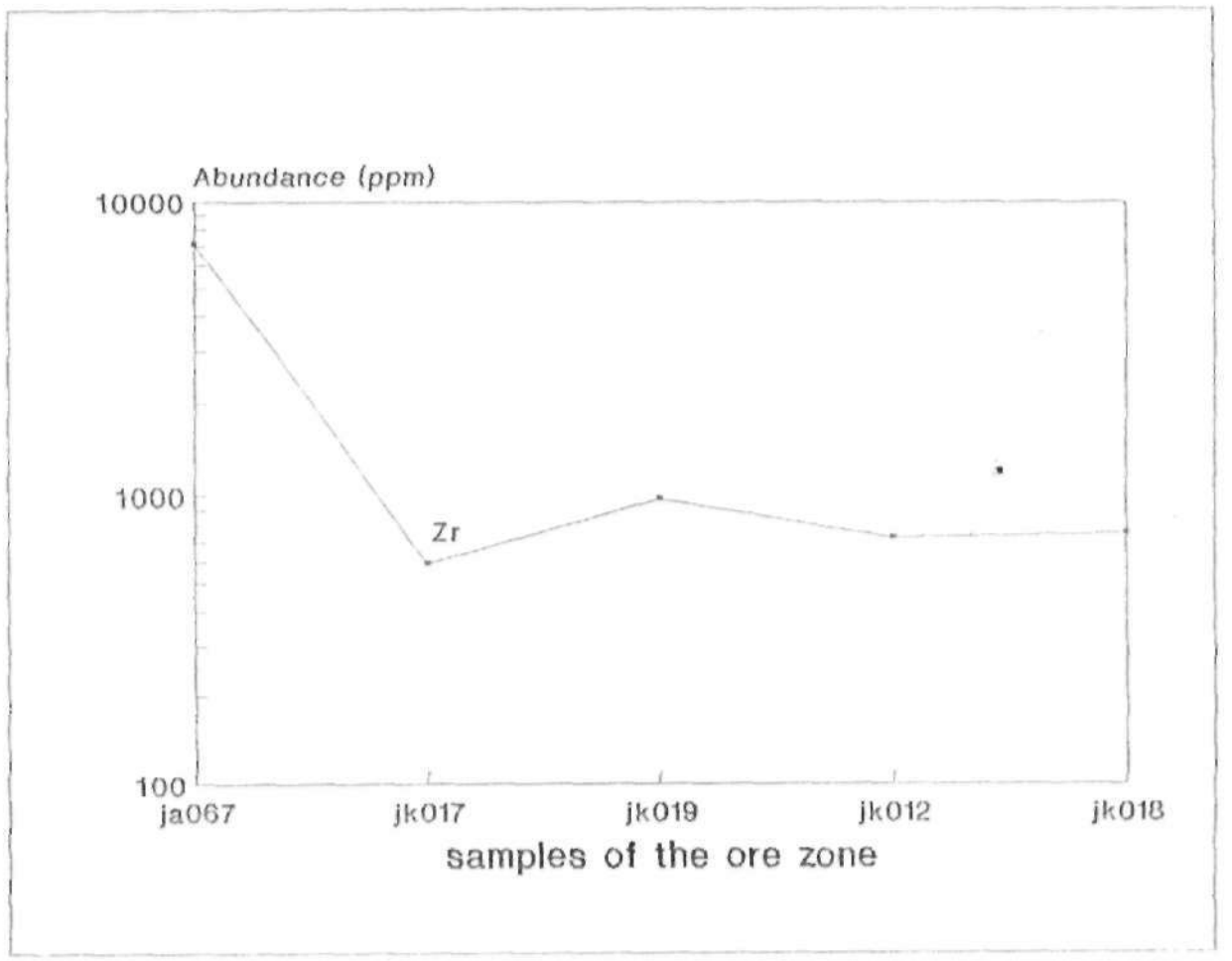


Figure 30. The Distribution of Zr in the riebeckite granite at the ore zone of the Kigom complex

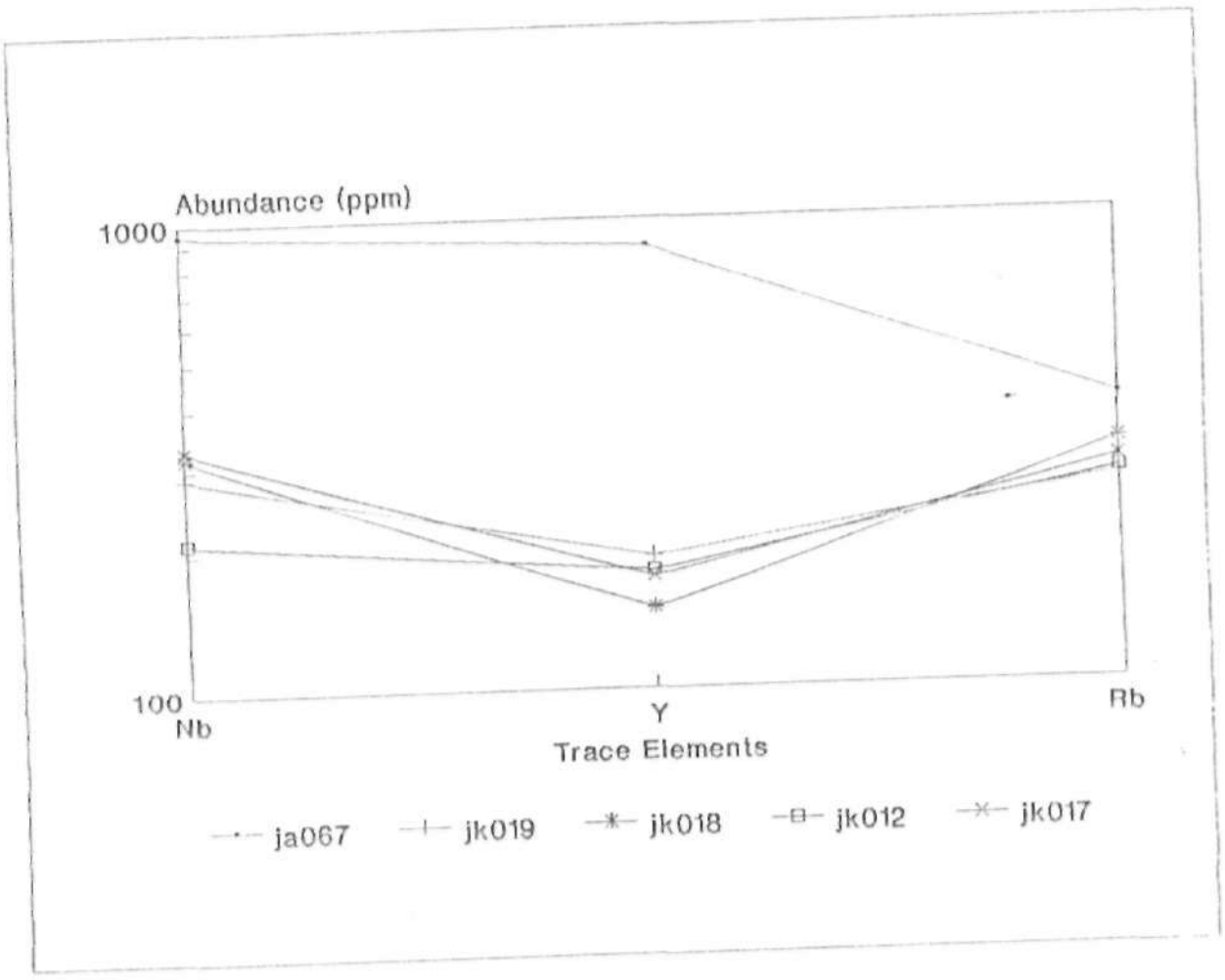


Figure 31. The Distribution of Nb, Y, and Rb at the ore zone of the Kigom complex.

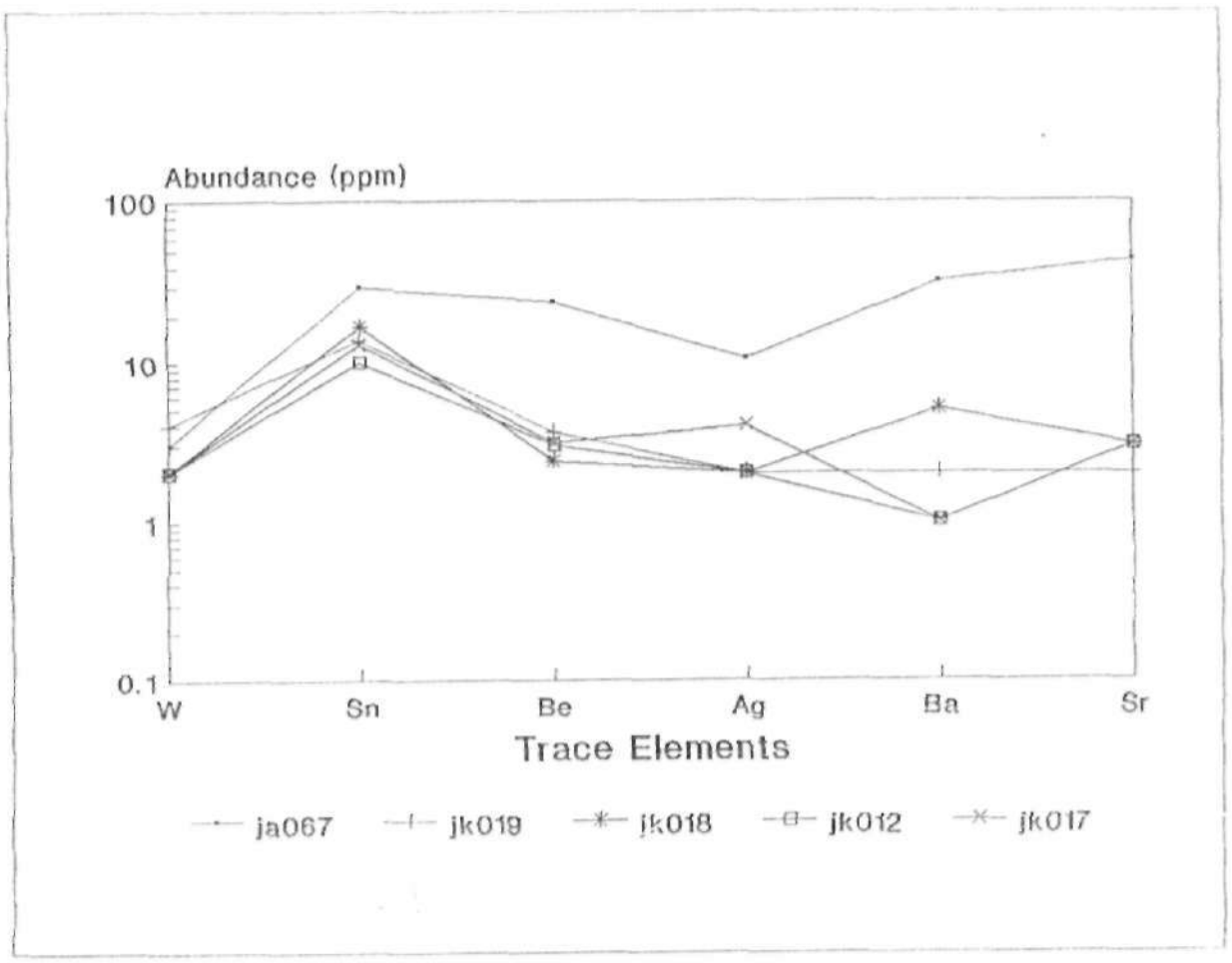


Figure 32. Distribution plot for the trace elements: W, Sn, Be, Ag, Ba and Sr for the ore zone of the riebeckite granite.

6.4 MINERAL CHEMISTRY

Fayalite

Fayalite in the aegirine microgranite consists of 29.3% SiO_2, 70.01% FeO, 1.5% MnO and 0.01% MgO (Table 12). The altered part of the mineral which is generally found in cracks and at margins has lower values of the major oxides, resulting in lower totals (Table 13). This extremely iron-rich composition indicates that the fayalite crystallised from a highly evolved magma. The alteration probably reflects a combination of hydration and oxidation owing to the introduction of H_2O from an external source into the microgranite.

Amphiboles

The sodic amphiboles in the riebeckite-bearing granites contain 49-50 wt% SiO_2, 7-8.11 wt% Na_2O, 14-18 wt% FeO, and 18-25 wt% Fe_2O_3 (Table 14). Minor amounts of Al_2O_3, K_2O, MnO, MgO, TiO_2 and CaO are also present. The riebeckites within the mineralised zone do, however, show a decrease in the K_2O, and this is reflected in their low totals. The riebeckites are F-rich having between 1.55% and 2.55% abundance. Cl is however rarely present having only traces of 0.01 wt% abundance in the minerals.

Table 12. The average composition of fayalite in the aegirine microgranite of the Kigom complex.

Oxides (wt%)	1	2
SiO_2	29.35	28.62
TiO_2	nd	nd
Al_2O_3	nd	nd
FeO	70.04	67.56
CaO	0.01	0.01
MnO	1.53	1.50
K_2O	nd	nd
Na_2O	nd	nd
Total	100.93	97.69

nd not determined

1 unaltered fayalite

2 altered fayalite

Table 13. The average composition of amphiboles from the Kigom complex.

Oxides (wt%)	arfvedsonite	riebeckite	riebeckite at ore zone
SiO_2	50.94	49.41	49.56
TiO_2	1.02	0.73	0.90
Al_2O_3	1.20	0.89	0.92
Fe_2O_3	14.67	16.21	17.27
FeO	19.26	20.11	17.28
MnO	0.32	0.36	0.49
MgO	0.02	0.00	0.01
CaO	0.06	0.42	0.30
Na_2O	8.03	7.78	7.60
K_2O	1.52	1.38	1.40
H_2O	0.84	0.91	1.04
F	2.27	2.09	1.83
Cl	0.00	0.00	0.02
O=F	-0.96	-0.88	-0.77
Total	99.21	99.42	99.85
number of ions on the basis of 24 anions			
Si^{IV}	7.95	7.79	7.77
Al^{IV}	0.05	0.16	0.17
Fe^{+3}	0.00	0.04	0.06
T site	8.00	8.00	8.00
Al^{VI}	0.17	0.00	0.00
Fe^{+3}	1.17	1.88	1.98
Ti	0.12	0.09	0.11
Mg	0.00	0.00	0.00
Fe^{+2}	2.51	2.65	2.53
Mn	0.04	0.05	0.07
Ca	0.01	0.07	0.05
M1,2,3 site	4.59	4.74	4.73
Ca	0.01	0.07	0.05
Na	1.99	1.93	1.95
M4 site	2.00	2.00	2.00
Ca	-0.01	-0.07	-0.05
Na	0.44	0.45	0.36
K	0.30	0.28	0.28
A site	0.73	0.66	0.59
O	22.00	22.00	22.00
OH	0.88	0.96	1.09
F	1.12	1.04	0.91
$Ca+Al^{IV}$	0.07	0.23	0.22
Si+Na+K	10.68	10.45	10.36

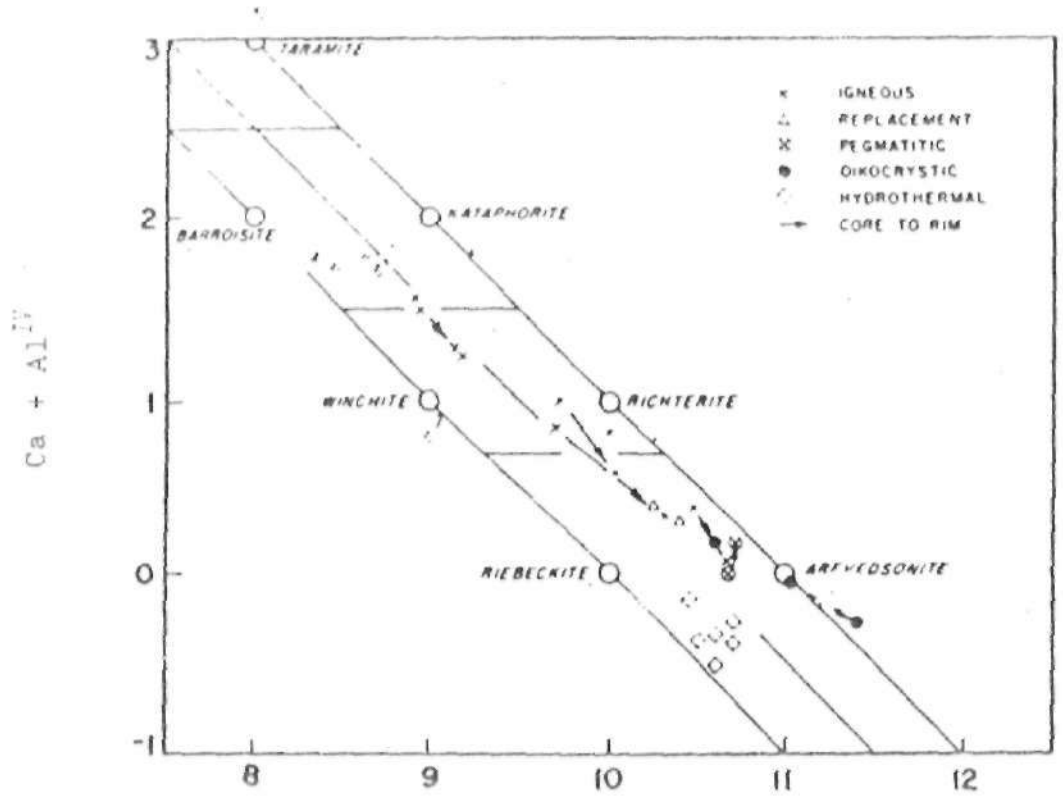


Figure 33. Amphibole classification diagram of Strong and Taylor (1984)

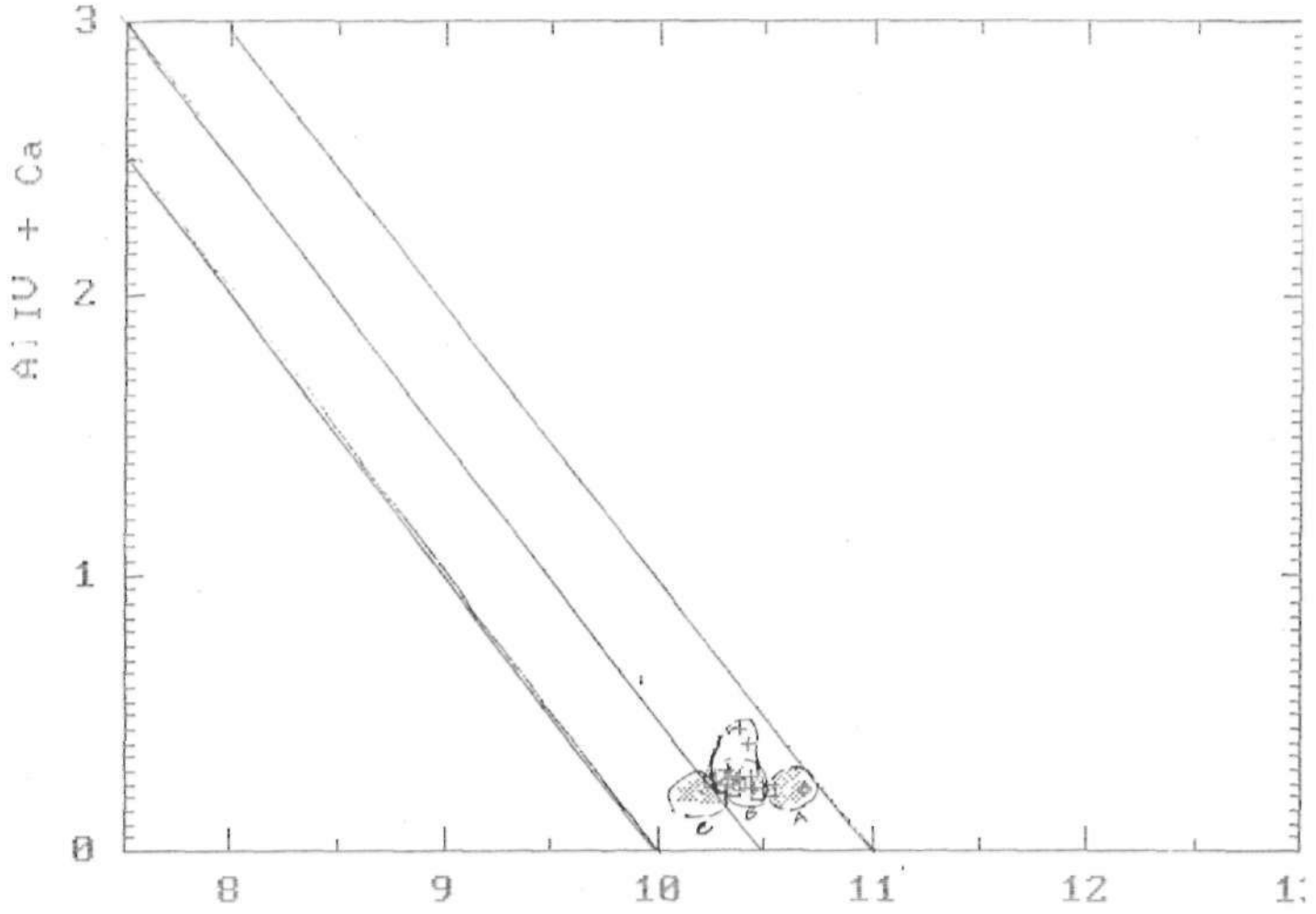


Figure 34. The Si + Na + K / Ca + Al^{IV} plot for the amphiboles in the Kigom complex. Note the increasing riebeckite composition from the amphiboles in the arfvedsonite granite (A) through those of the riebeckite-bearing granites (B) to the amphiboles from the ore zone (C).

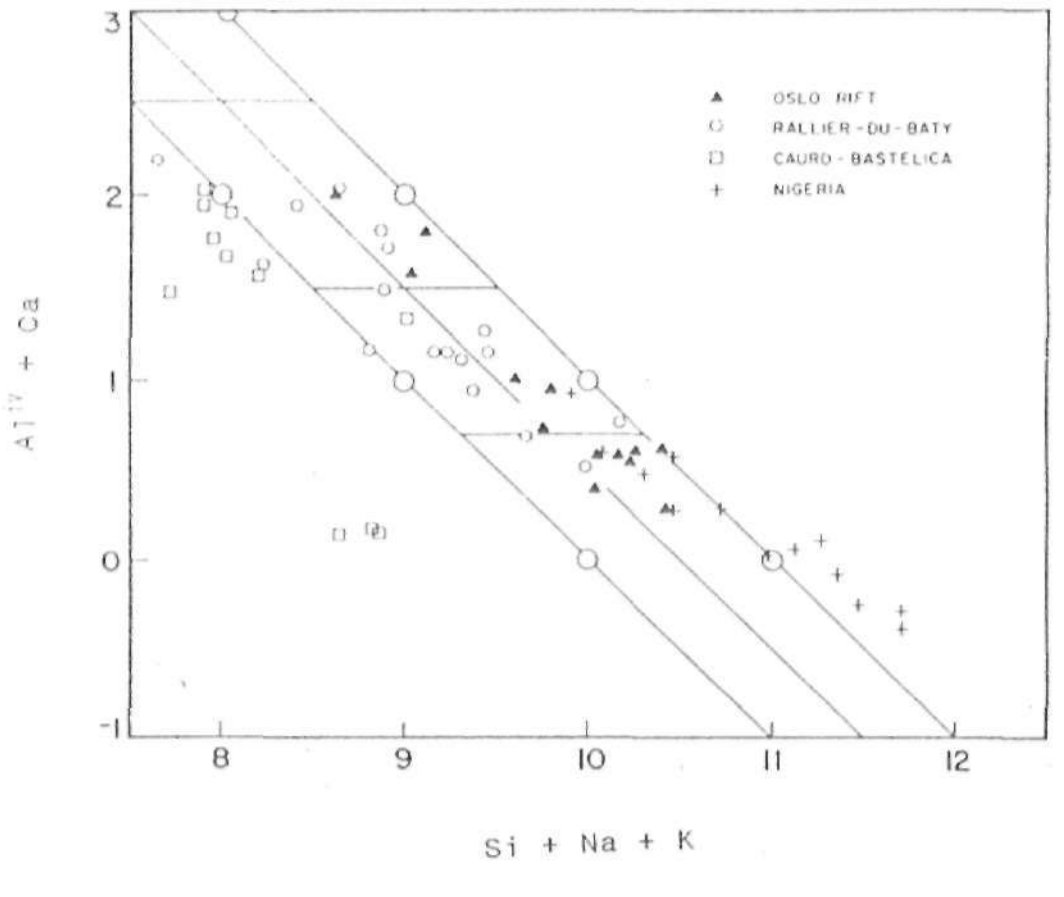


Figure 35. Plot of amphiboles from peralkaline rocks of the Oslo Rift (Neuman, 1976), the Rallier-du-Baty Pennisula, Kerguelen (Marot and Zimme, 1976), and Cauro-Bastelica, Corsica (Giret et al., 1980), and the Younger Granites of Nigeria (Borley, 1963).

The lower values of the K_2O in the riebeckite grains in the ore zone is due to the loss of K^+ used in the formation of metasomatic biotite in the post crystallisation hydrothermal alteration related to the latter influx of the mineralising fluids.

Compared with the riebeckites, the arfvedsonites show higher values of 2.6 wt% Ca and a complementary increase in F with a 3.4%: thus resulting higher totals (for example, sample 008d). There is, however, a decrease in the FeO content from 14 wt% in riebeckites to 11 wt% in the arfvedsonites indicating that the Ca^{2+} has substituted for the Fe^{2+} most likely due to similarity in charge.

The amphiboles are thus, generally rich in Si + Na + K, but are poor in Ca + ^{VI}Al, reflecting their alkali character. The ^{VI}Al + Ca^{2+} vs Si+Na+K plots for amphiboles (Fig. 33), define three groupings (Fig. 34): the arfvedsonites plotting in the arfvedsonite field of Giret et al. (1980) and Strong and Taylor (1984); the riebeckites from the riebeckite granites plotting in the arfvedsonite-riebeckite field; the riebeckites from the ore zone plotting in the riebeckite field. This trend of the amphiboles is indicative of oxidation (Stong and Taylor, 1984) during mineralisation, and it indicates that the amphiboles in the Kigom were primarily arfvedsonitic. Using the criteria of Giret et al (1980) and Strong and Taylor (1984), these texturally oikocrystic amphiboles can be referred to as "riebeckitic-arfvedsonites" and can be classed subsolidus amphiboles (Fig. 33). Similar compositional plots (Fig. 35) have been obtained from amphiboles from peralkaline granites of the Oslo rift (Neumann, 1976) and of

some of the Younger granites of Nigeria (Borley, 1963).

Biotite

Biotite, has a composition containing SiO_2 and Na_2O abundance of 35 wt% and 0.14 wt%, respectively, (Table 15) indicating a depletion compared to the values of those of the amphiboles. K_2O, Al_2O_3 and TiO_2 are, however, enriched having 9.7 wt%, 17.8 wt% and 1.8 wt%, respectively. FeO and Fe_2O_3 do not show significant changes with respect to the amphiboles. MgO is low.

The composition of the biotites is related to their hydrothermal origin (Chapter 4). The biotites have crystallised from post magmatic influx of K-rich fluids. MgO is normally not available during this stage of crystallisation and thus has very low abundances in the mineral. The composition of the hydrothermal fluid and the subsequent K-for-Na ion exchange between the amphiboles and the fluids are responsible for the high abundances of K_2O, Al_2O_3 and TiO_2 in the mineral.

Aegirine

Aegirine in the Kigom granites are FeO-, Na_2O-, and F-rich with 34.12% Fe, 6.9% Na, and 1.42% F, respectively (Table 15). Al_2O_3 is very low: 1.09% Al, and there are no K_2O, CaO, MgO and MnO in the aegirines indicating that sodic metasomatism was responsible for the formation of the mineral.

Table 14. The average composition of biotite in the Kigom complex.

Oxides wt%	
SiO_2	35.22
TiO_2	1.83
Al_2O_3	7.10
FeO	39.79
CaO	0.02
MnO	0.20
K_2O	9.00
Na_2O	0.02
H_2O	2.61
F	1.81
Cl	0.01
O=F	-0.76
Total	96.87
number of ions on the basis of 24 anions	
Si^{IV}	6.20
Al^{IV}	1.47
Ti^{IV}	0.24
T site	7.91
Fe^{+2}	5.86
Mn^{+2}	0.03
Mg	0.01
O site	5.89
Na	0.01
K	2.02
A site	2.03
O	20.00
OH	2.99
F	1.01

Table 15. The average composition of aegirine in the granites of the Kigom complex.

Oxides wt%	
SiO_2	49.74
TiO_2	0.65
Al_2O_3	1.10
FeO	34.12
CaO	0.01
MnO	0.43
K_2O	0.01
Na_2O	6.85
F	1.42
Total	94.44
number of ions on the basis of 6 anions	
Si^{IV}	2.16
T site	2.16
Al^{VI}	0.06
Ti	0.02
Fe^{+2}	1.24
Mn^{+2}	0.02
Na	0.58
M1, M2 site	1.91
O	6.00

ASTROPHYLLITE

Astrophyllite shows abundances of 5.4%, 2.8-3.0%, 34.4-35.4%, 8.3-8.7%, and 35.6-36.7%, respectively, of K_2O, Na_2O, SiO_2, TiO_2 and FeO. MnO varies between 1.10-1.12%, whereas Al_2O_3 and CaO have 0.05-0.16 and 0.1-0.71% abundances, respectively. Only traces of MgO are recorded (Table 16). The high values of TiO_2 and MnO are diagnostic of astrophyllite since structurally, it contains continuous sheets of $(Fe,Mn)O_6$ octahedra which are sandwiched between two sheets composed of chains of Si-O tetrahedra joined by Ti-O octahedra (cf: Deer et al., 1966). Alkali ions: K^+ and Na^+, separate the composite sheets.

The formation of astrophyllites is related to the metasomatic reaction of the alkali-rich fluid with feldspars and the amphiboles. In the ore zone, this mineral overlies molybdenite, indicating that the astrophyllite-formation precedes that of the molybdenite. The high values of TiO_2 in the astrophyllite is indicative of an increasing acidity of the fluid at time of formation. This is consistent with late crystallisation associated with alkali-rich fluids involved in postmagmatic metasomatism.

FELDSPAR

All the representative samples of the granites of the Kigom complex contain pure, ordered albite; the most potassic of albite has $Ab_{98.2}Or_{1.2}$ (Table 17). On the other hand, the K-feldspar is

microcline in all cases, but its composition and degree of Al-Si order vary a bit from sample to sample. In terms of composition Or content ranges from 87.8 to 99% Or, and degree of order ranges from t_1O = 0.93 to t_1O = 1.00. In end-member (pure) microcline, $KAlSi_3O_8$, N_{Or} = 100%. In fully ordered microcline, t_1O, the proportion of Al in the T_1O site, is 1.00.

The composition of the microcline from the fayalite-bearing aegirine microgranite and the riebeckite granite (including that at the ore zone) indicate that the conversion of orthoclase to microcline did not go in to completion in these rocks since their K-feldspars have $t_1O > 1.00$. Microcline from the arfvedsonite granite and the riebeckite-aegirine-biotite granite is fully ordered with t_1O = 1.00; this indicates that the conversion to microcline in these rocks was complete. The conversion of orthoclase to microcline and the degree of Al-Si order of albite and microcline are related to the metasomatic reaction between perthite and the-latter influx of alkali-rich hydrothermal fluid into the system. The degree of order is dependent on the reaction time between the fluid and the earlier crystallised minerals: the fayalite-bearing aegirine microgranite and the riebeckite granite that constitute the outer units of the Kigom complex had the least reaction time with the fluid due to loss of heat and high cooling rate, and therefore have the less ordered microcline. The arfvedsonite granite and the riebeckite-aegirine-biotite granite that constitute the inner units of the Kigom complex, on the other hand, have fully ordered microcline. Since microcline is stable in

nature at a temperature of ≤ 450 °C, the-latter granites of the Kigom complex with fully ordered microcline thus consolidated at temperatures of < 450 °C.

Table 16. The average composition of astrophyllite in the ore zone of the Kigom complex.

Oxides (wt%)	
SiO_2	35.37
TiO_2	8.29
Al_2O_3	0.05
FeO	36.66
CaO	0.12
MnO	1.10
MgO	0.00
K_2O	5.37
Na_2O	3.03
F	1.09
O=F	-0.46
Total	94.10
number of ions on the basis of 24 anions	
Si^{IV}	6.36
Al^{IV}	0.12
Ti^{IV}	1.12
T site	7.60
Fe^{+2}	5.52
Mn^{+2}	0.17
Mg	0.00
O site	5.69
Ca	0.02
Na	1.06
K	1.23
A site	2.31
O	20.00
OH	3.38
F	0.62

Table 17. Indicators of composition and Degree of Al-Si order in K-rich and Na-rich feldspars in Representative samples of the Kigom Younger Granite complex.

		K-rich feldspar			Na-rich feldspar			
S\No	Description	N_{Or}	t_1O	Δ	An	N_{Or}	t_1O	Δ_{131}
B000	rieb gr (ore)	99.0	0.93	0.91	0	0.7	1.00	1.086
003	rieb. aeg. grt	98.0	0.98	0.95	0	0.3	1.01	1.088
006	rieb gr (ore)	99.2	0.96	0.93	0	1.2	1.00	1.083
025	rieb. granite	96.0	1.00	1.01	0	1.2	1.01	1.097
034	Ae-Fa granite	96.0	0.95	0.91	0	1.0	1.00	1.099
044	arfv. granite	99.2	1.00	1.01	0	1.8	1.01	1.096
063	rieb. granite	87.8	0.94	0.95	0	1.1	1.01	1.089

Composition N_{Or} is expressed in mole % Or, and was calculated using the equation of Kroll and Ribbe (1983) relating unit-cell volume to N_{Or} for felspar compositions that are structurally ordered (i.e., that belong to the low microcline - low albite series). The degree of Al-Si order, expressed by t_1O, was computed using the equations of Blasi (1977). The error in N_{Or} and t_1O is believed to be ±0.015 in most cases. The obliquity Δ of a microcline is equal to 12.5 (d_{131} - d_{131}); it should have a value of 1.00 for fully ordered microcline.

CHAPTER SEVEN

DISCUSSION

7.1 INTRODUCTION

The petrogenesis of the Kigom granites and the genesis of the associated Mo are discussed in this chapter.

7.2 PETROGENESIS

7.2.1 Mode of Emplacement

The Kigom complex is one of the 40 Complexes within the Younger Granite Province of Nigeria that intruded during the Jurassic (Macleod et al., 1977). The Complexes form a northerly trending structurally controlled chain along existing Pan-African trends within the basement and continues southwards to South Africa along a zone of inferred crustal separation of the African and South American continents. These complexes thus evolved as a result of intracratonic rifting followed by mid-plate magmatism. The Younger Granite complexes of Nigeria thus belong to the intracratonic subgroup of the 'A-type Granites' as distinct from the 'post-orogenic A-type Granites'. Examples of the post-orogenic A-type granites are the Tertiary granites of the Colorado Mineral Belt, U.S.A.

The intrusion of most of the Younger Granite complexes was preceded by ring fracturing and cauldron subsidence. Many of the complexes thus occur as ring dykes. The Kigom complex, however, lacks any evidence of ring fracturing and cauldron subsidence. This, together with its sub-elliptical shape suggest that the Kigom intruded as a cupola most likely during the closing phases of the mid-plate magmatism in Nigeria.

7.2.2 Textural and Mineralogical Evidence

Texturally, the generally medium- to coarse-grained texture of the Kigom granites indicates crystallisation from a slowly cooled magma. Mineralogically, the Kigom granites show variations in the texture and in compositions of the sodic amphiboles and in the co-existing feldspars in microperthite. The microperthites show exsolution and hydrothermally modified exsolution textures in which the minerals become more albitic or pethitic depending on whether or not such perthite is close to a crystallising amphibole. In the sodic amphiboles, generally oikocrystic and interstitial to the perthites and optically riebeckitic but chemically arfvedsonitic, the variations follow a path of subsolidus oxidation as the granites undergo autometasomatism induced by the influx of alkali-rich hydrothermal fluids. These textures are typically associated with highly differentiated, shallow, high level, water-saturated magmatic intrusions of crustal origin (e.g., Tauch et al., 1986); the perthites differentiating early in the system. The absence of

the plagioclases in the mineral suite reflects the hypersolvus nature of the crystallising fluid.

7.2.3 Hydrothermal alterations

The first major effect of the hydrothermal fluid, also magmatic in origin, is noticed within the fayalite-aegirine microgranite where crystallisation began with fayalite and quartz and could have probably resulted in the formation of fayalite-bearing pegmatite but with the influx of alkali-rich fluid, this was aborted and aegirine had to form in addition to the feldspars and quartz. Thus the bulk of the remaining facies of the crystallising magma was water-saturated. The solidus temperature was therefore lowered and the crystallisation path was shifted from the feldspars which were crystallising as perthites to the amphiboles whose crystals could have been substantial in the subsolidus state. Two groups of post magmatic mineral alterations can, therefore, be recognised: the altered microperthites with modified exsolution textures (early post magmatic), and the altered amphiboles to aegirine, biotite and magnetite, while aegirine altered to hematite (late post magmatic). For the feldspars, it was a K^+ for Na_t ion exchange and for the amphiboles it was Na^+ for Fe^{3+}. The hydrothermal alteration was, therefore, mainly oxidation trend. The later minerals like astrophyllite were deposited under a more acidic condition i.e. lower Ph-higher Eh conditions. Subsequent minerals like zircon (some of which also are primary), fluorite,

and thorite were also crystallised from the hydrothermal fluids. Using these exsolution, modified exsolution and replacement textures, crystallisation can be grouped into the magmatic and the early and late postmagmatic or hydrothermal stages. Magmatic melts that have undergone this pattern of crystallisation are usually associated with mineral deposits especially tin deposits (Taylor, 1979; Martin and Bowden, 1981; Bowden, 1985; Kinnaird, 1985; Kinnaird et al., 1985) and Mo deposits (Westra and Keith, 1981; Mutschler et al., 1981).

7.2.4 Geochemical Evidence

The Kigom granites are characterised by high SiO_2, Na_2O+K_2O, but low CaO, MgO, MnO and TiO_2 and have bulk compositions of alkali feldspar granites that have undergone metasomatism as a result of the later influx of hydrothermal fluids. Like typical 'A' type granites, the Kigom granites are also characteristically enriched in trace elements: Zr, Rb, Nb, Y, and the REE, but also low in Ba and Sr. Some of the enriched trace elements could have been contained within the alkali amphiboles and pyroxenes since these minerals are known to be rich in trace elements such as Zr, Y and Nb (Borley, 1976; Teng and Strong, 1976; Bonin, 1986) and within the microperthites and the accessory minerals. The high-field trace elements are enriched following the early differentiation of the highly silicic magma (>74% SiO_2) and the low solidus temperatures which prevailed in the late-magmatic crystallisation, and the

excess alkali in the hydrothermal fluid (cf: Ludington et al., 1979; Hildreth, 1979). The enrichment of these elements, initially disseminated within the melt, was enhanced by the high fluorine content of the crystallising fluid since the kind of trace element enrichment like that of the Kigom rocks result from their transport as fluoride complexes in the alkali fluids responsible for metasomatism. This is more so since the basement migmatite which are likely to have contaminated the intruding granitic melts (cf: Hutchison and Chakraborty, 1979; Wright, 1970) are also enriched in these trace elements.

The high values of Zr/TiO_2, Rb/Sr, Rb/Ba, and Na_2O+K_2O/Al_2O_3 ratios clearly indicate that the Kigom represents highly differentiated peralkaline granites. The generally high Na_2O/K_2O ratios may also be related to the increased F content of the crystallising magma and the influx of alkali rich fluids, also magmatic, into the system (cf; Haapala, 1985). A similar process of volatile complexing is also thought to have controlled trace element behaviour in the W-Mo related Hjulsjo granite (Baker, 1985) and also the Grashojeden granite (Baker et al., 1987) both of which have anorogenic chemistry.

The trace elements geochemistry of the Kigom complex is indicative of enrichments that represent rest concentrations developed during the late magmatic-post magmatic stages of crystallisation following the precipitation and separation of the early magmatic phases (cf: Ewart et al., 1968). Hildreth (1979) has argued that such elements in granite Complexes reflet partial

confinement of the volatile phases within the roof facies of high level magma chambers. Similar enrichments have been reported from molybdenum-rich granites at Climax (Westra and Keith, 1981; Mutschler et al., 1981), Henderson (Desborough et al., 1978), Pine Groove (Keith, 1979; Bust et al., 1980).

7.2.5 Sequence of Evolution

The Kigom granites are clearly typical anorogenic 'A' type granites that crystallised from melts developed within the shallow regions of the crust. Their evolution, like those of the other complexes within the Province, is related to the intracratonic rifting along the N-S axis controlled by the existing basement lineaments (cf: van Breeman and Bowden, 1973; van Breeman et al., 1975; Rahaman et al., 1984). The plot of the granites in the region of the topaz-bearing granites (Fig. 34) which are, typically, late granites, indicates that the Kigom evolved as one of the marginal (closing) phases of magma intruded during the intracratonic rifting. The absence of basic rocks within the Kigom either before or after the crystallisation of the cupola indicates that the Kigom had little or no mantle input. This is supported by the fact that the fayalite and quartz are among the early minerals to crystallise and no mineral of basic character crystallised later not even as intrusives.

The pattern of crystallisation of the Kigom granites is clearly outlined using the Al/ANC vs AN/Al plot (Fig. 17). The

fayalite-aegirine microgranite, weakly perakaline, was the first part of the Kigom complex to crystallise. The more peralkaline arfvedsonite granite compared to the microgranite; and the moderately peralkaline riebeckite and riebeckite-aegirine-biotite granites follow in that order. This path of crystallisation of the Kigom granites is consistent with the peralkaline subsolidus/hydrothermal path for some of the Younger Granite complexes of Nigeria of Jacobson et al. (1958), and Bowden and Kinnaird (1976). In this classification (Fig. 36), the-latter granites are believed to have originated from the fayalite granite.

7.3 Genesis of the Mo Mineralisation

The last phase of the hydrothermal solution, also K-rich and chemically active, evolved from the initial hydrothermal fluid and followed the lithological contact between the already crystallised part of the Kigom complex and the basement migmatite towards the surface. Crystallisation of this fluid began with replacement reactions in perthites and the conversion of amphiboles to biotite, and finally the crystallisation of sulphides: pyrites (oldest), chalcopyrites, sphalerite, galena and molybdenite (youngest) which occur disseminated at the contact zone. The last stage of crystallisation involving the sulphides most likely included some degree of hydrogen metasomatism since the solution is, at this stage, sulphur-rich and the environment was more of a



Figure 36. Graphical representation of the evolution of rock types associated with the Nigerian ring complexes (Jacobson et al., 1958 and Bowden and Kinnaird, 1958).

reducing one. Similar molybdenite emplacements have been reported from the Mo-, Sn-mineralised Ackley Granite, Newfoundland, where the mineralisation occurs around the contact of the fine-grained marginal biotite granite lobe with Precambrian rhyolite (Tuach et al., 1986). Mo introduced into the hydrothermal system was derived from the crystallising magma since the aegirine microgranite which probably had longer reaction time with the basement migmatites, the host rock to the Kigom, does not show considerable enrichment in Mo to suggest that the Mo was leached from the basement into the crystallising magma during cooling and consolidation. Wallace et al. (1978) have similarly documented a magmatic origin for the hydrothermal solutions responsible for the deposition of the Urad and Henderson molybdenum deposits, Colorado, U.S.A.

The basement migmatite are considered to have contaminated the intruding granitic melts. If so, then the high Mo concentrations in the migmatite tend to suggest that the average Mo content in the melt was higher than the average crustal abundance of 1-2 ppm. The Mo could not, however, be concentrated in the granites with the silicates because of its incompatibility with the latter. This explains the apparent non-enrichment of the element in the Kigom granites and the later pegmatite and rhyolitic dykes associated with the Kigom.

The Mo mineralisation, like most of the enriched trace elements in the Kigom granites, was influenced by the high F content of the alkali-rich hydrothermal fluids. However, the deposition of Mo as MoS_2 is related to the supersaturation of the

vapour phase in Mo and S, and the associated Cu, Pb and Zn. The localisation of the MoS_2 mineralisation in parts of Na-rich amphiboles of the Kigom lends credence to a low temperature control on the mineralisation and the fact that the mineralisation represents remnants of the crystallising volatile fluids that were concentrated close to the contact with the basement; the contact serving as a form of structural control. This compares closely with the largest Bordvika Mo mineralisation (the Munka and the Bjorntjarn) which is located in the contact zone between the youngest granites and the gneissic supracrustals (Gyeti and Schonwandt,1979): a similar geologic setting to the Kigom. In terms of tectonic setting, the Borvida granites are, like the Kigom, rift related and form geophysically well defined diapiric structures representing copulas on top of an underlying batholith (Ohander and Nisca, 1982).

Following Mutschler et al's (1981) classification of Mo mineralised granites, the Kigom could represent a molybdenite granite system in which the lithophile elements underwent progressive enrichment under the influence of thermogravitational diffusion; especially if, as hitherto demonstrated, the Kigom is among the last of the complexes within the Province to evolve. It is certainly younger than the Ganawuri (dated about 150 Ma; Bowden et al., 1975) with which it has sharp contacts. Thus, it appears that the Kigom represents highly evolved magma that is enriched in lithophile and other trace elements including Mo. Though there is no geophysical evidence on the depth of the complex, it is likely

that the Kigom is not as deep-seated as the other complexes around it.

7.4 Mo Deposit Grade

The disseminated Mo mineralisation in the Kigom complex is relatively low-grade with 0.39% MoS_2. This is comparable to those of the Climax Mo deposit within the Colorado Mineral belt with a grade of 0.4% MoS_2. The lateral and vertical extent of the Kigom mineralisation is, however, yet to be established. When this is done, it should be possible to define the economics and recovery aspects of the deposit more closely. The adits of the Fidelity Mining Syndicate of Messrs N. Yassin is a springboard for further work. With more geophysical surveys, it should be possible to establish the configuration of the ore for purposes of planning and mining.

CHAPTER EIGHT

CONCLUSION AND RECOMENDATION

8.1 CONCLUSION

Field, geological, geochemical, and genetic studies of the Kigom Younger Granite complex and of its associated molybdenite mineralisation have been undertaken. Compared to the other complexes within the Younger Granite Province of Nigeria also intruded during the Jurassic intracratonic rifting along the N-S axis, the Kigom, is geographically distinct as a cupola: lacking the usually associated early volcanic rocks and enclaves of basement migmatite and gneisses within it. The emplacement of the Kigom was thus not preceded by ring fracturing and cauldron subsidence which are commonly associated with most of the other complexes.

The Kigom complex consists of 4 categories of granitic rocks: the aegirine microgranite, the arfvedsonite granite, the riebeckite granite and the riebeckite-aegirine-biotite granite. Crystallisation began with fayalite and quartz in the region of the aegirine microgranite close to the contact with the basement. With loss of volatiles and heat, and with an influx of water into the system, lower temperature minerals such as exsolution perthite and quartz began to crystallise. Oikocrystic sodic amphiboles: optically both riebeckite and arfvedsonite, but chemically

arfvedsonitic or riebeckitic-arfvedsonites, began crystallising in the magmatic and finally formed during the early hydrothermal (subsolidus) crystallisation. Replacing the amphiboles during hydrothermal reactions were: aegirine, astrophyllite, biotite, and magnetite as the alkalinity of the solution increased. Hematitisation also, was commonly associated with the early fayalite/aegirine in the microgranites. Also among the late minerals are zircon, fluorite and thorite. The minerals associated with the alteration thus indicate that the hydrothermal fluid was alkali-rich. This is also evident from the modification of exsolution textures within the perthites in which albitic blebs or orthoclase became dominant in perthites depending on whether or not the perthites are close to a crystallising amphibole. Using these exsolution, modified exsolution and replacement textures, crystallisation can be grouped into the magmatic, early hydrothermal or post magmatic and late hydrothermal. This mineralogy categorises the Kigom as hypersolvus A-type granites crystallised from an alkali-rich, water saturated peralkaline magma generated within shallow levels of the crust.

Whole-rock geochemistry of the Kigom granites indicates an increasing trend of peralkalinity (AN/Al and Al/ANC) from the aegirine microgranite, through the arfvedsonite granite, the riebeckite granite, to the riebeckite-aegirine-biotite granite; a trend consistent with the pattern of consolidation of peralkaline magmas. The granites also are characteristically poor in CaO, MgO, MnO and TiO_2. On the Q-Ab-Or triangular diagram, the granites plot

in the region of alkali-feldspars with a shift towards the Ab-end close to the eutectic minimum; an indication that there was alkali metasomatic alteration within the rocks. The granites also plot in the region of fluorine-bearing granites of Manning (1982) with 1-2% F and excess water at 1 kbar, indicating that the granites are fluorine rich. In terms of trace element geochemistry, the Kigom granites have very high values of Zr, Y, Rb, Nb and F, and very low values of Ba and Sr. The enriched trace elements are believed to have been concentrated in the volatile phases of crystallising fluid. This is characteristic of strongly peralkaline anorogenic A-type granites. The enrichment of the granites in these elements is consistent with a shallow subvolcanic origin of the magma. The granites plot on the Rb-Ba-Sr triangular diagram in the region described by Taylor (1986) for topaz-bearing granites or the so called late granites. This suggests that the Kigom most likely represents the marginal phases of the magmatic intrusions during the Jurassic northerly intracratonic rifting of parts of the Nigeria-Niger basement. The very low Mg/Mg + Fe ratio is consistent with a crustal source.

Molybdenite mineralisation is associated with the riebeckite granite unit of the Kigom at the contact with the basement migmatite. The sulphide mineralisation occurs disseminated and has an outer pyrite zone and an inner molybdenite with minor amounts of chalcopyrite, helvite, sphalerite, and galena. In both regions the ore minerals have inclusions of perthite which they replace. They also overlie metasomatic biotite and astrophyllite

indicating that the sulphides were the last minerals to form from the crystallising hydrothermal fluid. The mineralisation, thus, represents rest concentrations of elements which were initially incompatible with the silicates, deposited at relatively lower pH/Eh conditions at which stage the vapour phase was supersaturated in Mo. The Mo in the melt was most likely introduced into it from the source, more so that the migmatites considered possible contaminants to the magma, have enriched values of Mo above the normal background values. The pattern of Mo mineralisation in the Kigom compares most closely with the largest Borvida Mo deposit, the Munka and the Bjorntjan, located in the contact zone between the youngest granites (which are, like the Kigom, rift related and diapiric) and the gneissic supracrustals (Gyeti and Schownwandt, 1979).

The Mo deposit in the Kigom complex is low grade with 0.39% MoS_2. Compared with the Climax Mo deposit with a grade of 0.4% MoS_2, the Kigom molybdenum could be a mineable grade. Given a favourable mining environment, it should be possible to delineate the mineable ore and proceed with the development of the deposit and possible exploitation.

8.2 RECOMMENDATION

This study has highlighted the uniqueness of the Kigom complex in terms of its mode of emplacement, geology, geochemistry and genesis of the associated molybdenite mineralisation. No age determinations were, however, done. The Kigom is most likely comparable in age to the Afu complex dated 140 ma or slightly older. This speculation is based on the fact that the Kigom has an intrusive contact with the neighbouring Ganawuri complex dated 160 ma (Bowden et al., 1976).

An electromagnetic geophysical investigation could be used to study the depth of the Kigom and to delineate the ore zone. It is so necessary that the depth and internal configuration of the ore zone be properly delineated geophysically and the associated mineable grade determined through drilling. There is a possibility of a deep seated pipe which served as a passage way for the-latter ore related hydrothermal fluid. These should happen before financial commitments are made on developing the mine.

REFERENCES

Abaa, S.I., 1978. Some petrographic and chemical aspects of mineralisation in the Ririwai biotite granite, Nigeria. Bull. Geol. 1, Ahmadu Bello University, Zaria, Nigeria, p 1-18.

Abaa, S.I., 1985. Some geochemical characteristics of the alkaline rocks of the Mada Younger granite complex, Nigeria. Journal of African Earth Sci., 3, p115-121.

Abaa, S.I., 1991. Hydrothermal fluids responsible for the formation of precious minerals in the Nigerian Younger granite province. Mineral Deposita, v., 26, p 34-39.

Abaa, S.I., and Omada, J.I., 1990. Petrology and geochemistry of commendites from the Nigerian Younger granite province. In press [Journal of Nigerian Min. and Geosc. Soc.]

Anderson, R.N., Delong, S.E., and Schwarz, W.M., 1978. Thermal model for subduction with dehydration in the downgoing slab. Journ. Geology, v. 86, p 731-739.

Arutyunyan, I.A., 1969. Possibilities of migration of molybdenum in the form of haloid compounds. International Geology Rev., v. 11, no.,10, p 1200-1203.

Baker, J.H., 1985a. The petrology and geochemistry of 1.8-1.9 Ga granitic magmatism and related sub seafloor hydrothermal alteration and ore forming processes, W. Bergslagen, Sweden, GUA papers of Geology, Series 1, v. 21, 1-204.

Baker, J.h., Hellingwerf, R.H., and Hammergren, P., 1987. Geochemistry of a proterozoic high silica W-Mo granite from Vastra Grashojden, Central Sweden. Geologiska Foreningens i strockholm Forhandlingar, Vol. 109, Pt. 2, pp 111-121.

Black, R., 1963. Notes sur les complexes annularies de Tchouni-Zarniski et de Goure (Niger). Bull. Bur. Rech. geol. min., 1-1963, p. 31-45.

Blossom, J., 1989. Molybdenum. United States of America Molybdenum Minerals YearBook

Bookstrom, A.A., 1981. Tectonic setting and generation of Rocky Mountain porphyry molybdenum deposits. In: Dickinson, W.R., and Payne, W.D., eds., Relations of tectonics to ore deposits in the southern Cordillera: Arizona Geological Society Digest, v. 14, p 213-226.

Bonin, B., 1986. Ring complex granites and anorogenic magmatism. Elsevier, New York.

Borley, G. D., 1963. Amphiboles from the Younger Granites of Nigeria, Part 1: Chemical classification. Min. Mag. 33, pp 358-376.

Borley, G.D., 1976. Ferromagnessian mineralogy and temperature of formation of the Younger granites of Nigeria. In: Kogbe, C.A., ed., Geology of Nigeria, Elizabeth Press, Lagos.

Bowden, P., 1982. Magmatic evolution and mineralisation in the Nigerian Younger granite province. In: Evans, M.A. ed., Metallization Associated with Acid Magmaitsm, pp 51-56. John Willey, New York.

Bowden, P., and Jones, A., 1978. Mineralisation in the Younger granites of Northern Nigeria. In: Stemprok, M., Burnol, L., and Tischendorf, G., eds., Metallisation Associated with Acid Magmatism, v. 3, Geological Survey of Czechoslovakia, Prague, pp. 179-190.

Bowden, P., and van Breeman, O., 1972. Isotopic and chemical studies on the Younger granites from Northern Nigeria. In: Dessauvagle, T.F., and Whiteman, eds., African Geology, p 105-120. University of Ibadan Press, Nigeria.

Bowden, P., van Breeman, O., Hutchinson, J., and Turner D.C., 1976. Palaeozoic and Mesozoic age trends for some ring complexes

in Niger-Nigeria. Nature, v. 259, 1, p 297-299.

Bright, M.J., 1974. Primary geochemical dispersion associated with the Henderson molybdenum deposit, Colorado, [abs], Economic Geology, v. 69, p 1177.

Burt, D.M., Bikun, J.V., and Christansen, E.H., 1980. Distribution and petogenesis of topaz rhyolites, Western U.S.A., [abs] Geol. Soc. America, Abstracts with programs, V. 12, no. 7, p 396.

Cann, R.M., 1976. Geology of Kemess porphyry copper property, north-central British Columbia. Unpublished B.Sc. thesis, Depart. Geol. Sci., University of British Columbia.

Cann, R.M., and Godwin, C.I., 1980. Geology and age of the Kemess porphyry copper-molybdenum deposit, north-central British Columbia. C.I.M. Bull. 73, No. 821, pp. 94-99.

Chappell, B.W., and White, A.J.R., 1974. Two contrasting granite types. Pac. Geol. 8, pp. 173-174.

Deer, W. A., Howie, R. A., Zussman, J., 1966a. An Introduction to Rock-Forming Minerals. John Willey, New York.

Desborough, G.A., Mihalik, P., Kamilli, R., Gunow, A., and Taylor, B.B., 1978. Accessory minerals in the plutonic igneous host

of molybdenum ore, Henderson mine, Colorado. Regional Conf. Study Minerals in Polished Sections, on the Microscale, 8th Paris, Abstract v. 17, p. 1.

Erlande, A. J., Smith, H. S., Merchant, J. W., Cardose, M. P., and Ahrens, L. H., 1978. Zirconium, In: Wedepohl, K. H., ed., Handbook of Geochemistry, II-4. Springer-Verlag. Berlin-Heidelberg. New York.

Ewart, A., Taylor, S.R., and Capp, A.C., 1968. Geochemistry of the pantellerites of Mayor Island, New Zealand. Contributions Mineral. Petrol. v. 17, p. 116-140.

Gabrielse, H., Dodds, C.J., Mansy, J.L., and Elsbacher, G.H., 1977. Geology of Toodoggone River (94E) and Ware West-Half (95F). Geological Surv. Canada, Open file, 483.

Ganster, M.W., 1976. Evidence for the localised accumulation of hydrothermal fluids at the Henderson molybdenum deposit. Empire, Colorado [abs.]: Geol. Soc. America. Abstracts with programs, v. 8, No. 6, p. 880.

Garner, F.A., 1959. Memorandum on the molybdenite occurrence in the Kigom Hills - A short account of a visit to the molybdenite deposit and views on its exploitation. Geol. Surv. Nigeria Report No. 1230.

Geraghty, E.P., Carten, R.B., and Walker, B.M., 1988. Tilting of Urad-Henderson and Climax porphyry molybdenum systems, central Colorado, as related to Northern Rio Grande Rift tectonics. Geol. Surv. America v. 100, pp. 1780-1786.

Giret, A., Bonin, B., and Leger, J.M., 1980. Amphibole compositional trends in oversaturated and undersaturated alkaline plutonic ring-complexes. Can. Mineralogist 18, pp 481-495.

Glemser, O., and Wendlandt, H.G., 1963. Gaseous hydroxides Advances Inorganic chemistry. Radiochemistry v. 5, p. 215-258.

Glyuk, D.S., and Trufanova, L.G., 1977. Melting at 1000 kg/cm^2 in a granite-H_2O system with addition of HF, HCL, and Li, Na, and K fluorides, chlorides and hydroxides. Geokhimiya, no. 7, pp. 1003-1012.

Gyeti, A., and Schonwandt, H.K., 1979. Bordvika - a possible porphyry molybdenum occurrence within the Oslo rift, Norway. Economic Geology v. 74, pp. 1211-1220.

Haapala, I., 1977a. Petrography and geochemistry of the Eurojoki stock; a rapakivi-granite complex with greisen-type mineralisation in the Southwestern Finland. Geol. Surv. Finl. Bull. 286, 128p.

Haapala, I., 1985. Metallogeny of the Proterozoic rapakivi granites of Finland. In: Taylor, R.P., and Strong, D.F., eds., Recent Advances in the Geology of Granite-Related Mineral Deposits. Can. Inst. Min. Met. Special Volume 39, pp. 124-132.

Hannah, J.L., and Stein, H.J., 1986. Oxygen Isotope compositions of selected Larmide Tertiary granitic stocks in the Colorado Mineral Belt and their bearing on the origin of Climax-type granite-molybdenum systems. Contr. Min. Petr. v. 93, pp. 347-358.

Hannah, J.L., and Stein, H.J., 1990. Magmatic and hydrothermal processes in ore -bearing systems. In: Stein, H.J., and Hannah, J.L., eds., Ore-bearing Granite Systems; Petrogenesis and Mineralizing processes. Can. Inst. Min. Met. Special Paper 246, pp. 1-10.

Hess, P. C., 1989. Origins of Igneous Rocks. Harvard University Press, London.

Hildreth, W., 1979. The Bishop Tuff: Evidence for the origin of compositional zonation in silicic magma chambers. Geol. Soc. America Special Paper 180, pp. 43-74.

Hutchison, C.S., and Chakraborty, K.R., 1979. Tin: a mantle or Crustal Soruce ?. Geol. Soc. Malaysia Bull., v. 11, pp.71-79.

Ike, E.C., 1979. The Structure, petrology and geochemistry of the Tibchi Younger granite ring-complex, Nigeria. Unpublished Ph.D. thesis, University of St. Andrews.

Ike, E.C., Bowden, P., and Martin, R.F., 1985. Amphiboles in the porphyries of the Tibchi anorogenic ring-complex, Nigeria: product of deuteric adjustments. Can. Mineral. 23, pp.447-456.

Imeokparia, E.G., 1982. Geochemistry and relationship to mineralisation of granitic rocks from Afu Younger Granite Complex, Central Nigeria. Geol. Mag., v. 119, pp. 39-56.

Imeokparia, E.G., 1985. Mesozoic granite magmatism and tin mineralisation in Nigeria. In: Taylor, R.P. and Strong, D.F., eds., Recent Advances in the Geology of Granite-Related Mineral Deposits. C.I.M. special volume 39, pp. 133-141.

Isaksson, H., 1982. Kataburget, geofysisk undersokning. Internal report, FM 8204, Geol. Surv. Sweden. Lulea.

Isuk, E.E., 1976. Solubility of molybdenite in the system Na_2O-K_2O-SiO_2-MoS_2-H_2O-CO_2 with geologic implications [Ph.D. thesis]. Ames, University of IOWA.

Jacobson, R.R.E, MacLEOD, W.N., and Black, R., 1958. Ring complexes in the Younger granites of northern Nigeria. Geol. Soc. London, Memoir no.1, 72p.

Jenkins, R., and van Gelder, S., 1968. Determination of Low concentrations of Fluorine in cement by x-ray flourescent spectroscopy. Bull. Philips. Sci. Analyst. Equip., 8p.

Jensen, M.L., and Bateman, A.M. Economic Mineral Deposits [3rd ed.]. John Willey, New York. 1981.

Kamilli, R.J., 1978. The genesis of stockwork molybdenite deposits: implications from fluid inclusion studies at the Henderson mine [abs.]. Geol. Soc. America. Abstracts with programs, v. 10, no. 7, p.431.

Keith, S.B., 1978. Paleosubduction geometrics inferred form Cretaceous and Tertiary magmatic patterns in southwestern North America. Geology, v. 6, pp. 516-521.

Keith, S.B., 1979. Possible magmatic and metallogenetic products of 120 m.y. subduction in southwestern North America

[abs.].Geol. Soc. America. Abstracts with programs, v. 11, no. 7, p.455.

Khitarov, N.I., Arutyunyan, L.A., and Lebedev, E.B., 1967. Experimental study of separation of molybdenum from granitic melts at water vapour pressure up to 3000 atmospheres. Geokhimiya, no. 8, pp. 891-900.

Kinnaird, J.A., 1979. Mineralisation associated with the Nigerian Mesozoic ring-complexes. Stvdia Geologia (Salamanca) XIV, pp. 189-220.

Kinnaird, J.A., 1985. Hydrothermal alteration and mineralisation of the alkaline anorogenic ring-complexes of Nigeria. Journ. African Earth Sci. v. 3, no. 1, pp. 229-251.

Kinnaird, J.A., Bowden, P., Ixer, R.A., and Odling, N.W.A., 1985. *Mineralogy , Geochemistry and Mineral Deposits of the* Ririwai Complex, N. Nigeria. Journal of African Earth Sciences, v. 3, pp. 185-222.

Konnerup-Madsen, J., 1979. Fluid inclusions Associated with a metamorphosed molybdenite mineralisation in the Vest-Agder, South Norway. Economic Geology, v. 74, pp. 1221-1230.

Kovalengo, V.I., 1973. Distribution of fluorine in a quartz keratophyre dyke (ongonite) and solubility of fluorine in granitic melts. Geochem. Int., v. 10, pp. 41-49.

Kooiman, G.J.A., McLEOD, M.J., and Sinclair, W.D., 1986. Porphyry tungsten-molybdenum ore bodies, polymetallic veins and replacement ore-bodies, and tin-bearing greisen zones in the Fire Tower Zone, Mount Pleasant, New Brunswick. Economic Geology, v. 81, pp.1356-1373.

Krauskopf, K. B., 1979. Intoduction to geochemistry (2^{nd} ed.). McGraw-Hill Book Co., New York, 617p.

Ludington, D.L., Sharp, W.N., Mckowan, D., and Baker, F., 1979. The Redskin Granite - a Precambrian basin example of thermogravitational diffusion [abs.]. Geol. Soc. America., Abstracts with programs, v. 11. no. 7, p. 469.

Luth, W.C., Jahms, R.H., and Tuttle, O.F., 1964. The granite system at pressures of 4-10 kbar. Journ. Geophys. Res., v. 69, pp. 759-773.

Macdonald, G.A. 1968. Composition and origin of Hawaiian lavas. Geol. Soc. Amer. Mem. 116, pp 477-522.

MacLEOD, W.N., Turner, D.C., and Wright, E.P., 1977. The Geology of the Jos-Plateau - general geology. Geol. Surv. Bull. 32, 109p.

Manheim, F.T. Red sea geochemistry. In: Whitmarsh, R.B., Weser, O.E., Ross, D.A., eds., Initial Reports of the Deep sea Drilling Project, Washington, D.C., v. 23, 975, 1974.

Manheim, F.T., and Landergren, S., 1978. Molybdenum. In: Wedepohl, K.H., ed., Handbook of Geochemistry, II-4. Springer-Verlag. Berlin-Heidelberg. New York.

Manning, D.A.C., 1982. An experimental study of the effects of fluorine on the crystallization of granitic melts. In: Evans, A.M., ed., Metallization Associated with Acid Magmatism, pp 191-203. John Willey and Sons Ltd, New York.

Marot, A., and Zimme, S., 1976. Les complexes annulaires de syenites et granites alcalins dans la Peninsule Rallier-du-Baty, Iles Kerguelen (T.A.A.F.), these 3^{e} cycle, Universite Pierre-et-Marie Curie, Paris.

Martin, R.F., and Bowden, P., 1981. Peraluminous granites produced by rock-fluid interaction in the Ririwai nonorogenic ring-complex, Nigeria: mineralogical evidence. Can. Mineral. 19, pp. 65-82.

Mason, B., and Moore, B.C., 1982. Principles of Geochemistry, 4th Edition, John Willey, New York.

Matheis, G., Emofurieta, W.O., and Ohiwurei, S.F., 1982. Trace Element Distribution on Tin-bearing Pegmatite of Southwesthern Nigeria. In: Evans, A.M.. ed., Metallization Associated with Acid Magmatism, v. 6, pp. 205-220.

McCurry, P., 1976. The Geology of the Precambrian to Lower Paleozoic rocks of northern Nigeria - a review. In: C.A., Kogbe, ed., Geology of Nigeria, Elizabeth Publishing Co., Lagos. *pp* 15-39.

McLEOD, M.J., Taylor, R.P., and Lux, D.R., 1988. Geology, $^{40}Ar/^{39}Ar$ geochronology and Sn-W-Mo-bearing sheeted veins of the Mount Douglas Granite, Southwastern New Brunswick. Can. Inst. Min. Met. v. 81, no. 918, pp. 70-78.

Monger, J.W.H., 1977. The Triassic Takla Group in McConnel Creek map area, north-central British Columbia. Geol. Surv. Canada, Paper 76-29.

Monger, J.W.H., and Church, B.N., 1977. Revised stratigraphy of the Tarela Group north-central British Columbia. Canadian Journ. Earth Sci., v. 14, pp. 318-326.

Mutschler, F.E., Wright, E.G., Ludington, S., and Abbot, J.I., 1981. Granite Molybdenite Systems. Economic Geology, vol. 76, pp. 874-897.

Neumann, E. R., 1976. Compositional relations among pyroxenes, amphiboles, and other mafic phases in the Oslo region plutonic rocks. Lithos 9, pp 85-109.

Norman, G.W.H., 1945. Molybdenite deposits and pegmatite in the Preissac-La Corne Area, Abitibi County, Quebec. Economic Geology, v. XL, no. 1, 17p.

Norrish, K., and Chappell, B.W., 1967. X-ray flourescence spectography. In: Zussman, J., ed., Physical Methods in Determination, Acadenic Press, London, pp. 201-272.

Oftedahl, C., 1953. Studies on the igneous rock complex of the Oslo region, XIII, The Cauldrons. Skr. Norske Videnskaps-Akad. Oslo, 1. Mat.-Naturv. Kl. no. 3, 108p.

Ohander, B., 1985. Geochemistry of Proterozoic Molybdenite-mineralized aplites in Northern Sweden. Mineral Deposita v. 80, pp. 241-248.

Ohander, B., and Nisca, D.H., 1985. Tectonic controls of Precambrian molybdenite mineralisation in Northern Sweden. Econ. Geol., v. 80, pp. 505-512.

Olade, M.A., 1980. Geochemical characteristics of tin-bearing and tin-barren granites. Econ. Geology, v. 75, pp. 71-82.

Pitcher, W.S., 1983. Granite type and tectonic environment. In: Hsu, K., ed., Mountain Building Processes. Academic Press, *London, pp.* 19-40.

Rahaman, M.A., van Breeman, O., Bowden, P., and Bennett, J.N., 1984. Age migrations of anorogenic ring-complexes in Northern Nigeria. Journ. Geology, v. 92, pp.173-184.

Reece, C., Ruiz, J., Duffield, W.A., and Patchett, R.J., 1990. Origin of Taylor Creek Rhyolite magma, Black Range, New Mexico, based on Nd-Sr isotope studies. In: Stein, H.J., and Hannah, J.L., eds., Ore-bearing Granite Systems; Petrogenesis and Mineralising Processes. Canadian Inst. Min. Met. Special Paper 240, pp. 263-274.

Ruitenberg, A.A., 1967. Stratigraphy, Structure and metallisation, Piskahegan-Rolling Dam Area. Leise Geologische *Mededelingen, vol. 40, pp.* 79-120.

Ruitenberg, A.A., 1972. Metallisation episodes related to tectonic evolution, Rollingdam and Mascarene-Nerepis Belts, NewBrunswick. Econ. Geol., v. 67, pp 434-444.

Rye, O.R., Lufkin, J.L., and Wasserman, M.D., 1990. Genesis of the rhyolite-hosted tin occurrences in the Black Range, New Mexico, as indicated by stable isotope studies. In: Stein, H.J.,and Hannah, J.L., eds., Ore-bearing Granite Systems; Petrogenesis and Mineralising Processes. Canadian Inst. Min. Met. Special Paper 240, pp. 233-250.

Schmitz, C., and Burt, D.M., 1990. The Black Pearl Mine, Arizona; Wolfranite veins and stockscheider pegmatite related to an albitic stock. In: Stein, H.J.,and Hannah, J.L., eds., Ore-bearing Granite Systems; Petrogenesis and Mineralising Processes. Canadian Inst. Min. Met. Special Paper 240, pp. 221-232.

Schonwandt, H.K. and Gyeti, A., 1977. Detaljkottegning af de hydrotermale omdannelser ved Bordvika, Glitrevann. Internal report, Oslo, Norsk Hydro a.s., 13p.

Seedorff, E., 1985. Cyclic development of hydrothermal mineral assemblages related to multiple intrusions at the Henderson porphyry molybdenum deposit, Colorado. In: Taylor, R.P., and Strong, D.F., eds., Recent Advances in the Geology of

Granite-Related Mineral Deposits. Can. Inst. Min. Met. Special Volume 39, pp. 367-393.

Shand, S. J., 1951. Eruptive rocks. London: Murby.

Shesherba, G.N., 1970. Greisen, Part I. Internal Geology Rev., v. 12, no. 2, pp. 114-150.

Smith, R.W., Norman, D.I., and Popp, C.J., 1980. Calculated solubility of molybdenite in hydrothermal solutions [abs.]. Geol. Soc. America, Abstracts with programs, v. 12, no. 7, p.525.

Staudigel, H., Zindler, A., Hart, S. R., Leslie, T., Chen, T. Y., and Clague, D., 1984. The isotopic systematics of a juvenile intraplate volcano: Pb, Nd, and Sr isotope ratios of basalts from Loihi Seamount, Hawaii. Earth Planet. Sci. Lett. 69 pp 13-29.

Stein, H.J., 1985. A lead, strontium, and sulfur isotope study of Laramide-Tertiary intrusions and mineralisations in the Colorado Mineral Belt with emphasis on Climax-type porphyry molybdenum systems plus a summary of other newly acquired isotopic and rare earth element date [Ph.D. thesis]. Chapel Hill , University of North Carolina, 493p.

Stein, H.L., 1985. Genetic traits of Climax-type granites and molybdenum mineralization, Colorado Mineral Belt. In: Taylor, R.P., and Strong, D.P., eds., Recent Advances in the Geology of granite-related Mineral Deposits. Can. Inst. Min. Met. Special Volume 39, pp. 394-401.

Stein, H.L., and Hannah, J.L., 1985. Movement and origin of ore fluids in Climax systems. Geology, v. 3, pp. 469-474.

Strong, D. F., and Taylor, R.P., 1984. Magmatic-Subsolidus and Oxidation Trends in composition of Amphiboles from Silica-Saturated Peralkaline Igneous Rocks. Tschermaks Min. Petr. Mitt. 32, pp 211-222.

Tauch, J., Kerrich, R., Willmore, L.M., and Strong, D.F., 1985. Source terranes, magmatic evolution, and hydrothermal regimes in the Mo-, Sn-mineralized Ackley Granite, Newfoundland: evidence from combined geochemical and oxygen isotope data. In: Taylor, R.P., and Strong, D.F., eds., Recent Advances in the Geology of Granite-Related Mineral Deposits. Can. Inst. Min. Met. Special Volume 39, pp. 342-350.

Taylor, H.P., Jr., 1979. Oxygen and hydrogen isotope relationships in hydrothermal mineral deposits. In: Barnes, H.L. ed., Geochemistry of hydrothermal Ore Deposits (2nd ed.), John

Willey, pp. 236-277.

Teng, H.C., and Strong, D.R., 1976. Geology and geochemistry of the St. Lawrence peralkaline granites and associated fluorite deposits, Southeastern Newfoundland. Canadian Journ. Earth Sci., v. 13, pp. 1374-1385.

Thompson, G.A., and Burke, D.B., 1974. Regional geophysics of the Basin and Range province. Ann. Rev. Earth Planet Sci., v.2, pp. 213-238.

Thompson, M., and Walsh J.N., 1983. A handbook of inductively coupled plasma spectometry, Blackie and Lon Ltd. London.

Toksoz, M.N., Minear, J.W., and Julian, B.R., 1971. Temperature, field and geophysical effects of the downgoing slab: Journ. Geophys. Research. v. 76, p 1113-1138.

Turner, D.C., 1976. Structure and Petrology of the Younger granite ring-complexes. In: Kogbe, C.A., ed., Geology of Nigeria, Elizabeth Publ. Co., Lagos, pp. 143-159.

Tuttle, O.F., and Bowen, N.L., 1958. Origin of granites in the light of experimental studies in the system $NaAlSi_3O_8$-$KAlSi_3O_8$-SiO_2-H_2O. Geol. Soc. of America Mem. 74, 153p.

Uzkut, I., 1974. Zur Geochemie des Molybdans. Stuttgart, Gebruder, Borntraeger, p. 226.

Van Breeman, O. and Bowden, P., 1973. Sequential age trends for some Nigerian Mesozoic granites. Nature, v. 242, pp. 9-11.

Van Breemen, O., Hutchinson, J., and Bowden, P., 1975. Age and origin of the Nigerian Mesozoic granites: a Rb-Sr isotopic study. Contr. Miner. Petr., v. 50, pp. 157-172.

Van Breeman, O., Pigeom, R.T., and Bowden, P., 1977. Age and isotopic studies of some Pan African granites north-central Nigeria. Precambrian Research, V. 4, pp. 307-319.

Wallace, B.R., Mackenzie, W.B., Blair, R.G., and Muncaste, N.K., 1978. Geology of the Urad and Henderson Molybdenum section on a comparison of these deposits with those at Climax, Colorado. Economic Geology, v. 73, pp. 325-368.

Webster, J.D., and Holloway, J.R., 1990. Partitioning of F and Cl between magmatic hydrothermal fluids and highly evolved granitic magmas. In: Stein, H.J.,and Hannah, J.L., eds., Ore-bearing Granite Systems; Petrogenesis and Mineralising Processes. Canadian Inst. Min. Met. Special Paper 240, pp. 21-34.

Wendlandt, R.F., and Eggler, D.H., 1980. The origins of potassic magmas: 2. Stability of phlogopite in natural spinel herzolite and in the system $KAlSiO_4$-MgO-SiO_2-H_2O-CO_2 at high pressures and high temperatures. Amer. Journ. Sci., v. 280, p 346-358.

Westra, G., and Keith, S.B., 1981. Classification and genesis of Stockwork Molybdenum Deposits. Economic Geology, v. 76, pp. 844-873.

Whalen, J.B., Currie, K.L., and van Breeman, O., 1987. Episodic Ordovician-Silurian plutonism in the topsails igneous terrane, Western Newfoundland. Trans. Soc., Edinburgh Earth Sci.

White, H.J.R., and Chappell, B.W., 1983. Granitoid types and their distribution in the Lachlan Fold Belt, Southeastern Australia. Geol. Soc. America. Mem. 159, pp. 21-34.

Wright, J.B., 1970. Controls of mineralisation in the Older and Younger Tin Fields of Nigeria. Econ. Geol., v. 65, pp. 945-951.

Wyllie, P.J., 1979. Magmas and volatile components. American Mineralogist, v. 64, pp. 469-500.

Wyllie, P.J., and Tuttle, O.F., 1964. Experimental investigations of Silicate Systems containing two volatile components, 2: The effect of NH_3 and HF in addition to H_2O on the melting temperatures of albite and granite. American Journ. Sci., v. 262, pp. 930-939.

Yolder, H.S., and Tilley, C.E., 1962. Origin of basalt magmas: an experimental study of natural and synthetic rock systems. Journ. Petrol., v. 3, pp. 342-532.

APPENDIX

Table A.1. Whole-rock major oxides composition of the aegirine microgranite of the Kigom complex.

Oxides (wt %)	Sample jk034	Sample jk035	Sample jk040
SiO_2	76.92	76.80	76.93
TiO_2	0.12	0.10	0.11
Al_2O_3	12.20	12.18	12.16
Fe_2O_3	1.20	1.21	1.22
FeO	0.37	0.33	0.35
MnO	<0.01	<0.01	<0.01
MgO	<0.01	<0.01	<0.01
CaO	0.01	0.01	0.01
Na_2O	4.06	4.04	4.08
K_2O	4.40	4.14	4.56
P_2O_5	0.01	0.01	0.01
L.O.I	0.72	0.68	0.63
Total	100.01	99.95	99.96

Table A.2. Whole-rock major oxides composition of the arfvedsonite granite of the Kigom complex.

Oxides (wt %)	Sample jk025	Sample jk027	Sample jk030
SiO_2	76.14	76.10	76.13
TiO_2	0.08	0.09	0.08
Al_2O_3	11.87	11.90	11.79
Fe_2O_3	1.03	1.01	1.05
FeO	1.23	1.24	1.19
MnO	0.01	0.01	0.01
MgO	<0.01	<0.01	<0.01
CaO	<0.01	<0.01	<0.01
Na_2O	4.51	4.49	4.53
K_2O	4.31	4.33	4.29
P_2O_5	0.01	0.01	0.01
L.O.I	0.27	0.40	0.33
Total	99.53	99.58	99.41

Table A.3. Whole-rock major oxides composition of the riebeckite granite of the Kigom complex.

Oxides (wt %)	Sample jk001	Sample jk022	Sample jk049
SiO_2	74.97	75.14	75.25
TiO_2	0.10	0.08	0.13
Al_2O_3	11.79	11.87	11.77
Fe_2O_3	1.85	1.81	1.80
FeO	1.34	1.27	1.39
MnO	0.02	0.02	0.02
MgO	<0.01	<0.01	<0.01
CaO	0.06	0.03	0.04
Na_2O	4.53	4.52	4.43
K_2O	4.26	4.24	4.30
P_2O_5	0.01	0.01	0.01
L.O.I	0.29	0.28	0.33
Total	99.48	99.34	99.47

Table A.4. Whole-rock major oxides composition of the riebeckite-aegirine-biotite granite of the Kigom complex.

Oxides (wt %)	Sample jk023	Sample jk026	Sample jk033
SiO_2	75.46	75.44	75.39
TiO_2	0.08	0.08	0.08
Al_2O_3	11.61	11.65	11.70
Fe_2O_3	1.82	1.91	1.74
FeO	1.38	1.36	1.29
MnO	0.02	0.02	0.02
MgO	<0.01	<0.01	<0.01
CaO	0.01	0.01	0.01
Na_2O	4.70	4.69	4.68
K_2O	4.20	4.24	4.21
P_2O_5	0.01	0.01	0.01
L.O.I	0.29	0.28	0.31
Total	99.58	99.69	99.44

Table A.5. Whole-rock trace element composition of the aegirine microgranite of the Kigom complex (in ppm).

Elements	Sample jk034	Sample jk035	Sample jk040
Nb	208	210	209
Zr	530	550	525
Y	52	49	50
Sr	4	4	4
Rb	176	180	178
Pb	8	8	8
Th	34	35	34
U	4	4	4
Co	nd	nd	nd
Cu	33	32	33
Zn	79	77	79
Mo	1	1	1
W	4	4	4
Li	48	49	49
F	560	562	560
Sn	1	1	1
Ag	3	3	3
As	2	2	2
Be	3.9	4	4
Ba	4	4	4
Ni	1	1	1
Cr	28	27	28
V	1	1	1

Table A.6. Whole-rock trace element composition of the arfvedsonite granite of the Kigom complex (in ppm).

Elements	Sample jko25	Sample jk027	Sample jk030
Nb	118	115	120
Zr	457	460	455
Y	35	33	36
Sr	1	1	1
Rb	299	298	299
Pb	12	10	13
Th	34	34	34
U	5	5	5
Co	nd	nd	nd
Cu	125	124	125
Zn	285	284	285
Mo	2	2	2
W	2	2	2
Li	137	135	138
F	960	960	970
Sn	7	7	7
Ag	0.1	0.1	0.1
As	2	2	2
Be	6.9	7	7
Ba	1	1	1
Ni	10	10	11
Cr	33	33	32
V	1	1	1

Table A.7. Whole-rock trace element composition of the riebeckite granite of the Kigom complex (in ppm).

Elements	Sample jk001	Sample jk010	Sample jk052
Nb	74	76	77
Zr	512	513	510
Y	13	12	10
Sr	4	4	4
Rb	330	336	329
Pb	10	14	12
Th	22	24	23
U	nd	nd	nd
Co	nd	nd	nd
Cu	22	26	24
Zn	442	450	447
Mo	1	1	1
W	6	5	6
Li	216	220	229
F	1100	1150	1145
Sn	11	15	14
Ag	2	2	2
As	2	2	2
Be	5.8	6	6
Ba	7	7	7
Ni	7	6	7
Cr	29	28	26
V	1	1	1

Table A.8. Whole-rock trace element composition of the riebeckite-aegirine-biotite granite of the Kigom complex (in ppm).

Elements	Sample jk023	Sample jk029	Sample jk040
Nb	79	82	80
Zr	588	585	579
Y	21	20	19
Sr	2	2	2
Rb	290	296	288
Pb	17	20	18
Th	27	25	25
U	4	4	4
Co	nd	nd	nd
Cu	85	90	88
Zn	402	405	400
Mo	1	1	1
W	4	4	4
Li	111	111	112
F	1220	1230	1119
Sn	10	11	10
Ag	0.2	0.2	0.2
As	2	2	2
Be	7.3	7.3	7.4
Ba	1	1	1
Ni	10	11	9
Cr	30	29	27
V	1	1	1

Table A.9. The composition of unaltered fayalite in the aegirine microgranite of the Kigom complex.

Oxides (wt%)	jkfay	jkfay1	jkfay2	jkfay3	jkfay4
SiO_2	29.35	29.43	29.35	29.38	29.35
TiO_2	nd	nd	nd	nd	nd
Al_2O_3	nd	nd	nd	nd	nd
FeO	70.04	69.83	70.04	69.99	70.09
CaO	0.01	0.12	0.10	0.12	0.12
MnO	1.53	1.54	1.53	1.58	1.58
K_2O	nd	0.02	0.01	nd	nd
Na_2O	nd	0.05	0.03	0.03	0.03
Total	100.93	101.19	101.06	101.11	101.17

nd not determined

Table A.10. The composition of altered fayalite in the aegirine microgranite of the Kigom complex.

Oxides (wt%)	jkfay	jkfay1	jkfay2	jkfay3	jkfay4
SiO_2	28.62	29.65	28.65	28.62	29.35
TiO_2	nd	nd	nd	nd	nd
Al_2O_3	nd	nd	nd	nd	nd
FeO	67.56	65.91	67.04	67.56	67.39
CaO	0.10	0.09	0.10	0.01	0.01
MnO	1.50	1.46	1.45	1.50	1.48
K_2O	nd	0.01	0.01	nd	nd
Na_2O	0.03	0.05	0.03	nd	nd
Total	98.71	97.17	97.28	97.69	98.23

nd not determined

Table A.11. The composition of amphiboles grains at cores and arfvedsonite grains in the granites of the Kigom complex.

Oxides (wt%)	jk036h	jk008f	jk036a	jk036b	jk036f	jk036i
SiO_2	50.94	49.54	49.40	49.93	49.74	49.48
TiO_2	1.02	0.70	0.93	0.75	0.69	0.85
Al_2O_3	1.20	0.97	0.98	1.18	0.88	1.03
Fe_2O_3	14.67	15.22	14.44	15.84	14.01	13.49
FeO	19.26	20.60	20.65	19.76	20.94	21.27
MnO	0.32	0.32	0.39	0.38	0.40	0.35
MgO	0.02	0.03	0.00	0.04	0.03	0.01
CaO	0.06	0.26	0.46	0.13	0.30	0.20
Na_2O	8.03	7.93	7.91	7.84	8.09	8.22
K_2O	1.52	1.29	1.50	1.39	1.37	1.30
H_2O	0.84	0.78	0.71	0.90	0.64	0.56
F	2.27	2.36	2.48	2.13	2.62	2.79
Cl	0.00	0.01	0.01	0.00	0.01	0.01
O=F	-0.96	-0.99	-1.04	-0.90	-1.10	-1.17
O=Cl	0.00	0.00	0.00	0.00	0.00	0.00
Total	99.21	99.01	98.82	99.39	98.61	98.37

Table A.12. The composition of amphiboles grains at the rims and riebeckite grains in the granites of the Kigom complex.

Oxides (wt%)	jk008e	jk010b	jk010c	jk010j	jk008f	jk008i
SiO_2	49.74	49.70	49.44	48.47	48.67	49.48
TiO_2	0.68	0.59	0.57	0.55	0.86	0.65
Al_2O_3	1.03	1.06	1.01	0.95	1.10	1.03
Fe_2O_3	18.83	17.90	16.13	15.13	16.43	17.49
FeO	18.41	19.21	20.36	20.80	20.28	19.27
MnO	0.34	0.35	0.37	0.32	0.47	0.35
MgO	0.01	0.02	0.00	0.02	0.02	0.01
CaO	0.41	0.30	0.33	1.61	0.42	0.31
Na_2O	7.38	7.38	7.47	7.70	7.62	7.37
K_2O	1.42	1.33	1.39	1.39	1.42	1.30
H_2O	1.18	1.06	0.83	0.81	0.91	1.02
F	1.55	1.80	2.24	2.25	2.07	1.68
Cl	0.03	0.02	0.02	0.02	0.01	0.01
O=F	-0.65	-0.76	-0.95	-0.95	-0.87	-0.76
O=Cl	-0.01	0.00	0.00	0.00	0.00	0.00
Total	100.36	99.95	99.23	99.06	99.42	99.37

Table A.13. The composition of amphiboles grains in the riebeckite grains of the riebeckite granite at the ore zone of the Kigom complex.

Oxides (wt%)	jk007a	jk007b	jk007e	jk007g	jk007h	jk007d
SiO_2	50.50	50.24	50.52	50.48	51.34	51.44
TiO_2	0.65	0.48	0.55	0.79	0.45	0.47
Al_2O_3	0.92	1.03	0.94	1.04	0.91	0.72
Fe_2O_3	21.43	19.22	20.94	19.39	21.10	20.05
FeO	16.47	17.90	17.45	17.59	16.02	16.76
MnO	0.37	0.39	0.34	0.37	0.44	0.35
MgO	0.03	0.02	0.01	0.02	0.01	0.00
CaO	0.30	0.57	0.29	0.28	0.27	0.45
Na_2O	7.16	7.20	6.98	7.02	7.20	7.10
K_2O	1.31	1.34	1.40	1.43	1.40	1.37
H_2O	1.40	1.21	1.25	1.20	1.40	1.28
F	1.16	1.52	1.44	1.55	1.17	1.40
Cl	0.02	0.01	0.05	0.03	0.03	0.03
O=F	-0.49	-0.64	-0.61	-0.65	-0.49	-0.59
O=Cl	-0.01	0.00	0.01	0.01	-0.01	0.01
Total	101.22	100.50	100.70	100.53	101.24	100.83

Table A.14. The composition of aegirine in the granites of the Kigom complex.

Oxides (wt%)	jkaeg1	jkaeg2	jkaeg3
SiO_2	49.74	50.05	49.58
TiO_2	0.65	0.59	0.70
Al_2O_3	1.10	1.13	1.14
FeO	34.12	33.56	34.42
CaO	0.01	0.01	0.01
MnO	0.43	0.41	0.41
K_2O	0.01	0.01	0.01
Na_2O	6.85	6.89	6.85
F	1.42	1.50	1.46
Total	94.44	94.15	94.58

Table A.15. The composition of biotite in the granites of the Kigom complex.

Oxides (wt%)	jk36c1	jk36c2	jkbio11	jkbio12	jk035a	jk035b
SiO_2	35.58	35.27	35.84	35.22	34.97	35.33
TiO_2	1.78	1.77	1.93	1.83	1.87	1.22
Al_2O_3	7.55	7.75	6.49	7.10	7.98	7.73
FeO	39.08	38.80	41.25	39.79	39.76	38.96
MnO	0.40	0.45	0.30	0.20	0.41	0.48
MgO	0.22	0.20	0.01	0.02	0.22	0.21
CaO	0.00	0.00	0.01	0.02	0.01	0.00
Na_2O	0.18	0.12	0.05	0.02	0.14	0.18
K_2O	10.01	9.97	9.15	8.96	9.81	9.55
H_2O	2.46	2.47	2.40	2.34	2.28	2.16
F	2.68	2.59	2.05	2.18	2.97	3.15
Cl	0.11	0.09	0.32	0.31	0.09	0.20
O=F	-1.09	-1.09	-0.86	-0.92	-1.25	-1.33
O=Cl	-0.02	-0.02	-0.07	-0.07	-0.02	-0.05
Total	98.84	98.37	98.87	97.00	99.22	97.80